Automated Electromyogram Signal Classification Frameworks Based on Singular Spectrum Analysis Variants

Ph.D. Thesis

By

Makam Kiran Kumar

DEPARTMENT OF ELECTRICAL ENGINEERING

INDIAN INSTITUTE OF TECHNOLOGY INDORE

JUNE 2025

Automated Electromyogram Signal Classification Frameworks Based on Singular Spectrum Analysis Variants

A THESIS

submitted to the

INDIAN INSTITUTE OF TECHNOLOGY INDORE

in partial fulfillment of the requirements for

the award of the degree

of

DOCTOR OF PHILOSOPHY

By

Makam Kiran Kumar

DEPARTMENT OF ELECTRICAL ENGINEERING

INDIAN INSTITUTE OF TECHNOLOGY INDORE

JUNE 2025

INDIAN INSTITUTE OF TECHNOLOGY INDORE

CANDIDATE'S DECLARATION

I hereby certify that the work which is being presented in the thesis entitled **Automated Electromyogram Signal Classification Frameworks based on Singular Spectrum Analysis Variants** in the partial fulfillment of the requirements for the award of the degree of **Doctor of Philosophy** and submitted in the **Department of Electrical Engineering, Indian Institute of Technology Indore,** is an authentic record of my own work carried out during the time period from July 2018 to June 2025 under the supervision of Dr. Ram Bilas Pachori, Professor, Indian Institute of Technology Indore, Indore, India.

The matter presented in this thesis has not been submitted by me for the award of any other degree of this or any other institute.

13 Mar 26

Signature of the Student with Date

(Makam Kiran Kumar)

This is to certify that the above statement made by the candidate is correct to the best of my knowledge.

22.03.2026

Signature of Thesis Supervisor with Date

(Prof. Ram Bilas Pachori)

Makam Kiran Kumar has successfully given his Ph.D. Oral Examination held on **13 Mar 2026**.

22.03.2026

Signature of Thesis Supervisor with Date

(Prof. Ram Bilas Pachori)

ACKNOWLEDGEMENTS

I extend my sincere appreciation to all those who supported me throughout this research journey.

I am deeply grateful to my supervisor, **Prof. Ram Bilas Pachori**, for his constant guidance, valuable insights, and motivation. His mentorship played a pivotal role in shaping the depth and direction of my work.

I sincerely thank my research progress committee members—**Dr. Pavan Kumar Kankar**, **Prof. Anand Parey**, and **Dr. Swaminathan Ramabadran**—for their timely reviews and constructive suggestions. I also acknowledge the Head of the Department of Electrical Engineering and the administrative and technical staff of IIT Indore for their support.

I thank **Prof. Suhas Joshi**, Director, IIT Indore, for the opportunity to pursue my doctoral research at this esteemed institution.

Special thanks to my colleagues and friends—Vivek Kumar Singh, Shailesh Bhalarao, Nabasmita Phukan, Achinto Mondal, Aditya Nalwaya, Ashok Mahato, Kritiprasanna Das, and Vaibhav Mishra—for their camaraderie and encouragement.

I am forever indebted to my wife, **Makam Varalakshmi**, my children, **Makam Ganesh Kumar** and **Makam Charushree**, and my parents for their unconditional love and unwavering support. I also thank my father **Makam Ramakrishna**, mother **Makam Saraswati**, brother **Makam Nagaraju**, and sister-in-law **Makam Bharati** for being my pillars of strength.

Finally, I thank the Almighty for blessing me with the resilience to complete this journey.

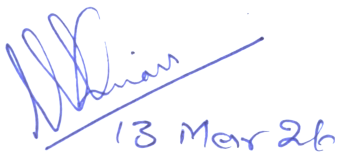

Makam Kiran Kumar

This thesis is dedicated to my loving wife, dear children, supportive parents and friends, whose unwavering encouragement and inspiration have made this work possible.

Abstract

The early diagnosis of neuromuscular disorders and the development of assistive technologies rely heavily on the accurate analysis of electromyogram (EMG) signals, which are inherently non-stationary, noisy, and complex. This thesis introduces novel frameworks that integrate advanced singular spectrum analysis (SSA) variants—namely, automatic SSA (Auto-SSA), sliding mode SSA (SM-SSA), and multivariate SM-SSA (MSSA)—with quantum convolutional neural networks (QCNNs) to enhance classification performance and robustness in biomedical signal processing tasks.

The proposed frameworks are validated across three key applications. For amyotrophic lateral sclerosis (ALS) detection, intramuscular EMG signals from benchmark datasets were decomposed using Auto-SSA, an adaptive method that selects decomposition parameters automatically, extracting most significant features of the signal via particle swarm optimization (PSO). The resultant QCNN classifier achieved a testing accuracy of 98.50% on 200 training samples, outperforming conventional classifiers. For eye movement detection, extraocular muscle EMG signals were analyzed using SM-SSA, which segments signals into overlapping frames for automated decomposition, followed by neighborhood component analysis (NCA)-based feature selection. The QCNN framework yielded a remarkable 98.70% accuracy on a publicly available six-class eye movement dataset with 256 training samples. For human activity recognition (HAR), multichannel surface EMG signals were processed using MSSA, which preserves inter-channel dependencies through channel-aligned decomposition. Multi-domain features—spanning time, frequency, and entropy characteristics—were extracted and refined using minimum redundancy maximum relevance (MRMR) before classification with a 10-qubit QCNN. The HAR framework achieved superior classification accuracies of 98.81%, 98.78%, and 98.86% for aggressive, normal, and combined activity classes, respectively, using an extensive dataset comprising 20 physical actions.

These frameworks leverage quantum entanglement and superposition to enable

expressive, compact models that generalize well in data-scarce and noisy conditions. By bridging classical decomposition techniques with quantum-enhanced learning, this work demonstrates significant improvements in diagnostic accuracy, computational efficiency, and robustness over state-of-the-art methods. Beyond biomedical applications, the proposed models have potential for real-time deployment in assistive prosthetics, defense-oriented eye-gaze interfaces, and rehabilitation systems, setting the stage for scalable and adaptive human-machine interaction solutions.

Keywords: Electromyogram signal analysis, Singular Spectrum Analysis variants, Quantum Convolutional Neural Network, Feature selection, Human Activity Recognition, Eye movement detection, Amyotrophic lateral sclerosis, Biomedical signal processing.

Contents

List of Figures

List of Tables

List of Abbreviations and Acronyms

ACC: Accuracy

ALS: Amyotrophic Lateral Sclerosis

ANN: Artificial neural network

ASSA: Automatic Singular Spectrum Analysis

CNN: Convolutional neural network

EMG: Electromyography

HAR: Human Activity Recognition

HAR-sEMG): sEMG-based HAR

HCI: Human Computer Interface

HMI: Human Machine Interface

KNN: K-nearest neighbor

ML: Machine learning

QML: Quantum Machine Learning

QCNN: Quantum Convolutional Neural Networks

RF: Random forest

SSA: Singular Spectrum Analysis

Auto-SSA: Automatic Singular Spectrum Analysis

SMSSA: Sliding Mode Singular Spectrum Analysis

MSSA: Multivariate Sliding Mode Singular Spectrum Analysis

PSO: Particle Swarm Optimization

NCA: Neighborhood Components Analysis

MRMR: Minimum Redundancy Maximum Relevance

SVM: Support Vector Machine

VMD: Variational mode decomposition

vs: versus

1D: One-dimension

2D: Two-dimension

Chapter 1

Introduction

This chapter provides a comprehensive overview of the thesis, outlining its primary objectives and key contributions. it begins with basic signal definitions and properties, establishing the necessity of using EMG signals and the rationale for employing variants of SSA and quantum computing for signal classification. the chapter also presents a detailed justification for favoring quantum computing over traditional techniques. following this, an overview of the ALS detection framework is provided, highlighting the integration of Auto-SSA with a QCNN for EMG signal analysis. The thesis further explores applications in HMI identification, focusing on decoding of eye movement from EMG signals of extraocular muscles using SMSSA, and HAR from sEMG utilizing MSSA combined with a QCNN quantum classifier. The chapter concludes by enumerating the thesis's specific objectives and contributions, and by outlining the overall structure and organization of the thesis.

1.1 EMG

The origins of electromyography (EMG) can be traced back to 1666, when Francesco Redi documented that electric ray fish possessed muscles capable of generating electricity [2]. In 1773, Walsh demonstrated that electric eels' muscle tissue could produce sparks, highlighting the electrical nature of muscular activity. Later, in 1792, Luigi Galvani published *De Viribus Electricitatis in Motu Musculari Commen-*

tarius [3], illustrating that electricity induces muscle contractions [4]. These foundational discoveries paved the way for modern EMG, which has since become a vital tool in biomedical research and clinical diagnostics.

EMG has evolved from invasive needle-based recordings to non-invasive surface electromyography (sEMG), enabling broader clinical and engineering applications [5, 6]. Advanced systems now integrate multi-channel sEMG electrodes with wireless technologies to facilitate muscle monitoring in both clinical and mobile environments [7, 8].

EMG records the electrical activity generated by skeletal muscles, primarily capturing myoelectric signals produced by motor neurons within the central nervous system (CNS). These signals reflect underlying neuromuscular activity and are crucial for diagnosing muscle injuries, nerve impairments, and various neuromuscular disorders. EMG is widely employed across diverse applications—from extracting basic signal features to enabling advanced machine learning algorithms for controlling prosthetic limbs and robotic systems, as well as in gait analysis and muscle activation tracking [9].

1.1.1 Signal characteristics and processing challenges

In signal processing, mathematical models are employed to represent signals and their underlying dynamics. EMG signals are inherently non-stationary, non-linear, and subject to varying noise conditions [10, 11, 12]. Non-stationarity means that the statistical properties of EMG signals—such as mean, variance, and frequency content—change over time, making them difficult to analyze using traditional signal processing techniques that assume time-invariance and stationarity. In other words, Specifically, the autocorrelation function $R_x(t_1, t_2)$ independant of time difference i.e. $\tau = t_2 - t_1$, i.e., $R_x(t_1, t_2) = R_x(\tau)$, which is the condition for stationary signals [13, 14]. Examples include speech signal (Figure 1.1(a)) and EMG signal (Figure 1.1(b)).

The non-linear nature of EMG arises from the complex interactions between motor units and muscle fibers, as well as the dynamic recruitment patterns during muscle contraction [15, 16]. This non-linearity is further evidenced by advanced entropy-

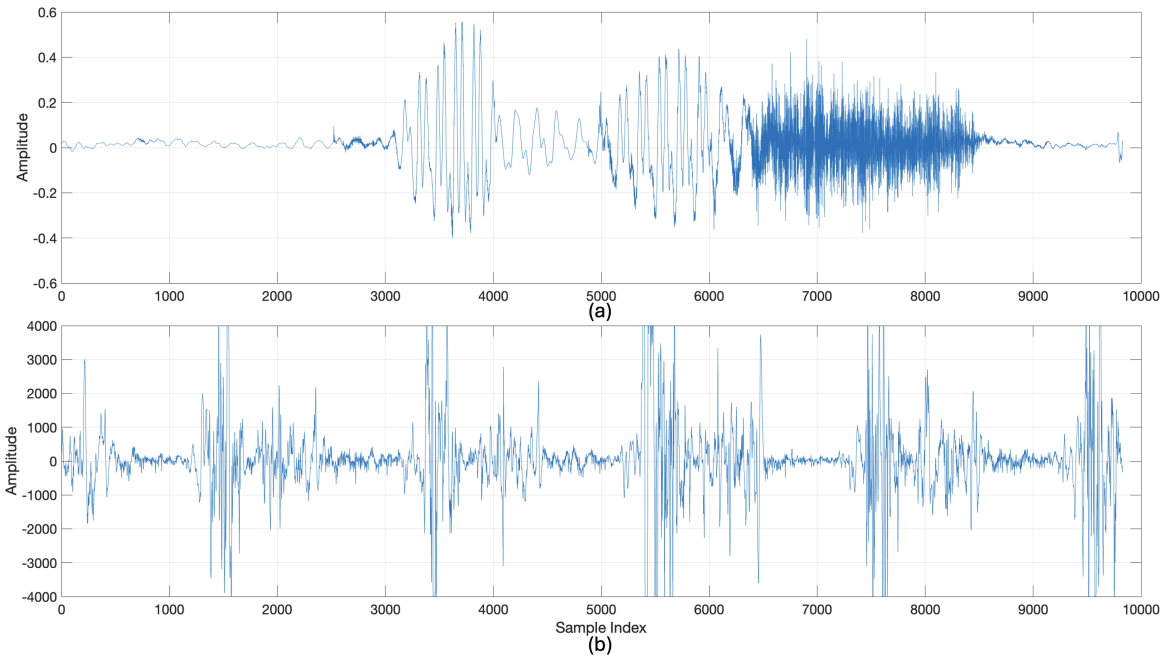

Figure 1.1: Real-time signal samples for (a) Audio signal from Matlab `speech_dft.wav` (plot from 4600–14429 samples) and (b) EMG Signal while bowing used in this thesis while bowing collected from right thigh [1].

based analyses, such as fixed sample entropy (fSampEn), which reveal sigmoidal-like behavior in EMG recordings as muscle activity increases [16].

Noise in EMG signals refers to unwanted electrical activity contaminating the true muscle signal. This can arise from external sources, such as power line interference, or internal sources, such as cross-talk from adjacent muscles or inherent sensor limitations [17, 7, 8]. The noise environment of EMG signals is not constant and varies over time, which further complicates analysis and classification tasks [11, 12].

Characteristic features of EMG signals include amplitude (peak-to-peak voltage), phase (initial negative cycle duration), rise time (interval between negative and positive peaks), total duration (between successive negative cycles), and satellite potentials—small signals trailing the main waveform [18]. These properties reflect muscle activation dynamics and are valuable for diagnosing disorders like ALS, guiding motor rehabilitation therapies, and expanding the utility of EMG in prosthetics and robotic control systems [19, 20].

1.1.2 Measurement and signal processing

The stationarity of signals can be evaluated using statistical tests such as the Augmented Dickey-Fuller (ADF) test and the Kwiatkowski-Phillips-Schmidt-Shin (KPSS) test, both of which assess the presence or absence of unit roots or trends in the signal [13]. However, physiological signals such as EMG are typically non-stationary, and traditional signal processing techniques—such as the Fourier Transform, which assumes stationarity and linearity—are inadequate for accurate analysis and interpretation [14]. To address these challenges, advanced, non-parametric spectral decomposition techniques such as empirical mode decomposition (EMD), empirical wavelet transform (EWT), and singular spectrum analysis (SSA) and its variants (SMSSA, Auto-SSA, MSSA) have been developed [21, 22, 23]. These methods excel at handling missing data, suppressing noise, and mitigating non-stationarity, decomposing complex EMG signals into interpretable amplitude- and frequency-modulated components.

Filtering and smoothing techniques, like Butterworth filters or SSA, are commonly used to mitigate noise in EMG recordings. Raw EMG signals typically have amplitudes between 0–10 mV. Various noise sources can degrade signal quality, including ambient noise from electrical sources, motion artifacts due to electrode movement, inherent electronic noise from amplifiers, and physiological variability [17, 7, 8]. Signal processing techniques such as wavelet transform, higher-order statistics, and machine learning are used to enhance signal fidelity and suppress noise [24, 25].

1.1.3 Types of EMG signals

Two primary types of electrodes are employed for recording EMG signals: needle electrodes and surface electrodes. Needle electrodes, which are approximately 1 mm^2 in size, are invasive and categorized into mono-polar single electrodes, single-fiber EMG electrodes, and concentric EMG electrodes. In contrast, surface electrodes, typically ranging from 0.5 to 2.5 cm in width, are non-invasive and placed on the skin surface. These operate based on electrolytic conduction, detecting electrical potential

differences between the muscle and skin interface. Surface electrodes are generally classified into gelled and dry types, depending on the contact medium used [18]. The type and placement of electrodes play a crucial role in determining signal quality, which directly impacts the performance of EMG-based clinical diagnostic tools and human-machine interfaces—particularly in tasks such as ALS detection, HAR, and eye-movement decoding.

Among electrophysiological measurements, EMG provides distinct advantages over electroencephalogram (EEG) and electrocardiogram (ECG) recordings. While EEG and ECG signals typically occupy lower frequency ranges (below 100 Hz), EMG signals span a broader spectrum from 5 Hz to 2 kHz. This wider frequency range enables EMG to capture more detailed muscle activation dynamics, although the signal patterns can be complex and challenging to interpret, which will be discussed in succeeding paragraphs.

1.1.4 EMG signal characteristics and processing

EMG signals represent the electrical activity generated by muscle contractions and relaxations and are shaped by both nervous system inputs and muscle anatomical structure [2]. These signals result from muscle fiber depolarization and are inherently complex due to noise contamination from surrounding tissues, deep muscle layers, and environmental artifacts. Accurate detection and processing are essential for clinical diagnostics, human-machine interfacing, prosthetic control, and biomechanical modeling.

1.1.5 Physiological and anatomical aspects of EMG

EMG captures *myoelectric activity*, reflecting the electrical potentials associated with muscle contractions. The signal-to-noise ratio (SNR), defined as the ratio of the desired EMG signal to background noise, is a key quality metric. Noise sources include electrical interference, motion artifacts, and physiological variability [15].

The motor unit action potential (MUAP), representing the summation of signals

from multiple muscle fibers, can be mathematically modeled as [15]:

$$Y(n) = \sum_{r=0}^{n-1} H(r)E(n-r) + W(n) \tag{1.1}$$

where: $Y(n)$ is the modeled EMG signal, $E(n)$ represents the processed muscle activity, $H(r)$ denotes the MUAP, $W(n)$ is additive white Gaussian noise, and n is the number of motor unit firings.

1.1.6 Electrical noise and EMG signal influencing factors

Noise in EMG signals refers to unwanted electrical activity contaminating the true muscle signal. This can arise from external sources, such as power line interference, or internal sources, such as cross-talk from adjacent muscles or inherent sensor limitations [17, 7, 8]. Filtering and smoothing techniques, like Butterworth filters or Singular Spectrum Analysis (SSA), are commonly used to mitigate noise in EMG recordings.

Raw EMG signals typically have amplitudes between 0–10 mV. Various noise sources can degrade signal quality: **Ambient noise** from electrical sources, **Motion artifacts** due to electrode movement, **Inherent electronic noise** from amplifiers, and **Physiological variability**.

Signal processing techniques such as wavelet transform, higher-order statistics, and machine learning are used to enhance signal fidelity and suppress noise [24, 25] Moreover the noise environment of the EMG signals is not constant and varies and hence traditional decomposition techniques where noise is assumed to be constant cannot efficiently process EMG signals [11, 12].

1.1.7 EMG applications

Electromyography (EMG) signals have become indispensable across a wide spectrum of biomedical and engineering applications, owing to their ability to capture neuromuscular activity with high temporal resolution and specificity. The versatility of EMG is reflected in its adoption for speech recognition, robotic control, prosthetic

devices, clinical diagnostics, rehabilitation robotics, and advanced human-machine interfaces. Each of these domains leverages the unique characteristics of EMG to address challenges that are difficult or impossible to solve with traditional sensing technologies.

1.1.7.1 Speech recognition

EMG-based speech recognition systems offer a robust alternative to traditional audio-based approaches, particularly in noisy environments or for individuals with vocal impairments. By monitoring the electrical activity of facial muscles during articulation, these systems can decode both sub-auditory and silent speech. Jorgensen et al. demonstrated an average success rate of 85.4% for sub-auditory speech recognition using EMG [26], while Meltzner et al. achieved 92.1% accuracy in silent speech recognition [27]. Jou et al. explored articulatory feature classification with surface EMG (sEMG), reaching 68% accuracy [28], and Lee's research using hidden Markov models reported 87% accuracy [29]. These results underscore the potential of EMG-based speech recognition to provide effective communication solutions for individuals with speech disabilities, as well as in scenarios where acoustic signals are unreliable or unavailable.

1.1.7.2 Robotic control and prosthetics

EMG signals serve as real-time biosignals for movement intention detection, enabling intuitive and adaptive control of robotic limbs and prosthetic devices. Osu and Gomi investigated joint muscle regulation via EMG, providing insights into muscle coordination and control [30]. Wang and Buchanan utilized neural networks to predict joint moments from EMG activations, advancing the field of biomechanical modeling and control [31]. The development of low-cost, portable EMG circuits has made prosthetic limb technology more accessible [32], while neuro-fuzzy control strategies have enhanced the adaptability and responsiveness of robotic exoskeletons [33]. Advanced gesture classifiers based on sEMG signals have enabled precise classification of upper limb movements [34], and decomposition-based control strategies have improved the precision and dexterity of multifunctional prosthetic hands [35, 36]. Signal condition-

ing and amplification techniques further ensure the fidelity and reliability of sEMG for prosthetic applications [37].

1.1.7.3 Diagnostics and Functional Assessment

In clinical settings, EMG signals are essential for assessing neuromuscular function and diagnosing a range of disorders. Applications include gait analysis, spasticity evaluation, and the assessment of motor unit disorders in conditions such as stroke and amyotrophic lateral sclerosis (ALS) [38, 9]. Machine learning pipelines, including K-nearest neighbors (KNN) classifiers, have demonstrated diagnostic accuracies as high as 99.1% for movement classification [39]. These capabilities highlight the diagnostic value of EMG in neurological, musculoskeletal, and rehabilitation medicine, supporting both clinical decision-making and patient monitoring.

1.1.7.4 Rehabilitation Robotics and Human-Machine Interfaces

EMG signal processing is critical for the real-time control of rehabilitation robots and adaptive human-machine interfaces. Noise-robust signal conditioning and advanced temporal pattern extraction enable adaptive robotic assistance tailored to individual user needs [40]. Machine learning algorithms such as support vector machines (SVM), convolutional neural networks (CNN), and long short-term memory networks (LSTM) enhance intent detection and user-specific adaptation in rehabilitation scenarios [41]. These interfaces are vital for improving recovery rates, facilitating effective collaboration between humans and robots, and enabling personalized rehabilitation programs that adapt to the evolving needs of patients.

1.1.7.5 Prosthetic Hand Control

With the number of amputees rising worldwide as a result of natural disasters, accidents, and conflicts [42, 43, 44], EMG-controlled prosthetic hands have become essential for restoring functional independence. Passive devices are limited in their capabilities and do not provide active control or feedback [45], whereas EMG-driven systems enable complex motor tasks and naturalistic control [46, 47, 48, 49]. Recent

advances in deep learning models have further improved control precision, bringing EMG prosthetics closer to the dexterity and intuitiveness of natural hand function [50]. These innovations are transforming the lives of amputees, enabling them to perform daily activities with greater independence and confidence.

In summary, the broad and growing range of EMG applications reflects its importance as a foundational technology for biomedical engineering, clinical diagnostics, and assistive robotics. Continued advances in signal processing, machine learning, and hardware design promise to further expand the impact of EMG in improving human health, mobility, and quality of life.

1.2 Motivation

Traditional signal processing techniques are grounded in key assumptions such as linearity, time-invariance, and stationarity [51]. These simplifications facilitate mathematical tractability and computational efficiency, enabling the widespread adoption of methods like the Fourier transform and linear filters in a variety of engineering and biomedical applications. However, these assumptions often break down when applied to real-world signals, especially those generated by biological systems.

Electromyography (EMG) signals—which record the electrical activity produced by muscle contractions—are inherently non-linear, non-stationary, and highly susceptible to noise from both physiological and environmental sources [10, 51]. The dynamic nature of neuromuscular activity, influenced by factors such as varying muscle force, fatigue, and electrode placement, results in signal characteristics that evolve rapidly over time. This variability poses significant challenges for accurate analysis, interpretation, and real-time classification, limiting the effectiveness of conventional signal processing approaches.

Despite these challenges, EMG signals provide a rich and indispensable source of information for biomedical and engineering applications. They are essential for the early detection and continuous monitoring of motor neuron diseases such as ALS, myopathies, and stroke-related impairments [52, 53]. Advanced machine learning al-

gorithms, including support vector machines (SVM) and random forests (RF), have demonstrated remarkable classification accuracies exceeding 90% in differentiating motion states and identifying pathological patterns [53]. These capabilities underscore the potential of EMG-based systems as high-precision diagnostic tools for neuromuscular disorders, enabling timely medical intervention and personalized rehabilitation strategies.

Beyond clinical diagnostics, EMG signals play a transformative role in the development of advanced prosthetic devices and intelligent robotic systems. Myoelectric prosthetics harness EMG signals to provide intuitive and natural control of upper and lower limb prostheses, restoring functional independence for amputees [52, 54]. Hybrid systems that integrate EMG with electroencephalography (EEG) further enhance adaptability, enabling the control of exoskeletons and assistive devices in complex environments such as defense and remote healthcare settings [55, 56, 57]. These integrated platforms empower individuals with paralysis or limb loss to achieve enhanced mobility, control fidelity, and improved quality of life.

The inherent non-stationarity and noise in EMG signals complicate their analysis, particularly when traditional methods that assume linearity, time-invariance, and stationarity are employed [10]. To address these limitations, advanced, non-parametric spectral decomposition techniques such as empirical mode decomposition (EMD), empirical wavelet transform (EWT), and singular spectrum analysis (SSA) and its adaptive variants (SMSSA, Auto-SSA, and MSSA) have been developed [17, 7, 58]. These methods excel at handling missing data, suppressing noise, and mitigating non-stationarity, decomposing complex EMG signals into interpretable amplitude- and frequency-modulated components. This enhanced signal quality is critical for downstream tasks such as classification, motion intent analysis, and real-time control.

Recent advances have pushed the boundaries of EMG signal processing by integrating SSA and its adaptive variants with quantum machine learning models such as QCNNs [59]. QCNNs leverage quantum parallelism to process high-dimensional features extracted via SSA, enabling accurate classification of binary and multiclass EMG datasets even under low-data regimes. This synergy combines SSA's adaptive decom-

position capabilities with QCNNs' capacity for efficient feature learning, effectively addressing both signal variability and data scarcity in EMG-based systems.

In summary, the use of EMG signals for detecting neuromuscular diseases and developing adaptive control systems for prosthetics and rapid-response robotic platforms operating in dynamic environments represents a significant advancement in both clinical and defense sectors. By leveraging sophisticated signal processing and classification frameworks, this research aims to contribute to the creation of more responsive, reliable, and user-friendly assistive technologies. The motivation for using EMG signals in ALS detection, eye movement decoding, and human activity recognition (HAR) stems from their ability to capture neuromuscular activity in real time, enabling actionable insights into human health, behavior, and intent. These signals enable improved diagnostic accuracy, enhanced patient care, and the development of more effective data-driven health management solutions.

1.2.1 ALS signal

Amyotrophic lateral sclerosis (ALS) is a neurodegenerative disorder primarily affecting the motor system, with emerging recognition of extra-motor manifestations. The gradual degeneration of upper and lower motor neurons causes muscle weakness and atrophy, eventually leading to paralysis [60]. ALS has a low global incidence and prevalence, with rates ranging from 0.26 to 23.46 per 100,000 person-years and prevalence from 1.57 to 11.80 per 100,000, depending on the region [61]. Inheritance modes include dominant, recessive, compound heterozygosity, and de novo mutations linked to the SOD1 gene [62].

1.2.2 EMG of EOM

EMG signals from extraocular muscles (EOM) are crucial for diagnosing conditions such as ALS, neuropathies, and muscle disorders [63]. These signals reflect nervous system control of muscle fibers and are influenced by muscle anatomy and physiology [64]. EOM EMG signals may be acquired using:

1. Surface electrodes: Non-invasive conductive pads placed near the eyes.

2. Needle electrodes: Invasive electrodes inserted into extraocular muscles [65].

The collected signals are processed using filtering, wavelet transforms, and advanced analysis [66, 67]. EOM EMG is pivotal for fatigue monitoring, human-machine interaction, robotic navigation [68], and real-time control applications [69]. Electrode types include mono-polar, single-fiber, concentric needle, and surface electrodes [70].

1.2.3 EMG for HAR

The HAR dataset used in this study consists of EMG signals from upper and lower limb muscles during physical actions. Data were collected from four subjects (three males, one female, aged 25–30) performing ten normal and ten aggressive activities, using a Delsys EMG wireless apparatus in the Essex robotic arena, equipped with a professional kick-boxing standing bag [1].

Eight surface electrodes were placed on biceps, triceps, thighs, and hamstrings, recording from channels corresponding to right biceps (ch1), right triceps (ch2), left biceps (ch3), left triceps (ch4), right thigh (ch5), right hamstring (ch6), left thigh (ch7), and left hamstring (ch8). This dataset supports real-time classification for prosthetics, rehabilitation, and assistive technologies, and has become a benchmark for EMG-based HAR algorithm evaluation.

The preceding discussion highlights the complexity of electromyography (EMG) signals, which are characterized by non-stationary, non-linear behaviors, and susceptibility to diverse sources of noise. These complexities challenge conventional signal processing approaches, rendering techniques like Fourier transforms inadequate for accurate analysis and interpretation. To address these issues, advanced signal decomposition techniques have been developed to adaptively decompose EMG signals into their constituent components, enabling enhanced feature extraction, noise reduction, and classification performance. The following section details these data-driven decomposition methods, including singular spectrum analysis (SSA) and

its variants, which are central to the frameworks proposed in this thesis.

1.3 Signal decomposition techniques

Decomposition techniques are essential for handling the complexities of analyzing biomedical signals, particularly those exhibiting non-stationary and non-linear characteristics like EMG. In the context of SSA, Auto-SSA, SMSSA, and MSSA decomposition refers to breaking down complex time-series signals into smaller, more tractable components for further analysis, noise suppression, and feature extraction.

Biomedical signals such as EMG are inherently non-stationary and non-linear, and are often contaminated with time-varying noise. These properties pose significant challenges for traditional signal processing techniques like Fourier transform (FT), which assumes stationarity and linearity [71, 22]. To address these challenges, modern signal decomposition (SD) techniques aim to deconstruct complex signals into amplitude-modulated (AM) and frequency-modulated (FM) components, enabling a more accurate representation of physiological dynamics [21].

Traditional transforms like FT or wavelet-based methods fall short when dealing with signals exhibiting complex, time-varying characteristics, such as EMG. In real-life scenarios, the natural entanglement of time and frequency domains results in phenomena like mode-mixing and poor localization in conventional spectral analysis [72]. This necessitates the adoption of data-driven approaches, which make fewer assumptions about signal structure and adaptively extract inherent oscillatory components [23, 73].

Popular data-driven SD techniques include empirical mode decomposition (EMD) and its variants, variational mode decomposition (VMD), synchrosqueezed transform (SST), and SSA [21, 22, 73, 23]. These methods excel in adaptively decomposing non-stationary signals into intrinsic mode functions (IMFs) or components, capturing both amplitude and frequency modulations inherent in physiological signals like EMG. Specifically, SSA and its extensions, such as Auto-SSA, SMSSA, and MSSA, demonstrate robustness in dealing with noise, missing data, and adaptively adjusting to signal properties [23].

Moreover, real-life EMG signals often contain multiple overlapping modes, dynamic amplitude-frequency variations, and transient noise artifacts. Data-driven SD methods, by virtue of their local and adaptive nature, effectively isolate these components, providing meaningful insights into neuromuscular function. Their ability to handle both narrow- and wide-band components further strengthens their applicability in biomedical applications, where signal characteristics can vary significantly [22, 73].

In summary, the decomposition of EMG and similar biomedical signals necessitates robust, data-driven approaches capable of addressing the inherent non-stationarity, non-linearity, and varying noise conditions of real-life data. The integration of SSA variants—including Auto-SSA, SMSSA, and MSSA—into signal processing pipelines is essential for accurate feature extraction, noise suppression, and interpretation of complex physiological processes.

1.3.1 SSA

Singular Spectrum Analysis (SSA) is a methodology used for analyzing and forecasting time series data. It integrates concepts from traditional time series analysis, multivariate statistics, dynamical systems, and signal processing. From an algorithmic perspective, SSA is a multistep process for signal analysis. The basic SSA framework consists of two main phases: decomposition and reconstruction [74].

1.3.1.1 Embedding for SSA

The algorithm starts with embedding of a trajectory matrix $\mathbf{T}$ of size $L \times (N-L+1)$ constructed from the time series $Y(t) = \{y_1, y_2, \ldots, y_N\}$ using an window length L. This can be expressed as follows:

$$\mathbf{Y}_i = \{y_i, y_{i+1}, \ldots, y_{i+L-1}\},$$

where L gives the lentgh of the vector $\mathbf{Y}_i$ and $K = N - L + 1$.

The crucial parameter L dictates the separability of different eigenmodes. The classical limit for window length is $2 \leq L \leq \frac{N}{2}$ [75]. If the data has a low-frequency

component at $f_{\min}$, then setting the window length to $\frac{1}{f_{\min}}$ is appropriate.

THe lagged autocorrelation of the data may compute the length of the window.In this case, the window length is given by half of the difference between the lags corresponding to any two successive points of the same phase on the autocorrelation plot:

$$L = \frac{1}{2}\left(\text{Lag}_{i+1} - \text{Lag}_i\right),$$

where Lag_i and Lag_{i+1} represent the lags corresponding to points with the same phase on the autocorrelation plot.[76]

1.3.2 Auto-SSA

Auto SSA is an advanced adaptation of traditional Singular Spectrum Analysis (SSA) designed to address the challenges posed by non-stationary and complex signals [23]. While classical SSA requires manual selection of parameters such as the window length and grouping strategy, Auto SSA incorporates algorithms to automatically determine these critical parameters, optimizing the decomposition process for each specific dataset thus outperforming the classical SSA. This automation is particularly valuable in scenarios involving rapidly changing signal characteristics or when analyzing large volumes of data, as it reduces the need for expert intervention and enhances reproducibility. By leveraging techniques such as adaptive windowing, automatic component grouping, and sometimes machine learning-based feature selection, Auto SSA improves the accuracy and robustness of signal decomposition, noise reduction, and feature extraction. As a result, Auto SSA is increasingly applied in fields like biomedical signal processing, vibration analysis, and industrial diagnostics, where dynamic and variable signal properties demand adaptive and efficient analytical tools [77].

1.3.3 SMSSA

Sliding Mode Singular Spectrum Analysis (SMSSA) extends the separation capabilities of Singular Spectrum Analysis (SSA) to non-stationary signals containing amplitude- and frequency-modulated (AM-FM) components, addressing key limitations of classical approaches [23]. The development of SMSSA is motivated by several technical challenges inherent to real-world signal analysis, such as the weak correlations between elementary components of a single signal, which complicate reliable unsupervised grouping. Additionally, the spectral overlap between different signal components can result in mixing modes, making it difficult to distinguish between distinct signal features. The dynamic nature of real signals, characterized by the transient appearance and disappearance of components over time, further complicates traditional decomposition methods. To overcome these issues, SMSSA employs a sliding, locally adaptive analysis window that adjusts to the time-varying characteristics of the signal, thereby enhancing the robustness and accuracy of component extraction. This adaptive framework is particularly well-suited for applications involving complex, non-stationary signals such as EMG, where traditional methods that assume signal stationarity and fixed component structure often fail to provide reliable results [23]. By continuously updating the analysis window and component grouping strategy, SMSSA effectively mitigates the effects of noise, spectral overlap, and component transience, resulting in improved signal reconstruction quality and fidelity for downstream tasks such as classification and motion intent analysis [78, 79].

The sliding window mechanism in SMSSA effectively captures the non-stationary property of a signal and the resulting components due to use of SMSSA on a multi-component signal have a better quality reconstruction factor (QRF) as compared to those of other SD methods, such as EMD and synchrosqueezing technique. Therefore, the SMSSA-based signal-driven approach will be effective for the removal of cross-terms in the time–frequency representation obtained using WVD of the multi-component signal [80]. The sliding window mechanism in SMSSA effectively addresses non-stationarity in signals, enabling high-fidelity decomposition of multi-component

signals. Compared to other signal decomposition (SD) methods—such as empirical mode decomposition (EMD) and synchrosqueezing, SMSSA achieves superior component reconstruction quality, as quantified by the quality reconstruction factor (QRF) [81]. This enhanced reconstruction capability makes SMSSA particularly effective for suppressing cross-term artifacts in the Wigner-Ville Distribution (WVD) time–frequency representations of multi-component signals [80].

1.3.4 MSSA

MSSA is a robust technique for analyzing multichannel time-series data, such as sensor arrays or physiological recordings (e.g., EMG). By integrating sliding window analysis with singular spectrum decomposition, MSSA extracts underlying trends, periodicities, and amplitude-modulated components while suppressing noise and mode mixing artifacts. The method operates through three key steps: (1) constructing a trajectory matrix via a sliding window, (2) decomposing the matrix into orthogonal components, and (3) applying hierarchical clustering post-diagonal averaging to group reconstruction components (RCs) for each channel. This approach is particularly effective for nonstationary signals with time-varying components, such as those encountered in healthcare monitoring or human motion analysis, where it outperforms conventional methods in feature extraction and cross-term mitigation. The sliding window mechanism ensures adaptability to dynamic signal variations, addressing challenges like spectral overlap and transient component emergence [82, 64].

While signal decomposition techniques like SSA and its variants effectively extract meaningful components from complex EMG signals, the resultant high-dimensional feature space still presents challenges for real-time classification and interpretation. To address these challenges, dimensionality reduction techniques are employed to distill essential features, reduce computational complexity, and improve classification performance. The following section explores advanced methods, including PSO, NCA, and MRMR, which enhance EMG signal analysis by refining feature sets and ensuring efficient model deployment.

1.4 Dimensionality reduction

Both SSA and MSSA achieve a reduction in dimensionality by decomposing the signal into components with the highest singular values. These dominant components capture the most significant patterns in the data, while less important or noisy components are discarded. This process allows for reducing the dimensionality of the signal representation. The dimensionality reduction technique is an essential method for sEMG signal pattern recognition and classification, especially for real-time applications such as prosthesis control. This technique can reduce the high dimension extracted feature into a lower dimension space feature which helps the classifier work more properly.[83]

1.4.1 PSO

PSO is a population-based optimization algorithm inspired by the collective movement of social organisms, such as bird flocks or fish schools. Originally introduced by Kennedy and Eberhart [84], PSO has been widely applied in solving complex global optimization problems due to its simplicity and the ability to explore large search spaces effectively.

PSO operates by maintaining a swarm of candidate solutions, referred to as particles, which traverse the solution space based on their own best-found positions and those of neighboring particles. Each particle iteratively adjusts its position by updating its velocity according to a set of mathematical equations that incorporate both individual experiences and the collective intelligence of the swarm. This cooperative interaction allows PSO to navigate complex, multimodal landscapes efficiently, making it particularly well suited for problems with multiple local minima.

Unlike traditional gradient-based optimization techniques, PSO does not require the function being optimized to be differentiable. This makes it an attractive choice for high-dimensional, nonlinear, or poorly defined objective functions where conventional approaches struggle [85]. However, like many metaheuristic algorithms, PSO does not guarantee convergence to the global optimum and may require fine-tuning

of hyperparameters, such as inertia weight and acceleration coefficients, to balance exploration and exploitation.

1.4.1.1 PSO for clustering and dimensionality reduction

One notable application of PSO is in data clustering, where it has demonstrated superior performance over traditional methods such as K-means. The PSO clustering algorithm dynamically updates the cluster centroids by optimizing an objective function that minimizes intra-cluster distances [86]. Studies have shown that PSO-based clustering can yield more compact and well-separated clusters compared to conventional approaches. However, when dealing with high-dimensional datasets, the computational cost of PSO increases significantly, leading to performance bottlenecks.

To address this challenge, dimensionality reduction techniques are often employed before applying PSO to clustering tasks. By transforming high-dimensional data into a lower-dimensional representation, these techniques help mitigate the **curse of dimensionality** and improve computational efficiency while preserving essential data structures. Principal component analysis (PCA), singular value decomposition (SVD) and feature selection methods are commonly used in conjunction with PSO to enhance clustering performance [87, 88].

Additionally, hybrid approaches that integrate PSO with feature selection methods have been proposed to identify the most relevant attributes, further reducing noise and improving clustering accuracy. Such hybrid models leverage the exploratory nature of PSO to find an optimal subset of features that maximizes cluster compactness and separation while minimizing computational overhead.

1.4.1.2 Algorithmic representation of PSO

A standard PSO algorithm begins with a swarm of S particles, each representing a potential solution in a n dimensional space [89]. The optimization process follows these key steps:

1. Initialize particle positions $\mathbf{x}_i$ and velocities $\mathbf{v}_i$ randomly within predefined

bounds.

2. Evaluate the fitness of each particle using the objective function $f(\mathbf{x}_i)$.

3. Update each particle's best-known position $\mathbf{p}_i$ and identify the global best position $\mathbf{g}$ found by the swarm.

4. Adjust particle velocity using the update rule:

$$\mathbf{v}_i(t+1) = \omega \mathbf{v}_i(t) + c_1 r_1(\mathbf{p}_i - \mathbf{x}_i) + c_2 r_2(\mathbf{g} - \mathbf{x}_i), \tag{1.2}$$

   where ω is the inertia weight, c_1 and c_2 are cognitive and social coefficients, and r_1, r_2 are random values in [0,1] [89].

5. Update particle position:

$$\mathbf{x}_i(t+1) = \mathbf{x}_i(t) + \mathbf{v}_i(t+1). \tag{1.3}$$

6. Repeat steps 2–5 until convergence criteria (e.g., maximum iterations or acceptable error threshold) are met [89].

PSO's adaptability and efficiency make it a preferred choice for various real-world applications, including feature selection, robotics, supply chain optimization, and neural network training. However, advancements in adaptive PSO variants and hybrid models continue to enhance its robustness and applicability to emerging computational challenges.

1.4.2 NCA

Neighborhood-based feature selection is a supervised technique that aims to enhance classification performance by identifying a set of influential features [90]. This method operates by learning a transformation of input variables that optimizes classification accuracy using a leave-one-out (LOO) approach. Unlike traditional nearest-neighbor methods, which rely on strict distance measures, adaptive neighborhood

analysis incorporates a stochastic approach to selecting reference points, thereby improving robustness in high-dimensional spaces.

1.4.2.1 Mathematical formulation

Consider a classification problem with a dataset containing N training samples:

$$S = \{(\mathbf{x}_i, y_i) | i = 1, 2, \ldots, N\}, \tag{1.4}$$

where $\mathbf{x}_i \in \mathbb{R}^d$ are feature vectors, $y_i \in \{1, 2, \ldots, C\}$ are class labels, and C represents the number of categories [90]. The objective is to learn a classifier $g : \mathbb{R}^d \to \{1, 2, \ldots, C\}$ that maps feature vectors to their respective classes.

A probabilistic reference selection scheme is defined as follows. Instead of deterministically choosing the nearest neighbor, we define the probability of selecting a reference point $\mathbf{x}_j$ for a given input $\mathbf{x}$:

$$P(Ref(\mathbf{x}) = \mathbf{x}_j | S) \propto \exp\left(-\frac{d_w(\mathbf{x}, \mathbf{x}_j)}{\sigma}\right), \tag{1.5}$$

where $d_w(\mathbf{x}_i, \mathbf{x}_j)$ is the weighted distance function:

$$d_w(\mathbf{x}_i, \mathbf{x}_j) = \sum_{r=1}^{d} w_r^2 |x_{ir} - x_{jr}|, \tag{1.6}$$

and w_r are the feature importance weights. The parameter σ controls the sensitivity of the selection process to distance variations [90].

1.4.2.2 Optimization objective

To optimize classification performance, we define the expected probability of correct classification for a sample $\mathbf{x}_i$:

$$q_i = \sum_{j=1, j \neq i}^{N} P(Ref(\mathbf{x}_i) = \mathbf{x}_j | S_{-i}) I(y_i = y_j), \tag{1.7}$$

where $I(y_i = y_j)$ is an indicator function that returns 1 if the labels match and 0 otherwise. The overall classification accuracy function is given by [90]:

$$F(w) = \frac{1}{N}\sum_{i=1}^{N} q_i - \lambda \sum_{r=1}^{d} w_r^2. \tag{1.8}$$

Here, λ serves as a regularization parameter, ensuring that irrelevant features are assigned near-zero weights to enhance model sparsity [90].

1.4.2.3 Feature weight optimization

Finding the optimal weight vector w is framed as the following minimization problem:

$$\hat{w} = \arg\min_{w} \left(\frac{1}{N} \sum_{i=1}^{N} \sum_{j=1, j\neq i}^{N} P_{ij} L(y_i, y_j) + \lambda \sum_{r=1}^{d} w_r^2 \right), \tag{1.9}$$

where the loss function is given by $L(y_i, y_j) = 1$ if $y_i \neq y_j$ and 0 otherwise. This objective function minimizes classification error while enforcing feature selection through regularization [90].

Since the regularization parameter applies uniformly to all feature weights, inconsistencies in feature scaling can affect weight optimization. To address this, feature standardization is performed to ensure all features have zero mean and unit variance before applying adaptive neighborhood analysis.

The NCA provides a robust mechanism for feature selection in high-dimensional classification tasks. By integrating a probabilistic reference selection approach and optimizing feature importance weights, the technique achieves improved classification accuracy while minimizing redundant information.

1.4.3 MRMR

When dealing with large-scale datasets comprising numerous features, feature of selection plays a crucial role in machine learning applications. In fields like digital marketing, where predicting user behavior and preferences is vital, an abundance of features can potentially improve model performance if utilized effectively. However,

incorporating all available features without filtering can lead to overfitting, increased computational complexity, and decreased interpretability.

To address this challenge, feature selection techniques are employed to identify and retain only the most relevant and non-redundant features. This not only enhances computational efficiency but also improves prediction accuracy and reduces maintenance efforts related to feature management [91]. Among various methods, MRMR stands out as a widely adopted approach due to its ability to balance feature relevance and redundancy.

The MRMR method aims to select features that are both highly relevant to the target variable and minimally redundant among themselves. The relevance of a feature is typically measured through mutual information, while redundancy is quantified by assessing the mutual dependence between features. By achieving this balance, the MRMR method enhances model generalization and reduces noise in the input data.

1.4.3.1 Background

Feature selection methods can broadly be categorized into three groups: filter methods, wrapper methods, and embedded methods. Filter methods are favored for their computational efficiency and independence from specific learning algorithms, making them suitable for scenarios requiring rapid model adaptation. The MRMR method, being a filter-based technique, has gained significant traction due to its efficacy in maintaining high relevance while minimizing redundancy.

The original MRMR framework, introduced by Peng et al. [92], utilizes mutual information to quantify both relevance and redundancy. Subsequent advancements have aimed to enhance its efficiency and accuracy. One such extension, the Normalized Mutual Information Feature Selection (NMIFS) method [93], addresses the challenge of normalizing redundancy measures. Another improvement involves normalizing the relevance term itself [94]. More recent approaches, such as the maximum relevance-minimum multi-collinearity (MRmMC) method [95], use conditional variance and multiple correlation to achieve a refined balance.

Furthermore, the computational demands of the MRMR method prompted the de-

velopment of Fast-MRMR [91], which leverages distributed computing environments for speed optimization. Other methods, like the F-statistic-based MRMR variant, aim to reduce complexity while maintaining high accuracy [96]. Despite these advancements, the core principle remains the same: selecting features that maximize relevance to the output while minimizing redundancy within the selected subset.

1.4.3.2 MRMR framework

Given a set of m features, the MRMR criterion evaluates the importance of a feature $\mathbb{X}_i$ as follows [94]:

$$f_{MRMR}(\mathbb{X}_i) = I(\mathbb{Y}, \mathbb{X}_i) - \frac{1}{|S|} \sum_{\mathbb{X}_s \in S} I(\mathbb{X}_s, \mathbb{X}_i)$$

Here, Y denotes the response variable, S represents the set of selected features, and $I(\cdot, \cdot)$ is the mutual information between two variables. The equation balances relevance, quantified as $I(Y, \mathbb{X}_i)$, and redundancy, quantified as the average mutual information between the candidate feature and each already-selected feature.

For discrete variables, mutual information can be expressed as:

$$I(Y, \mathbb{X}) = \sum_{y \in \Omega_Y} \sum_{\mathbb{X} \in \Omega_{\mathbb{X}}} p(\mathbb{X}, y) \log \left(\frac{p(\mathbb{X}, y)}{p(\mathbb{X}) p(y)} \right)$$

During the selection process, the algorithm iterates through the unselected features to identify the one with the highest MRMR score, subsequently adding it to the selected set [94]. Variants of the MRMR method have been introduced to address computational efficiency and incorporate non-linear associations [97]. These include modifications such as the Mutual Information Quotient (MIQ) and F-test Correlation Quotient (FCQ) [96], which leverage alternative metrics to measure relevance and redundancy.

Through rigorous empirical evaluations on both synthetic and real-world datasets, the MRMR framework has proven its robustness and scalability. By balancing relevance and redundancy effectively, it serves as a powerful technique for enhancing model

accuracy and computational efficiency in various machine learning applications. Having decomposed complex EMG signals and extracted a reduced set of high-quality features using methods like Auto-SSA, SMSSA, MSSA, PSO, NCA, and MRMR, the next phase involves leveraging advanced computational frameworks for classification. QML, and specifically QCNNs, offer a powerful approach to analyzing such feature-reduced biomedical data. The integration of quantum computing principles into neural architectures enables superior classification performance, robustness, and adaptability in dynamic environments.

1.5 QML

Quantum computers leverage quantum mechanics to perform tasks beyond the capabilities of classical machines, with potential applications ranging from cryptography, signal analysis to drug design. These advances are driven by quantum algorithms that offer speedups or efficiency improvements over classical approaches. Although large-scale quantum computers are not yet available, research in quantum algorithms has been active for over two decades, focusing on practical methods with demonstrable performance. Contrary to the widespread belief that quantum computers have limited applications, the field of quantum algorithms has grown explosively, with resources such as the "Quantum Algorithm Zoo" listing with 518 papers on the subject [98]. Several comprehensive surveys provide further insights into this rapidly evolving area [99, 100, 101].

Within this context, Quantum Machine Learning (QML) has emerged as a vibrant interdisciplinary field at the intersection of quantum computing and classical machine learning, offering novel approaches to data processing and pattern recognition. While early QML research primarily addressed classification and clustering, the scope has since expanded to encompass optimization, regression, and generative modeling. QML methodologies can be broadly categorized into four paradigms based on the nature of the data and computational substrate.

- **Classical-Classical (CC)**: Classical algorithms inspired by quantum principles

(e.g., quantum-inspired optimization) executed on classical hardware. Example: Quantum annealing-inspired neural networks.

- **Classical-Quantum (CQ)**: Quantum algorithms (e.g., QCNNs, quantum kernel methods) applied to classical data, often seeking computational advantages through quantum feature maps or variational circuits. Example: Quantum-enhanced image classification.

- **Quantum-Classical (QC)**: Classical learning models (e.g., SVMs, neural networks) processing quantum-state data, typically for quantum system characterization. Example: Quantum error correction pattern recognition.

- **Quantum-Quantum (QQ)**: Fully quantum algorithms operating on quantum data, enabling tasks like quantum state discrimination. Example: Quantum autoencoders for state compression.

Among these, the CQ and CC paradigms dominate current research due to their compatibility with near-term quantum hardware and hybrid architectures [102].

1.5.1 Quantum computing foundations

QML implementations leverage three fundamental quantum phenomena:

1.5.1.0.1 Qubit representation The quantum bit (qubit) generalizes classical bits through superposition [103]:

$$|\psi\rangle = \alpha|0\rangle + \beta|1\rangle \quad (\alpha, \beta \in \mathbb{C},\ |\alpha|^2 + |\beta|^2 = 1)$$

where $|0\rangle, |1\rangle$ form an orthonormal basis in Hilbert space $\mathcal{H}_2$.

1.5.1.0.2 Quantum gates State evolution in quantum computing is governed by unitary operators, denoted as U, which satisfy the condition ($UU^\dagger = I$). Key single-qubit gates include [103]:

- Pauli-X (σ_x): Bit-flip ($|0\rangle \leftrightarrow |1\rangle$)
- Hadamard (H): Creates superposition ($|0\rangle \rightarrow \frac{|0\rangle+|1\rangle}{\sqrt{2}}$)
- Rotation gates (R_x, R_y, R_z): Parameterized state manipulation

State evolution in quantum computing is governed by unitary operators, denoted as U, which satisfy the condition $UU^\dagger = I$, ensuring that quantum states remain normalized and probabilities are preserved [103]. Among the fundamental single-qubit gates, the Pauli-X gate (σ_x) performs a bit-flip operation, interchanging the states $|0\rangle$ and $|1\rangle$ [104].

$$Pauli - X(\sigma_x) : Bit - flip(|0\rangle \leftrightarrow |1\rangle)$$

The Hadamard gate (H) is essential for creating superposition, transforming the basis state $|0\rangle$ into

$$\frac{|0\rangle + |1\rangle}{\sqrt{2}}$$

thereby enabling quantum parallelism.

Additionally, rotation gates (R_x, R_y, R_z) allow for precise, parameterized manipulation of qubit states by rotating them around the x-, y-, or z-axes of the Bloch sphere, which is crucial for implementing quantum algorithms and quantum machine learning circuits [103, 104].

Multi-qubit gates enable entanglement and correlated operations, which are foundational for quantum circuit design and quantum computation [104]. The controlled-NOT (CNOT or CX) gate, for example, flips the state of a target qubit conditioned on the control qubit being in the state 1, thereby facilitating quantum entanglement between qubits. This operation is essential for constructing quantum circuits that exploit parallelism and non-classical correlations. Additionally, the SWAP gate exchanges the states of two qubits, mapping $\psi \otimes \phi$ to $\phi \otimes \psi$, which is valuable for redistributing quantum information and enabling efficient communication across different parts of a quantum register i.e. SWAP: Exchanges qubit states as shown below [104]:

$$(|\psi\rangle \otimes |\phi\rangle \rightarrow |\phi\rangle \otimes |\psi\rangle)$$

These multi-qubit gates are central to the implementation of quantum algorithms such as Shor's factorization and Grover's search, as well as quantum error correction protocols, underscoring their importance in both theoretical and practical quantum computing applications [104].

1.5.1.0.3 Quantum advantage The exponential state space of n-qubit systems ($\dim(\mathcal{H}) = 2^n$) enables parallel computation through superposition, while entanglement facilitates non-classical correlations. These properties underpin potential quantum advantages in QML tasks [103].

1.6 QCNNs

QCNNs represent an emerging direction in quantum machine learning, integrating quantum computing principles into convolutional architectures to address limitations and enhance performance in supervised learning tasks [105, 106]. Introduced by Cong et al. [107], QCNNs utilize quantum entanglement and hierarchical structures inspired by the multiscale entanglement renormalization ansatz (MERA) and quantum error correction (QEC), demonstrating effectiveness in classification tasks, noise resilience, and scalability.

Recent research highlights QCNNs' versatility and performance across diverse domains. In image classification, including remote sensing and autonomous vehicle perception, QCNNs and hybrid quantum-classical models have demonstrated strong results [108, 109, 110, 111, 112, 113, 114, 115, 116]. In physics, QCNNs have been successfully used for quantum phase recognition, high-energy physics data analysis, and detection of quantum critical points [117, 118, 119, 120, 121, 122, 123]. Their role in communications, IT, and foundational aspects of hybrid quantum-classical computing has also been explored [105, 124, 125, 59, 126]. These advances position QCNNs as adaptable and scalable tools for solving complex supervised learning problems, including biomedical signal analysis.

1.6.1 Basic QCNN architecture

This work adopts a modular QCNN architecture integrating three primary subsystems: data encoding, convolutional, and classifier, designed to maximize quantum computational advantages while maintaining flexibility for EMG data processing (Figure 1.2). The architecture follows principles from Cong et al. [107].

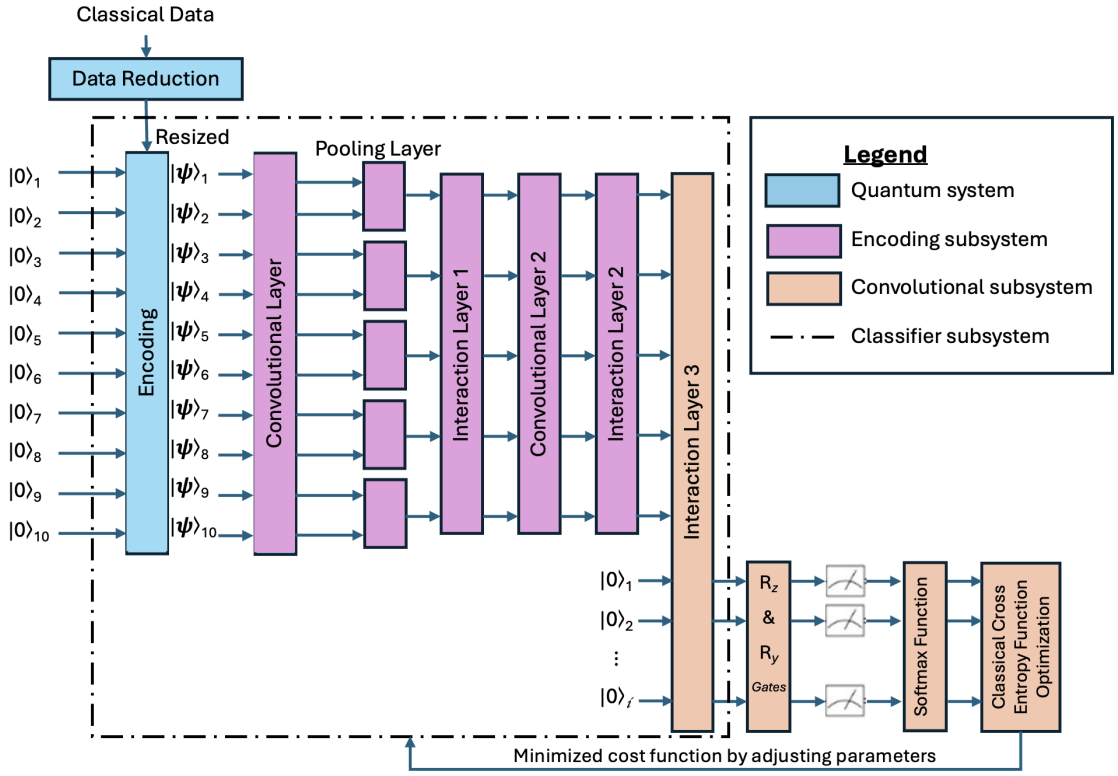

Figure 1.2: Basic QCNN Architecture.

1.6.1.1 Data encoding subsystem

Amplitude encoding is used to efficiently map classical EMG features into quantum states, leveraging quantum systems' exponential encoding capability to represent high-dimensional data within logarithmic qubit space. This encoding balances feature richness and limited qubit resources typical of near-term intermediate-scale quantum (NISQ) devices. Autoencoders perform initial dimensionality reduction and resizing prior to quantum encoding. Angle encoding, though robust against certain noise

types, was not chosen due to its one-qubit-per-feature requirement, which was limiting scalability.

This subsystem encodes classical data into quantum states employing: **Amplitude Encoding** involves encoding classical data points into the amplitudes of quantum states. This approach efficiently represents data because an exponential number of features can be encoded using a logarithmic number of qubits. This makes Amplitude Encoding particularly suitable for handling large datasets or high-dimensional feature spaces, effectively reducing the number of qubits required for computation. The primary advantage of amplitude encoding is its compact representation, allowing for the efficient utilization of limited quantum resources available on current quantum hardware. Data is dimensionally reduced using autoencoders and resized to suit quantum hardware capabilities.

1.6.1.2 Convolutional subsystem

Quantum convolutional layers apply local unitary operations to neighboring qubits using parameterized circuits (ansätze), incorporating rotation gates (Rx, Ry, Rz) and controlled gates. Pooling layers measure specific qubits and apply conditional unitaries, further reducing dimensionality. Toffoli-based interaction layers are explicitly integrated between convolutional blocks, introducing complex multi-qubit entanglement and significantly enhancing the network's expressibility and feature correlation learning. These interactions strengthen the QCNN's capacity to extract meaningful patterns from decomposed and dimensionally reduced EMG signals, improving classification performance [107]. QCNN architecture is depicted in Figure 1.3. The brief description of subsystems within the architecture is enumerated below and the same is given as in Table 1.1.

1.6.1.3 Classifier subsystem

Classification is executed via ancilla qubits entangled with processed qubits, enhanced by Toffoli-based interaction layers. Rotations (Rx, Ry, Rz) fine-tune the output, with measurement outcomes converted into classical probabilities using Pauli-Z

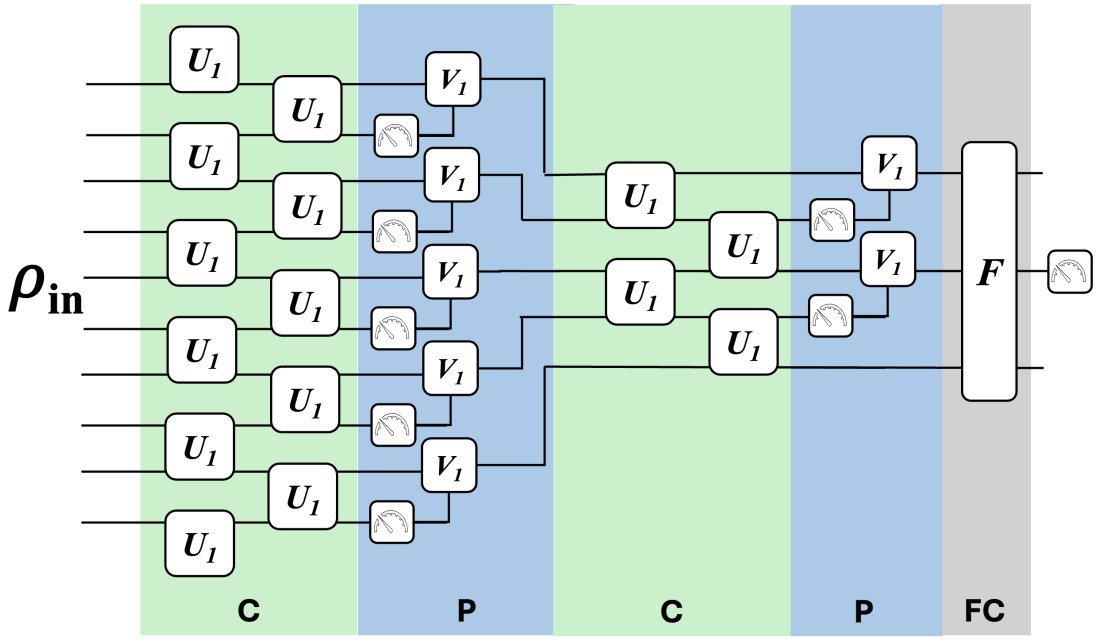

Figure 1.3: General architecture of QCNN with layered unitaries and measurements. A sequence of classical layers i.e.—convolution (C), pooling (P), and fully connected (FC) are depicted.

Table 1.1: Summary of QCNN subsystems

Subsystem	**Role**	**Key mechanism(s)**	**Output**
Classifier subsystem	Classification	Ancilla qubits, Toffoli-based interaction layers, Pauli-Z expectation, softmax	Classical probabilities
Quantum convolutional layer	Feature extraction	Local unitaries (U3, IsingXX/YY/ZZ), Parameterized ansätze, entanglement	Hierarchical quantum features
Quantum pooling layer	Dimensionality reduction	Measurement of qubits, conditional operations	Reduced quantum state subspace

expectations and softmax functions. This subsystem's expressibility and resilience to noise are enhanced by interaction layers.

1.6.1.4 Quantum convolutional layer

The Quantum Convolutional layer in QCNN applies local unitary operations on neighboring qubits to extract meaningful quantum features from encoded data. These layers use parameterized quantum circuits, known as ansätze, which include U3 gates capable of performing arbitrary single-qubit rotations. Additionally, the convolutional layers implement Ising-type gates (IsingXX, IsingYY, and IsingZZ), facilitating controlled entanglement between adjacent qubits. This entanglement is crucial as it allows the QCNN to learn complex correlations inherent in quantum data. The structure of quantum convolutional layer is given at Figure 1.4.

By applying these parameterized gates iteratively, quantum convolutional layers extract hierarchical quantum features similar to classical convolutional operations. The translational invariance and locality of these operations ensure consistency and efficient learning across different regions of the quantum input state. The primary advantage of this layer is its ability to systematically leverage quantum entanglement, significantly improving the expressibility and accuracy of the network.

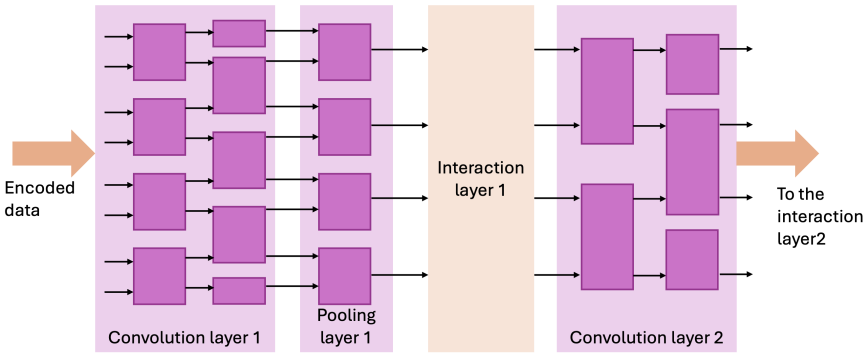

Figure 1.4: Structure of quantum convolutional layer.

1.6.1.5 Quantum pooling layer

Quantum pooling layers in QCNN perform dimensionality reduction on quantum states. Unlike classical pooling, quantum pooling involves measuring selected qubits and applying conditional operations based on the measurement outcomes. The measured qubits effectively collapse the state to a subspace containing the most relevant

quantum features, enhancing computational efficiency by discarding less significant quantum information [107].

This measurement-driven approach to pooling uniquely benefits quantum neural networks by inherently leveraging quantum mechanics' probabilistic nature. The conditional quantum operations applied after measurement further refine the quantum state, ensuring the preservation of essential information for subsequent processing layers. Quantum pooling thus maintains the delicate balance between information retention and dimensionality reduction, crucial for effective quantum learning.

1.6.1.6 Dense (Fully Connected) layer

The final classification task in QCNN is executed by the Dense or Fully Connected quantum layer, implemented using arbitrary unitary gates. This layer transforms the processed qubit states into outputs suitable for classification tasks by applying general, parameterized unitary transformations that allow maximal flexibility in manipulating quantum states [107].

By using an arbitrary unitary gate, the dense layer can adapt to various data patterns without restriction to specific predefined transformations. The flexibility offered by arbitrary unitaries enables the network to robustly handle different classification tasks with high accuracy. Measurement of the final qubit states after these transformations provides classical outputs used to calculate probabilities and predict class labels.

1.6.1.7 Optimization and training

Optimization employs classical methods—specifically Nesterov Momentum—to minimize mean squared error (MSE) [107]:

$$\text{MSE} = \frac{1}{2M}\sum_{\alpha=1}^{M}(y_\alpha - f_{\{U_i,V_j,F\}}(|\psi_\alpha\rangle))^2 \tag{1.10}$$

where $(|\psi_\alpha\rangle, y_\alpha)$ denote training pairs. Quantum differentiable programming enables the integration of quantum circuits into classical machine learning optimization work-

flows, allowing gradients of quantum operations to be computed and utilized for hybrid model training.

1.6.1.8 Performance evaluation and applications

QCNNs outperform classical and conventional quantum methods, as already demonstrated on datasets like MNIST, fashion MNIST, and Iris [127]. QCNNs are notably effective in quantum phase recognition tasks, such as identifying phases in the $\mathbb{Z}_2 \times \mathbb{Z}_2$ symmetry-protected topological (SPT) systems, described by Hamiltonians of the form:

$$H = -J \sum_{i=1}^{N-2} Z_i X_{i+1} Z_{i+2} - h_1 \sum_{i=1}^{N} X_i - h_2 \sum_{i=1}^{N-1} X_i X_{i+1} \tag{1.11}$$

QCNN applications have shown exponential sample complexity gains compared to traditional order parameters like string order parameters [107].

1.6.1.9 Quantum error correction and scalability

QCNN architectures integrate quantum error correction (QEC) mechanisms, optimizing encoding and decoding maps under noise channels:

$$F_q = \sum_{|\psi_l\rangle \in \{|\pm x\rangle, |\pm y\rangle, |\pm z\rangle\}} \langle \psi_l | M_q^{-1}(\mathcal{N}(M_q(|\psi_l\rangle\langle\psi_l|)))|\psi_l\rangle \tag{1.12}$$

as shown in [107]. This architecture ensures high-fidelity operation, vital for real-world deployment of quantum-assisted classification frameworks in biomedical and defense systems.

1.6.2 Theoretical outlook and applications

QCNNs inherently support generalization, robustness to noise, and scalability in NISQ environments [128]. Applications span quantum phase recognition, high-energy physics, and biomedical pattern recognition. Experimental validations in [107, 127] demonstrate QCNNs' superior performance and sample complexity efficiency.

The detailed exploration of QCNNs underscores their potential in addressing the inherent complexities of biomedical signal classification, particularly for non-stationary, high-dimensional EMG datasets. This introductory chapter so far has established the theoretical framework and technical foundation for the subsequent experimental work. Building on this, the following sections articulate the specific research objectives pursued in this thesis, followed by a comprehensive summary of the contributions made and the structural layout of the thesis. These upcoming sections connect the foundational principles of QCNNs and related signal processing techniques to their practical applications in neuromuscular disorder detection, eye-movement decoding, and HAR, thereby setting the stage for the experimental chapters that follow.

1.7 Objectives

In this thesis, the following research objectives have been pursued to develop quantum-enhanced frameworks for biomedical signal analysis and human-machine interaction:

Objective 1: To design a data efficient QCNN architecture that leverages quantum principles such as entanglement and superposition for robust pattern recognition in EMG signals.

Objective 2: To develop a theoretical understanding of how trainable quantum gates and the amount of training data affect generalization in QML.

Objective 3: To develop QCNN based diagnostic models for neuromuscular disorders, specifically for the detection of ALS using intramuscular EMG signals, using Auto-SSA-based decomposition techniques with PSO.

Objective 4: To design a QML assisted framework for decoding eye movements from extraocular EMG signals using SMSSA and NCA.

Objective 5: To benchmark the proposed QCNN frameworks, developed using multichannel EMG signals and MSSA decomposition and MRMR feature extraction, against state-of-the-art classical models in terms of classification accuracy, generaliza-

tion, and computational efficiency, and to validate their cross-domain applicability in biomedical diagnostics, human computer interface, and defense systems.

1.8 Contributions

Contribution I: To develop a QCNN-based framework for ALS detection from EMG signals

This contribution presents a quantum-enhanced automated classification system for detecting amyotrophic lateral sclerosis (ALS), a progressive neuromuscular disorder, using intramuscular EMG signals. The framework integrates automated signal decomposition via Auto-SSA for adaptive handling of nonstationary EMG signals and employs PSO for optimal feature selection. Extracted features are used to train a hyperparameter-tuned QCNN, which achieves a classification accuracy of 98.50% on benchmark EMG datasets, outperforming conventional CNN and handcrafted feature-based methods reported in literature [129, 130]. A systematic analysis of training size versus accuracy and loss demonstrates strong generalization and minimal overfitting, particularly at $N = 200$ training size, as validated on the EMG dataset from [131]. Unlike traditional classifiers, the QCNN architecture processes the extracted features through a low-parameter quantum variational circuit, demonstrating robustness and generalization capability even with small and imbalanced datasets, a common bottleneck in early detection of neuromuscular disorders. The use of Auto-SSA enables real-time, adaptive decomposition, making the framework suitable for diagnostic tools in telemedicine, with potential impact in remote and resource-constrained settings. This contribution addresses the objective of developing a robust quantum-assisted framework for neuromuscular disorder classification using intramuscular EMG signals.

Contribution II: Eye-movement decoding from extraocular EMG using SMSSA and QCNN

This contribution presents a novel framework for decoding eye movement patterns from extraocular EMG signals, combining SMSSA with a QCNN. The SMSSA technique decomposes noisy, nonstationary signals into reconstructed components (RCs),

enhancing robustness against temporal irregularities. Features including entropy, complexity, and frequency-domain descriptors are extracted and reduced to a 64-dimensional set using NCA. These features are classified by a hyperparameter-tuned 6-qubit QCNN model, achieving an accuracy of 98.70%, outperforming traditional classifiers like SVM and neural networks (see Table 3.1 and Table 3.3). The QCNN's low training data requirement and adaptive learning capability enable operator-specific configurations, making it viable for sensitive environments such as neuroadaptive cockpits or combat gear interfaces. The framework is designed for real-time assistive devices, including eye-controlled prosthetics and mobility aids, and extends to defense applications such as UAVs and hypersonic aircraft with eye-gaze-controlled interfaces. By demonstrating quantum feature space encoding for biomedical signals, this work introduces a paradigm for precision eye-controlled technologies bridging assistive tools and defense-oriented human-computer interaction (HCI) systems.

Contribution III: To develop HAR from multi-channel sEMG using MSSA and optimized QCNN

This contribution presents a robust HAR framework for classifying twenty distinct human activities using multichannel surface EMG (sEMG) signals. A novel signal decomposition approach based on MSSA decomposes signals across all channels while preserving spatial synchrony and mitigating noise. Multi-domain features are extracted from the decomposed signals, and MRMR is employed to select a 64-dimensional subset of the most informative features. These features are classified using a custom-designed QCNN architecture, achieving a peak classification accuracy of 98.81% across twenty activity classes, demonstrating superior performance and robustness compared to existing methods [132]. Evaluation metrics in Table 3.1 and visual results in Fig. 3.5 illustrate consistent improvements across varying training sizes. This framework extends the applicability of quantum machine learning to complex multi-class problems and is validated on real-world biomedical datasets. It is suitable for wearable sensor platforms used in rehabilitation, physical therapy, and activity monitoring, and can also be deployed in military and security settings such as exoskeleton suits or autonomous humanoids for task replication, load-bearing sup-

port, or mission-specific training. The system is adaptable to new users with minimal retraining, enabling deployment in demanding environments with frequently changing operators, such as in defense scenarios. This contribution highlights the potential of combining adaptive multivariate decomposition with quantum-enhanced learning for advanced prosthetics and human-computer interaction systems.

Overall impact: The collective contributions of this thesis establish a comprehensive framework for EMG signal analysis, integrating adaptive decomposition, dimensionality reduction, and quantum-based classification. These innovations demonstrate the feasibility and effectiveness of quantum machine learning for robust biomedical and physiological signal classification, validated across multiple datasets and use cases. The proposed frameworks are immediately applicable in both biomedical and defense domains, enabling real-time decision-making, advanced operator augmentation through eye-controlled systems, adaptive exoskeletons, and next-generation prosthetics for rehabilitation and combat support. With low data requirements, strong generalization, and adaptability to environmental variability, these systems are ideally suited for dynamic military operations, remote diagnostics, and adaptable rehabilitation programs. By bridging advanced signal processing with quantum computing, this work lays a strong foundation for the future integration of quantum models into edge devices and smart assistive systems. This paves the way for transformative advances in human-computer interaction, real-time diagnostics, and human performance augmentation in complex operational environments.

1.9 Organization of the thesis

This thesis is organized into seven chapters. The title and short summary of the chapters are structured as follows:

Chapter 1 (Introduction)

This chapter describes the background of EMG, the motivation, and the contribution of this thesis.

Chapter 2 (QCNN-based Framework for ALS detection from EMG Sig-

nals)

This chapter proposes a framework for detecting ALS using EMG based new QML classifier. The introduced method shows the efficacy of the new classifier over classical convolutional neural networks.

Chapter 3 (Eye-movement decoding from extraocular EMG using SM-SSA and QCNN)

This chapter has proposed a framework based on SMSSA and QML for the detection and classification of eye movements using EMG of EOM signals.

Chapter 4 (HAR from multi-channel sEMG using MSSA and optimized QCNN)

In this chapter, we presented a novel QCNN-based framework to classify HAR. The introduced framework are used to for automatic classification of HAR, both aggressive and normal.

Chapter 5 (Conclusions and future scope)

This chapter provides a summary and findings of the thesis. This chapter also listed the information of future work.

Chapter 2

QCNN-based Framework for ALS Detection from EMG Signals

In this chapter, we present a novel framework for the automatic detection of Lou Gehrig's disease medically known as ALS using EMG signals. The proposed approach integrates automatic singular spectrum analysis (Auto-SSA) for signal decomposition and QCNNs for classification. Additionally, PSO is employed for feature selection to identify the most discriminative components. The chapter discusses the advantages of the Auto-SSA method over traditional decomposition techniques and the effectiveness of QCNN in handling biomedical signal features. A comprehensive evaluation of the classification performance validates the superiority of the proposed method in comparison to state-of-the-art ALS detection models. The following sections elaborate on the methodology, implementation, and performance analysis of the framework.

2.1 Introduction

ALS is a fatal neurological condition characterized by progressive motor neuron degeneration in the brain and spinal cord, resulting in muscle weakness, twitching, and finally leading to dyspnea [133]. It mainly impacts people aged from 40 to 70 years, with a notable occurrence in those 80 years old or above (10.2 per 100,000 in men; 6.1 per 100,000 in women), emphasizing the need for early diagnosis of ALS [133]. EMG signals are essential for detecting motor neuron dysfunction in ALS, where

sensors capture abnormal electrical activities like fasciculations and fibrillation, which indicate muscle denervation. Depending on the sensor placement, EMG signals are classified into surface EMG and intramuscular EMG. These signals can be complex and noisy, often corrupted by muscle activity and external interference [134, 135]. In order to extract relevant information from EMG signals, advanced signal processing techniques are required [13].

Doulah et al. confirmed that EMG signals can be used to detect ALS by extracting mel-frequency cepstral coefficients from signals and classfying them using the K-nearest neighbourhood algorithm [136]. Sengur et al. designed a transfer learning-based framework for ALS detection in which the spectrogram of EMG signals were used for training a pretrained convolutinal neural network (CNN) [129]. Hassan et al. proposed a dilated one dimensional CNN named ALSNet to detect ALS from raw EMG signals [130]. Sengur et al. proposed a framework for ALS detection from EMG signals using a spectrogram obtained from short-time Fourier transform and CNN [137]. Mokdad et al. developed a framework based on continuous wavelet transform and machine learning techniques for ALS detection from EMG signals [138]. Chatterjee et al. developed a framework for ALS and myopathy classification of time-frequency domain features extracted from the Stockwell transform of EMG signals using machine learning classifiers [139]. Mishra et al. used empirical mode decomposition to extract time-frequency domain features from EMG signals and machine learning techniques to classify these features for ALS detection [140].

Hou et al. investigated the effectiveness of singular spectrum analysis (SSA) in processing EMG signals to remove electrocardiogram interference [141]. Their findings demonstrate the efficacy of the SSA in EMG signal analysis. However, numerous component grouping methods were proposed separately for SSA to reconstruct sinusoids, trends, and noise, each requiring manual adaptation based on the specific signal [23]. In contrast, the automatic SSA (Auto-SSA), employs an agglomerative hierarchical clustering-based component grouping method that provides physically interpretable components, regardless of the component type [23]. Recently, De et al. developed a framework for driver drowsiness detection based on quantum machine learning from

EMG, electroencephalogram, and pulse rate signals [142]. Caro et al. have proven through their studies that the quantum CNN (QCNN) trained on very few training data can provide good performance [59]. These aforementioned studies motivated us to propose Auto-SSA and quantum machine learning methods-based ALS detection framework from EMG signals.

This chapter introduces a new automated ALS detection framework based on Auto-SSA and QCNN from EMG signals. The EMG signals are decomposed into reconstructed components (RCs) using Auto-SSA. The features are extracted from RCs using PSO to explore unique characteristics of ALS in EMG signals. The QCNN is developed and trained to classify the extracted features into the ALS class and healthy class. The proposed framework is found outperforming the state-of-the-art methods from the literature.

The manuscript is structured as follows: Section 2.2 details the proposed hybrid method, including dataset specifications, problem definition, and algorithm; Section 2.3 discusses the results comprehensively; and Section 2.4 concludes the manuscript with insights into potential future work.

2.2 Methodology

The proposed methodology uses Auto-SSA, PSO, and QCNN for ALS detection from EMG signals. In this framework, the EMG signals are decomposed using Auto-SSA into 12 RCs. The RCs provide more informative, noise-reduced representations than the raw EMG signals. PSO is used to extract a total of 64 features from the obtained RCs. The QCNN is used to classify the extracted features into ALS and healthy classes. The block diagram of the aforementioned framework is presented in Figure 2.1.

2.2.1 Dataset

The dataset of EMG signals used in this study is a benchmark for ALS detection [131]. The EMG signals were recorded using a special Teflon-insulated monopo-

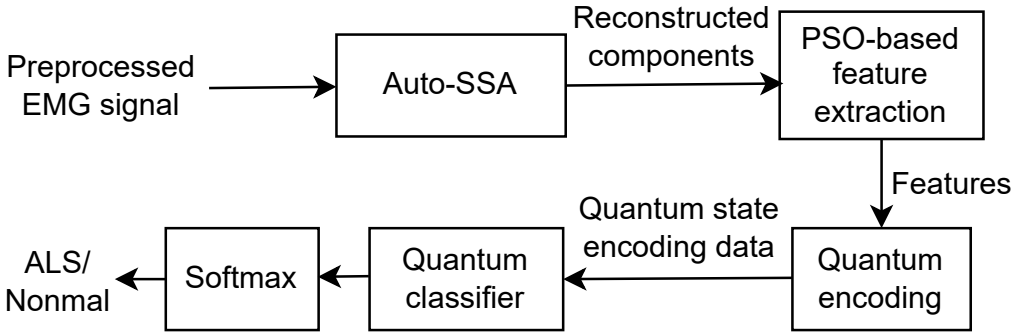

Figure 2.1: Block diagram of the proposed framework for ALS detection using EMG signal.

lar needle electrode or sensors, at a sampling rate of 23.435 kHz. These sensors are characterized by their high signal quality and low impedance, providing clear and precise electromyographic recordings due to the effective Teflon insulation that minimizes noise interference. They are durable and flexible, making them suitable for reliable intramuscular measurements in various biomedical applications. The signals were recorded at different insertion levels of sensors (deep, medium, and low), from the biceps brachii and medial vastus muscles. The EMG signals were band-pass filtered in the frequency range 2 Hz to 10 kHz. There are 955 EMG signals corresponding to both healthy (control group) and pathological (ALS and myopathy) classes. Table 2.1 presents the detailed dataset information. The 10000 sample length EMG signal from sample numbers 601 to 10600 corresponding to the healthy class (record number N2001C01BB51) and an ALS class (record number N2001A01VM01) are shown in Fig. 2.2. The dataset is divided into two parts for simulation purposes: 80% for training and 20% for testing.

In this chapter, Section 2.3 focuses on ALS–Control classification, while Section 2.5 reports additional analyses including Myopathy and multiclass experiments using the same dataset.

Table 2.1: Dataset information.

Group	Males	Females	Age group	Number of signals
Healthy/control	6	5	21-37	325
ALS	4	4	19-67	305
Myopathy	2	5	19-63	325

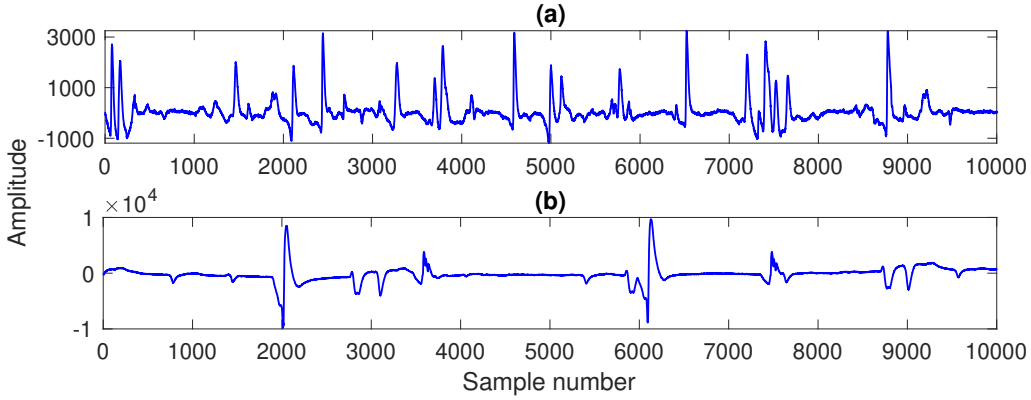

Figure 2.2: EMG signals of (a) the normal and (b) the ALS subjects.

2.2.2 Proposed framework

The proposed framework for ALS detection using EMG signal is explained in the following subsubsection:

2.2.2.1 Auto-SSA

The Auto-SSA decomposes the EMG signal $\varphi[n]$ for $n = 0, 1, \ldots, L$ into a set of K RCs using the following steps:

Step 1. Obtain a Hankel matrix $\mathbb{P}$ of the signal $\varphi[n]$, which is expressed as follows [23, 143]:

$$\mathbb{P} = \begin{bmatrix} \varphi[1] & \varphi[2] & \ldots & \varphi[C] \\ \varphi[2] & \varphi[3] & \ldots & \varphi[C+1] \\ \vdots & \vdots & \ddots & \vdots \\ \varphi[E] & \varphi[E+1] & \ldots & \varphi[L] \end{bmatrix} \tag{2.1}$$

where E is the embedding dimension, and $C = L - E + 1$.

Step 2. The singular value decomposition of matrix $\mathbb{P}$ with R rank ($R = \min(E, C)$)

is expressed as [23, 143],

$$\mathbb{P} = U\Sigma V^T = \sum_{i=1}^{R} \mathbb{P}_i \quad \text{with } \mathbb{P}_i = \sigma_i u_i v_i^T \tag{2.2}$$

where $U = (u_1, u_2, \ldots, u_R)$, $V = (v_1, v_2, \ldots, v_R)$, $\Sigma = \text{diag}(\sigma_1, \sigma_2, \ldots, \sigma_R)$, and u_i, v_i, and σ_i are i^{th} left singular vector, right singular vector, and singular value, respectively.

Step 3. The diagonal averaging of i^{th} trajectory matrix $\mathbb{P}_i$ is performed to obtain the i^{th} elementary component $\varphi_i[n]$. This is mathematically expressed as [143, 23],

$$\varphi_i[n] = \begin{cases} \frac{1}{n}\sum_{m=1}^{n} \mathbb{P}_i(m, n-m+1), & \text{for } 1 \leq n < E \\ \frac{1}{E}\sum_{m=1}^{E} \mathbb{P}_i(m, n-m+1), & \text{for } E \leq n < C \\ \frac{1}{L-n+1}\sum_{m=1}^{n-C+1} \mathbb{P}_i(m, n-m+1), & \text{for } C+1 \leq n < L \end{cases} \tag{2.3}$$

where $\mathbb{P}_i(m, n)$ is the m^{th} row and n^{th} column indexed element $\mathbb{P}_i$.

Step 4. The obtained elementary components are grouped into a set of K RCs using hierarchical agglomerative clustering (HAC) [23, 143]. Finally, the signal $\varphi[n]$ is approximately represented in terms of RCs as,

$$\varphi[n] = \sum_{i=1}^{K} \varphi_i[n] \tag{2.4}$$

For simulation, the values of parameters E and K are considered as 40 and 12, respectively. Further, the length of the EMG signals is considered as $L = 10000$ samples.

2.2.2.2 PSO

PSO is employed in the proposed framework to extract the most significant features from the RCs obtained via Auto-SSA. PSO was chosen because the feature selection problem in EMG analysis involves optimization in a high-dimensional continuous feature space [144]. Compared with genetic algorithms, PSO has fewer control parameters, simpler implementation, and faster convergence while maintaining com-

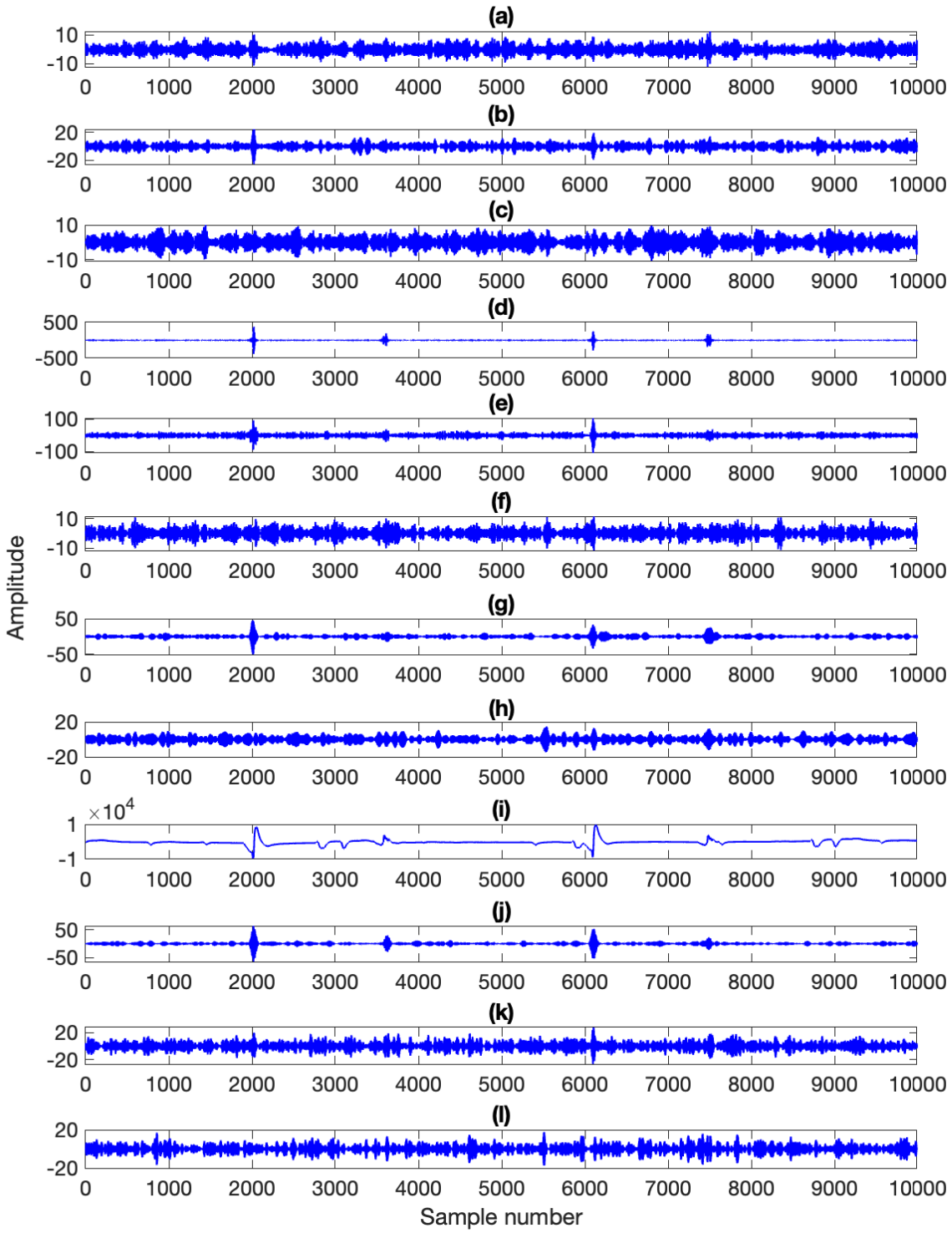

Figure 2.3: Plots in (a)–(l) are the reconstructed components of the EMG signal corresponding to ALS subject (shown in Fig. 2(b)) obtained using Auto-SSA.

petitive global search capability [145]. This also makes it computationally efficient for wrapper-based feature selection in biomedical signal classification problems [145]. In

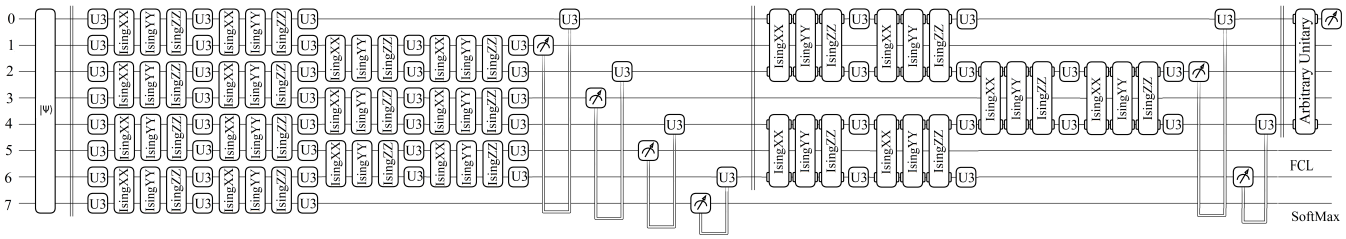

Figure 2.4: Proposed block diagram of 8-qubit QCNN classifier.

this study, a population size of 20 and a maximum of 10 iterations are empirically chosen to balance computational efficiency and feature relevance [146].

For feature selection, PSO initializes a population of particles, where each particle represents a binary feature subset. The algorithm iteratively adjusts particle velocities and positions based on both individual and global best solutions. At every iteration, the fitness of each feature subset is evaluated using a predefined fitness function—the mean of the input data—optimizing the selection process towards subsets with improved classification potential.

Mathematically, given 12 reconstructed components as input, PSO extracts 64 most significant features, which are subsequently used to train the QCNN classifier for ALS detection.

The Auto-SSA technique used to generate these RCs operates as follows: a trajectory matrix $\mathbb{P}$ is constructed from the signal $\varphi(n)$ of length N with embedding dimension Len, resulting in $C = N - \text{Len} + 1$ shifted frames:

$$\mathbb{P} = \begin{bmatrix} \varphi(1) & \varphi(2) & \dots & \varphi(C) \\ \varphi(2) & \varphi(3) & \dots & \varphi(C+1) \\ \vdots & \vdots & \vdots & \vdots \\ \varphi(\text{Len}) & \varphi(\text{Len}+1) & \dots & \varphi(N) \end{bmatrix}$$

Singular value decomposition (SVD) is applied:

$$\mathbb{P} = UXV^T = \sum_{i=1}^{Rk} \mathbb{P}_i, \quad \text{where } \mathbb{P}_i = \sigma_i u_i v_i^T$$

Diagonal averaging (Hankelization) is then applied to each $\mathbb{P}_i$ to derive component

matrices:

$$x_i(n) = \begin{cases} \frac{1}{n}\sum_{l_o=1}^{n} s(l_o, n-l_o+1), & \text{for } 1 \le n < \text{Len} \\ \frac{1}{\text{Len}}\sum_{l_o=1}^{\text{Len}} s(l_o, n-l_o+1), & \text{for Len} \le n < C \\ \frac{1}{N-n+1}\sum_{l_o=1}^{n-C+1} s(l_o, n-l_o+1), & \text{for } C+1 \le n < N \end{cases}$$

Hierarchical agglomerative clustering is used to group these components into r clusters. For this study, Len = 12 and $M = 40$ are used, which yield informative RCs used by PSO for feature extraction.

The optimal 64 features obtained through PSO are then reshaped into an 8×8 matrix and encoded into quantum states for classification via QCNN (see Fig. 2.4). This pipeline ensures that the final ALS detection framework leverages both signal decomposition and optimal feature representation.

2.2.2.3 QCNN for classification

QCNNs, introduced by Cong et al. [147], are quantum analogs of classical CNNs designed to exploit hierarchical patterns in data using quantum circuits. In the present framework, QCNN is used to classify ALS and healthy samples based on the 64 most significant features extracted using PSO.

Each feature vector x is encoded into a quantum state $\rho(x)$ using a quantum feature map, and subsequently processed by the QCNN circuit $\mathcal{E}_\alpha(\cdot)$, where $\alpha = (\theta, k)$ represents the trainable parameters of the model. Here, θ denotes the continuous parameters inside quantum gates, and k denotes the discrete gate structure [59].

Given a training dataset $\{x_i, y_i\}_{i=1}^{N}$, the empirical loss over the training set is defined as:

$$R(\alpha) = \frac{1}{N}\sum_{i=1}^{N} \mathcal{L}(\alpha; x_i, y_i) \tag{2.5}$$

where $\mathcal{L}(\cdot)$ is the task-specific loss function, and N is the training set size [59].

In the proposed framework, the 64 selected features are reshaped into an 8×8 matrix and encoded as quantum states to match the 8 qubit topology i.e. with each row mapped to one qubit line. These are then input to an 8-qubit QCNN classifier

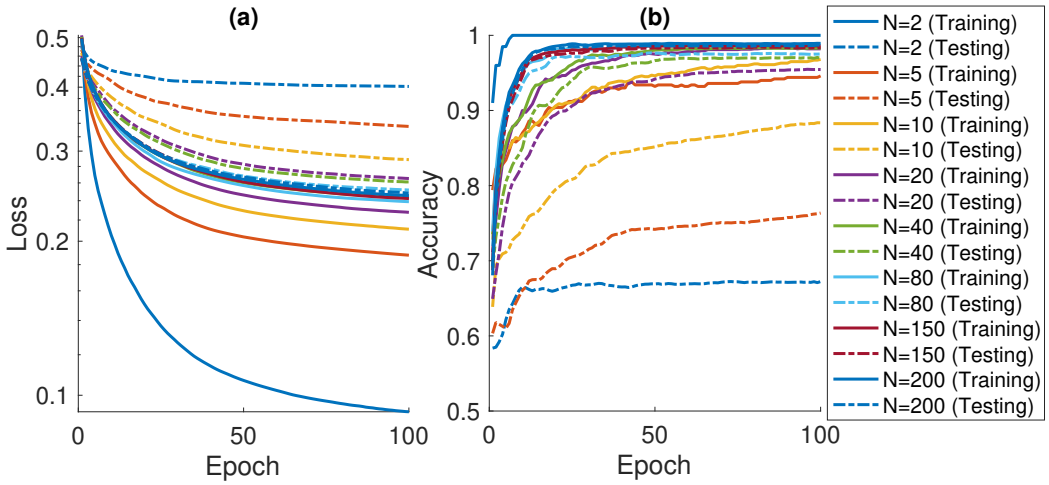

Figure 2.5: Plots of the loss versus epoch in (a) and accuracy versus epoch in (b) of the proposed ALS detection framework for various training set sizes.

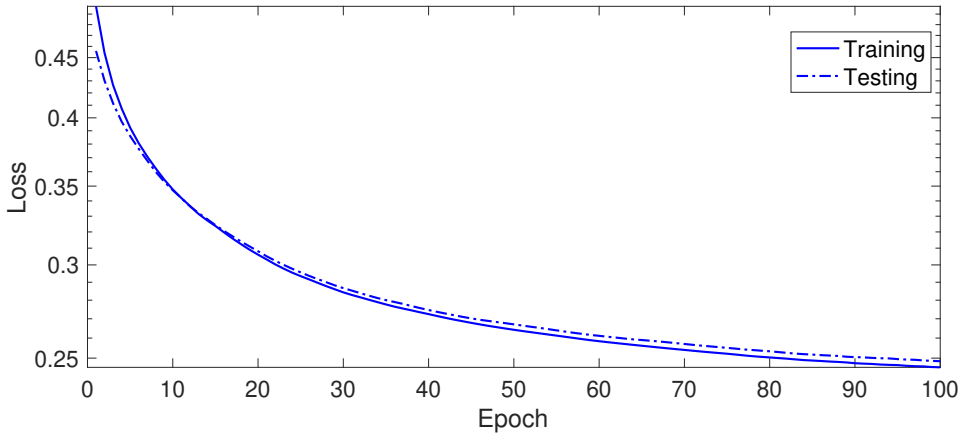

Figure 2.6: Training and testing loss versus epoch plot of the proposed ALS detection framework for the value of training set size $N = 200$.

whose structure is illustrated in Fig. 2.4. The QCNN comprises parameterized single-qubit U3 gates for arbitrary rotations and entangling gates such as IsingXX, IsingYY, and IsingZZ, which enable correlations between qubit pairs by applying controlled rotations about corresponding axes.

The use of QCNN allows for the extraction of quantum hierarchical representations from the input data, potentially offering better generalization performance, especially when the number of training samples is limited.

2.3 Results and discussion

The performance of the proposed ALS detection framework was evaluated across varying training set sizes $N = \{2, 5, 10, 20, 40, 80, 150, 200\}$, using 80% of the EMG dataset for training and the remaining 20% for testing. Table 2.2 presents the loss and accuracy metrics for each training size. The results indicate a clear trend: as the training set size increases, the disparity between training and testing performance reduces, reflecting improved generalization of the model.

Figures 2.5(a) and 2.5(b) illustrate the epoch-wise progression of loss and accuracy for different training sizes. For smaller training sizes ($N = 2$ to 20), the model demonstrates signs of overfitting—training accuracy remains high while testing accuracy lags significantly. For instance, with $N = 2$, the training accuracy is 100% while the test accuracy drops to 72.92%, revealing poor generalization.

At higher training sizes, especially $N = 200$, the training and testing performance converge. As depicted in Figures 2.6 and 2.8, the overlap of training and testing loss and accuracy curves confirms that the model generalizes well without overfitting. Additionally, Figure 2.9 highlights the reduction in the generalization gap with increasing N, plateauing around $N = 150$, where test accuracy reaches 98.75%.

2.3.1 Performance of classical CNN on extracted features

To assess the baseline performance of conventional deep learning models, a classical Convolutional Neural Network (CNN) was trained using the same 64 prominent features extracted via PSO. The full dataset, consisting of 630 EMG signal instances, was used for training and evaluation.

Figure 2.10 illustrates the resulting classification performance of the classical CNN. Despite tuning and employing standard convolutional layers, the network achieved a peak testing accuracy of only 65%. This outcome underscores the limitations of classical CNN architectures in capturing complex nonlinear relationships present in EMG signals for ALS detection, especially in a low-sample regime.

These findings reinforce the merit of the proposed quantum CNN (QCNN)-based

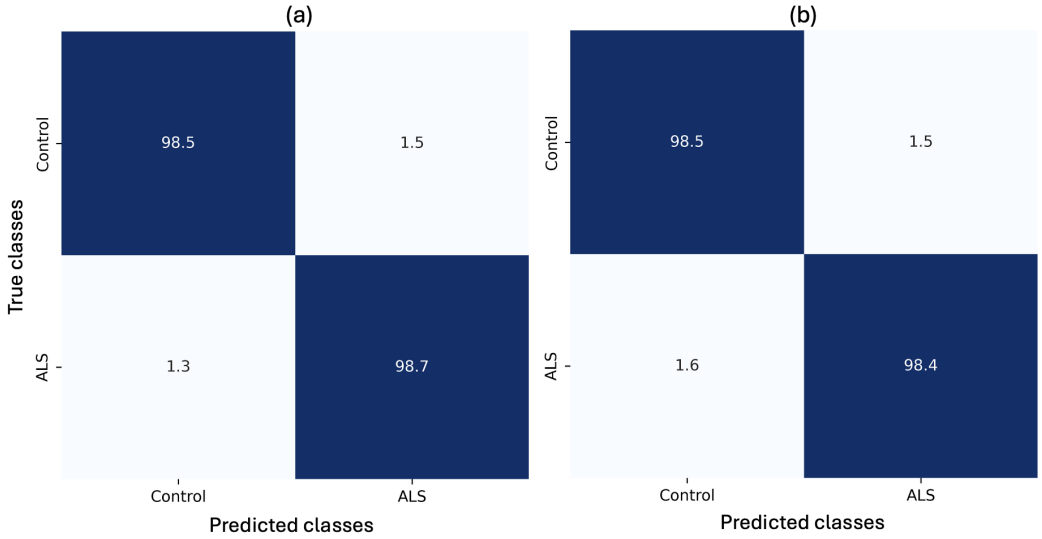

Figure 2.7: Confusion matrix for $N = 200$

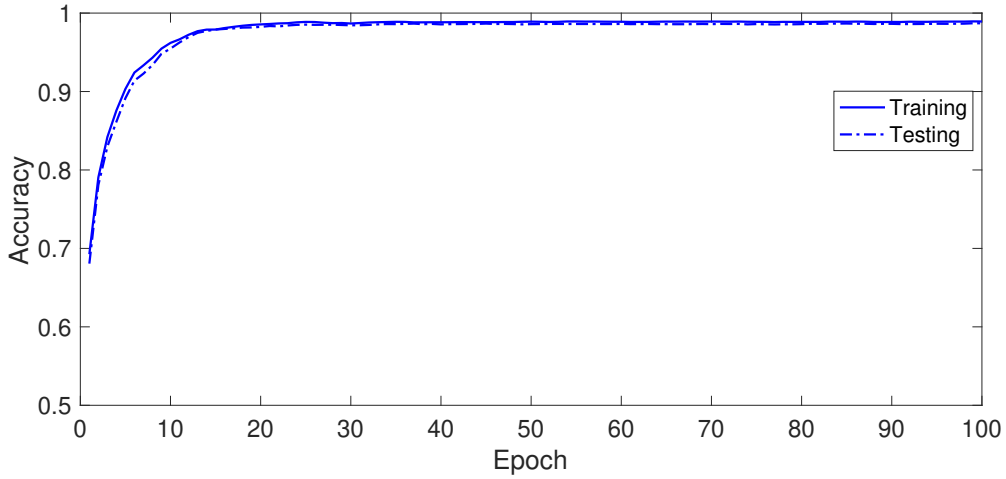

Figure 2.8: Training and testing accuracy versus epoch plot of the proposed ALS detection framework for the value of training set size $N = 200$.

framework, which demonstrated significantly higher classification accuracy (up to 98.50%), thereby justifying the use of quantum computing paradigms for nuanced biomedical signal interpretation.

The best testing accuracy of 98.50% is achieved at $N = 200$, with training accuracy closely following at 98.61%, and corresponding losses of 0.2425 (training) and 0.2458 (testing). The confustion matrix is shown in Figure 2.7 and the additional performance metrics are given in Table 2.3.The low loss values and high classification accuracy across larger training sets substantiate the robustness of the QCNN classifier.

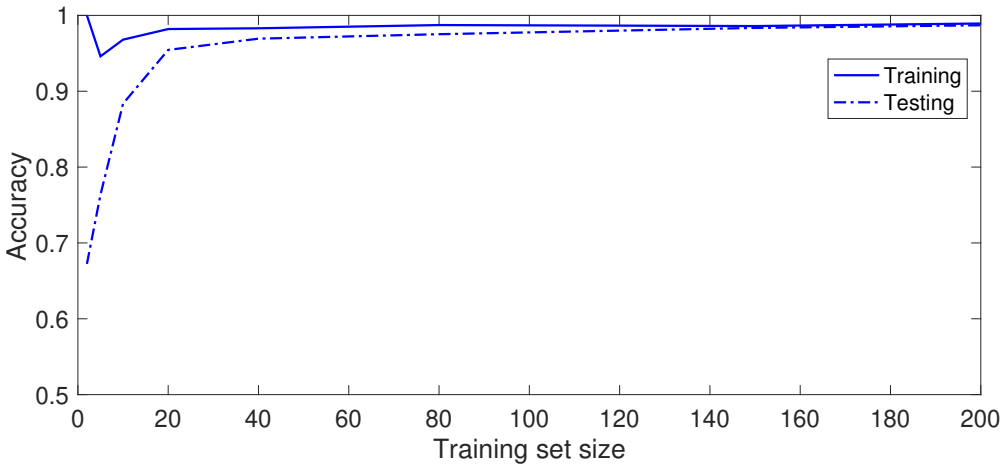

Figure 2.9: Accuracy (training and testing) versus training set size plot for the proposed framework.

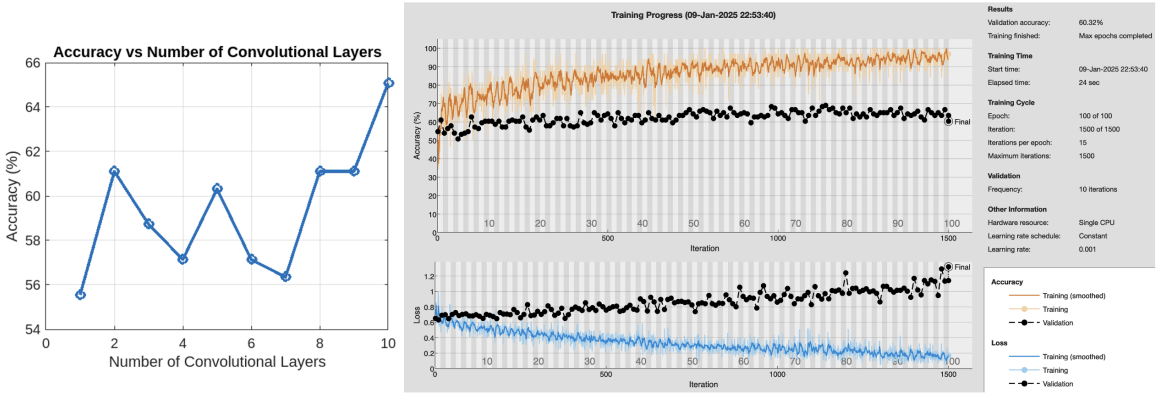

Figure 2.10: Performance of classical CNN on the ALS dataset using 64 prominent features post PSO. The maximum classification accuracy achieved was 65%.

Table 2.2: Performance metrics (accuracy and loss) of the proposed framework for various training set sizes.

Training set size	Loss		Accuracy (in %)	
	Training	Testing	Training	Testing
2	0.1093	0.3773	100	72.92
5	0.1834	0.3134	97	83.91
10	0.2064	0.2910	96.50	87.33
20	0.2244	0.2693	97.40	93.10
40	0.2401	0.2561	98.30	97.43
80	0.2418	0.2518	98.84	98.25
150	0.2445	0.2473	98.87	98.75
200	0.2425	0.2458	98.61	98.50

Table 2.3: Performance metrics of the proposed framework for ALS-Control classification.

	Training	Testing
Loss	0.2424	0.2458
Accuracy	0.9861	0.9850
Precision		0.9877
Recall		0.9846
Specificity		0.9861
F1-score		0.9877

Table 2.4: Performance comparison of the proposed framework with other existing methods from the literature.

Authors	**Methodology**	**Dataset**	**Accuracy (%)**
Doulah et al. [136]	MFCC, KNN	ALS + Control [131]	92.50
Aicha et al. [138]	CWT, SVM	ALS + Control [131]	95.80
Sengur et al. [137]	TFR, EMD, CNN	ALS + Control [131]	96.80
Sengur et al. [129]	Spectrogram, CNN	ALS + Control [131]	97.70
Hassan et al. [130]	ALSNet	ALS + Control [131]	97.74
Proposed Method	Auto-SSA, PSO, QCNN	ALS + Control [131]	**98.50**

Table 2.4 compares the performance of the proposed framework with existing state-of-the-art methods using the same dataset [131]. The proposed Auto-SSA + PSO + QCNN pipeline surpasses all prior works, including ALSNet [130], which reported the highest previously known accuracy of 97.74%. This 0.76% gain is especially significant given that the QCNN operates effectively even with relatively compact training data due to quantum state encoding.

The proposed framework not only achieves superior classification performance but also demonstrates scalability with respect to dataset size and robustness in generalization. This indicates the viability of quantum machine learning approaches for biomedical signal analysis.

Despite current limitations in deploying QCNNs due to hardware constraints, the trajectory of quantum computing advancements suggests imminent feasibility. Future integration of such models with edge-based diagnostic tools could facilitate rapid, remote ALS detection in the field or telemedicine settings, particularly where access

to neuromuscular specialists is limited.

2.4 Summary

This chapter presented an Auto-SSA and QCNN-based framework for the detection of amyotrophic lateral sclerosis (ALS) using surface electromyography (EMG) signals. The EMG data were decomposed into reconstructed components (RCs) using Auto-SSA, significant features were selected through particle swarm optimization (PSO), and the resulting feature vectors were classified using a quantum convolutional neural network (QCNN). The model achieved a maximum testing accuracy of 98.50% with a training set size of 200, outperforming several existing ALS detection approaches in the literature. Subject to prospective clinical validation, this framework offers promise for tele-neurological screening and remote diagnosis. Furthermore, the demonstrated performance suggests strong potential for extending the framework to the broader differential diagnosis of neuromuscular disorders, including the classification of ALS, myopathy, and normal EMG patterns.

2.5 Additional studies

Amyotrophic lateral sclerosis (ALS) and myopathies are major neuromuscular disorders characterized by progressive weakness and muscle wasting. Although their underlying pathophysiology differs—ALS arises from motor neuron degeneration, whereas myopathies originate from primary muscle fiber pathology—both conditions manifest with overlapping clinical features such as impaired gait, reduced limb strength, and functional decline in motor tasks [148]. These similarities make their early differentiation clinically challenging.

Electromyography (EMG) remains central to the diagnostic workflow for distinguishing neurogenic from myogenic patterns. Myopathy typically produces short-duration, low-amplitude, polyphasic motor unit potentials (MUPs) with early recruitment, while ALS is characterized by fibrillation potentials, positive sharp waves, fas-

Table 2.5: Performance metrics of the proposed framework for Myopathy–Control classification.

	Training	Testing
Loss	0.2421	0.2454
Accuracy	0.9886	0.9866
Precision		0.9807
Recall		0.9877
Specificity		0.9892
F1-score		0.9907

ciculations, and long-duration, high-amplitude MUPs reflecting chronic denervation and reinnervation [149]. These electrophysiological signatures guide diagnosis and influence biopsy or genetic testing strategies [148].

To evaluate the generalizability of the proposed framework beyond ALS vs Control (initial study), three additional classification paradigms were explored:

1. Myopathy vs Control

2. ALS vs Myopathy

3. ALS vs Myopathy vs Control (multiclass)

These additional experiments assess whether the model can adapt to clinically relevant combinations and maintain diagnostic discriminability across different neuromuscular conditions.

2.5.1 Myopathy vs Control

Objective: Evaluate the capability of the classifier to distinguish myopathic EMG activity from that of healthy individuals.

Rationale: Healthy EMG patterns provide a physiological baseline, while myopathic signals exhibit reduced amplitude, shortened duration, and rapid recruitment. These differences constitute a clear signal subspace that an automated classifier should identify.

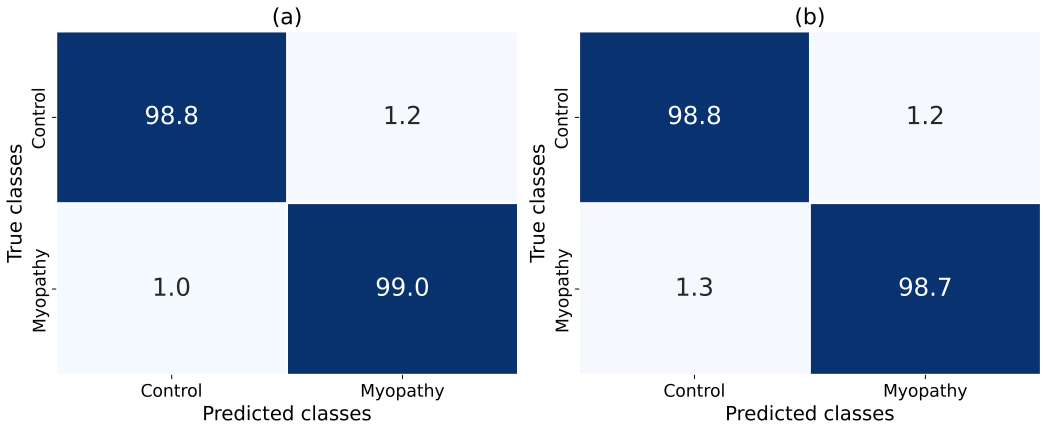

Figure 2.11: Confusion matrix: Myopathy vs Control.

Methods: EMG data from myopathy patients and healthy controls underwent identical preprocessing, AutoSSA decomposition, feature extraction, and QCNN classification. Stratified sampling ensured balanced representation in training and testing splits. The methodological pipeline is shown in Figure 2.1.

Evaluation metrics: Accuracy, sensitivity, specificity, precision, F1-score, and ROC–AUC were computed.

Results and interpretation: As shown in Table 2.5, the classifier performs strongly in distinguishing myopathic signals from normal physiology. The confusion matrix in Figure 2.11 demonstrates clear separation with minimal misclassification.

2.5.2 ALS vs Myopathy

Objective: Assess whether the classifier can differentiate neurogenic (ALS) from myogenic (myopathy) EMG signals.

Rationale: Unlike the Myopathy–Control analysis, both classes in this paradigm represent pathological EMG but with distinct underlying mechanisms. ALS presents with neurogenic MUPs and widespread denervation, whereas myopathy exhibits structurally impaired muscle fibers. Distinguishing these two is clinically crucial yet challenging—making this a rigorous test of classifier robustness.

Methods: ALS and myopathy EMG recordings were processed using the proposed hybrid AutoSSA–QCNN pipeline. Balanced sampling ensured parity across

Table 2.6: Performance metrics of the proposed framework for ALS–Myopathy classification.

	Training	Testing
Loss	0.2468	0.2432
Accuracy	0.9888	0.9868
Precision		0.9901
Recall		0.9902
Specificity		0.9911
F1-score		0.9901

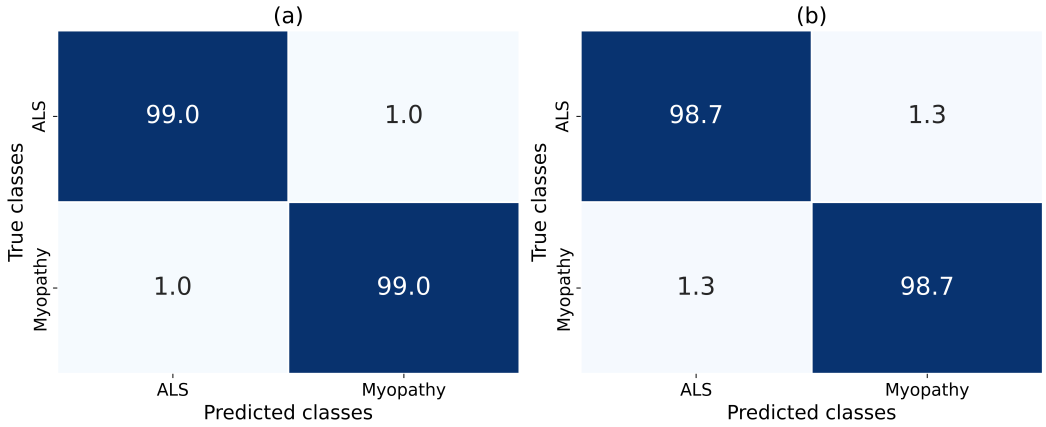

Figure 2.12: Confusion matrix: ALS vs Myopathy.

neuromuscular categories.

Evaluation metrics: Accuracy, sensitivity, specificity, precision, F1-score, and ROC–AUC.

Results and interpretation: Table 2.6 shows excellent performance in distinguishing ALS from myopathy, reflecting the framework's ability to capture neurogenic–myogenic divergence. The confusion matrix in Figure 2.12 corroborates the observed performance.

2.5.3 ALS vs Myopathy vs Control

Objective: Evaluate multiclass discrimination among ALS, myopathy, and control subjects—representing a realistic clinical decision-support scenario.

Rationale: This experiment tests whether the model generalises beyond binary conditions and can simultaneously distinguish (i) neurogenic pathology, (ii) myogenic

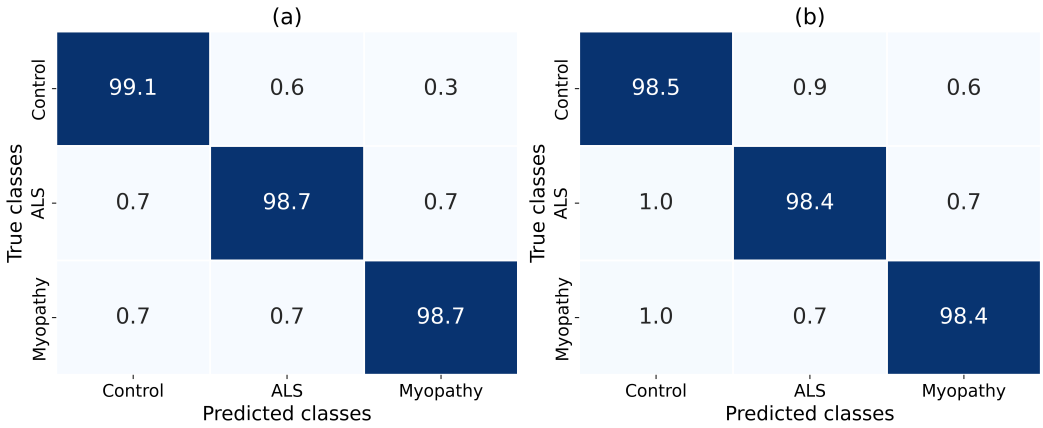

Figure 2.13: Confusion matrix: ALS–myopathy–control multiclass classification.

pathology, and (iii) healthy neuromuscular function. Such multiclass evaluation is essential for developing automated triage systems.

Table 2.7: Performance metrics for ALS–Myopathy–Control multiclass classification.

	Training	Testing
Loss	0.2417	0.2473
Accuracy	0.9877	0.9841
Precision		0.9901
Recall		0.9969
Specificity		0.9952
F1-score		0.9985

Methods: All three classes were jointly processed through the AutoSSA decomposition, feature selection, and QCNN classification pipeline. Stratification ensured balanced representation for multiclass training.

Evaluation metrics: Macro-averaged precision, recall, specificity, F1-score, and accuracy were computed.

Results and interpretation: Table 2.7 demonstrates excellent multiclass performance with strong macro-level metrics and minimal confusion across groups. High recall and F1-scores indicate robust separation of neurogenic and myogenic patterns, and specificity above 0.99 highlights a low false-positive rate. The confusion matrix in Figure 2.13 shows clear diagonal dominance with minimal inter-class leakage. The additional studies show that the proposed framework not only classifies ALS vs Control

but also is efficient in detecting Myopathy in a binary class classification and works equally well in multiclass detection i.e. ALS vs myopathy vs control.

Conclusion of additional studies

The additional studies conducted in this chapter demonstrate that the proposed AutoSSA–QCNN framework is not limited to ALS detection alone but generalises effectively across multiple neuromuscular classification scenarios. Beyond accurately distinguishing ALS from healthy controls, the model exhibits robust performance in detecting myopathy in a binary setting and maintains high discriminative capability in a more demanding multiclass environment involving ALS, myopathy, and control subjects. These results confirm that the framework captures clinically meaningful electrophysiological distinctions across neurogenic, myogenic, and normal EMG activity. Collectively, the findings reinforce the versatility, scalability, and clinical promise of the proposed approach for broader neuromuscular disorder assessment.

Chapter 3

Eye-movement decoding from extraocular EMG using SMSSA and QCNN

In this chapter, we present a framework for the automatic classification of eye movement tasks using electromyographic (EMG) signals derived from extraocular muscle activity. The chapter introduces a multi-resolution decomposition method known as Sliding Mode Singular Spectrum Analysis (SMSSA), designed to handle the non-stationary and nonlinear characteristics of EMG signals. In conjunction with SMSSA, Neighborhood Component Analysis (NCA) is applied for effective feature selection. The proposed framework further employs a Quantum Convolutional Neural Network (QCNN) to classify EMG signals corresponding to various extraocular movement tasks. The architecture and performance of this quantum-enhanced classification model are discussed in detail in the following sections, demonstrating its superior accuracy compared to conventional approaches.

3.1 Introduction

EMG signals from extraocular muscles (EOM) are critical for understanding eye movement mechanisms, diagnosing oculomotor disorders, and enabling advanced clinical practices [150]. Accurate classification of these signals is essential in developing assistive technologies and human-computer interaction (HCI) systems [151]. For instance, Singh et al. [152] demonstrated eye movement detection using multichannel

EMG and machine learning techniques.

Despite their diagnostic value, EMG signals—particularly from extraocular muscles—are inherently noisy, nonlinear, and non-stationary due to muscle artifacts and environmental interference [134, 135]. This complexity presents significant challenges for conventional classification approaches. To address this, advanced signal processing and machine learning methods have been proposed, including entropy-based techniques [153], fractal theory [154, 155, 156], wavelet transforms [157], and feature extraction with machine learning models [158, 159].

Singular Spectrum Analysis with Sliding Windows (SMSSA) has emerged as a robust method for decomposing non-stationary time-series data into meaningful reconstructed components [23, 160]. In this study, we build upon this foundation by integrating SMSSA with a quantum convolutional neural network (QCNN) for automated classification of extraocular EMG signals. Feature selection is further enhanced using Neighborhood Component Analysis (NCA), ensuring only the most relevant characteristics are retained.

The key contributions of this work are as follows:

1. Development of a novel SMSSA-QCNN framework for decoding eye movement tasks from extraocular EMG signals.

2. Extraction of optimized features using Neighborhood Component Analysis to enhance task classification.

3. Implementation of a custom-tuned QCNN architecture that achieves a classification accuracy of 98.70%, outperforming existing methods.

Advances in quantum computing, including room-temperature qubit control [161] and miniaturized quantum processors [162], indicate the feasibility of quantum intelligent sensors for real-time, edge-based pathological diagnostics. This work represents a step toward the practical integration of such technologies in biomedical applications.

The manuscript is structured as follows: Section 3.2 reviews existing literature on EMG signal classification and machine learning approaches. Section 3.3 details the

proposed hybrid method, including dataset characteristics and algorithmic workflow. Section 3.4 presents the experimental results, and Section 3.5 concludes with insights and directions for future research.

3.2 Related work

The classification of EMG signals, particularly from extraocular muscles, has drawn significant research interest due to its application in clinical diagnostics and HCI systems. The human eye processes luminous stimuli through complex oculomotor control, and these dynamics are reflected in EMG patterns [163]. Prior work has explored entropy-based measures [153, 164], wavelet-domain analysis [157], machine learning algorithms [165, 159], and fractal analysis techniques [166, 154, 155, 156] for EMG classification.

SMSSA is particularly well-suited for EMG signals due to its capacity to isolate oscillatory components in noisy, non-stationary environments. Nazmi et al. [160] demonstrated the utility of SSA for biomedical signal decomposition. Building on this, our study integrates SMSSA with a quantum convolutional neural network (QCNN), leveraging the generalization strengths of quantum models. Our method achieves an accuracy of 98.70%, a significant improvement over existing literature.

This direction aligns with ongoing advancements in quantum computing, which point toward real-time edge integration through miniaturized quantum processors and improved qubit stability [161, 162]. The convergence of quantum learning models with EMG signal classification could redefine the landscape of neuromuscular diagnostics and assistive interface technologies in entertainment industry as well as targeting systems in the future.

3.3 Methodology

The proposed methodology integrates SMSSA with a QCNN classifier for classifying EMG signals from extraocular muscle (EOM) movements. Figure 3.2 presents

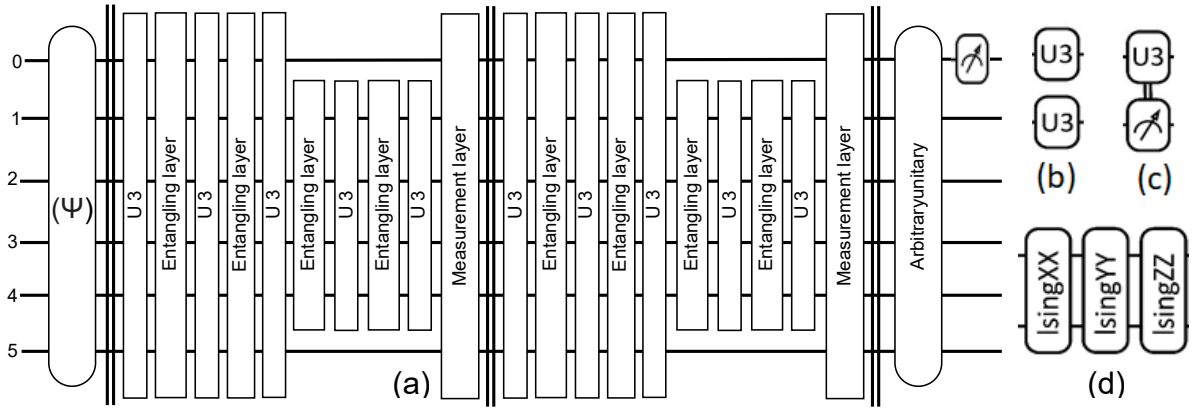

Figure 3.1: (a) Block diagram of 6-Qbit QCNN classifier. Figures (b) U3 layer: Single-Qbit rotation, (c) Measurement Layer components, and (d) Entanglement Layer operation between two Qbits in each layer.

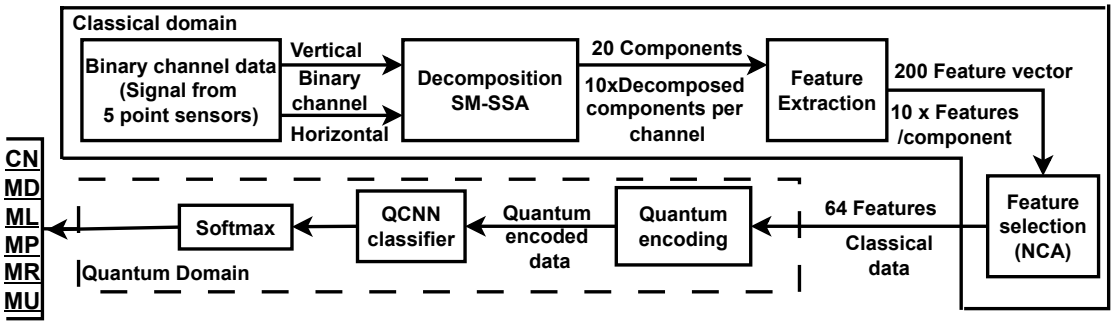

Figure 3.2: Block diagram of the proposed framework.

the complete pipeline. Initially, pre-processed EMG signals are obtained from a public dataset [167]. These signals are decomposed using SMSSA [168], and significant features are extracted via NCA. The top 64 optimized features are then used to train a QCNN classifier for detecting the specific type of eye movement.

3.3.1 Dataset description

The EMG signals were collected using five surface electrodes following the setup described in [67]. Electrode D serves as the reference point on the forehead. Electrodes A and B are placed vertically above and below the eyes to capture vertical eye movements, while electrodes C and E are placed laterally to capture horizontal eye movements. Signals were amplified using an AD620 instrumentation amplifier and

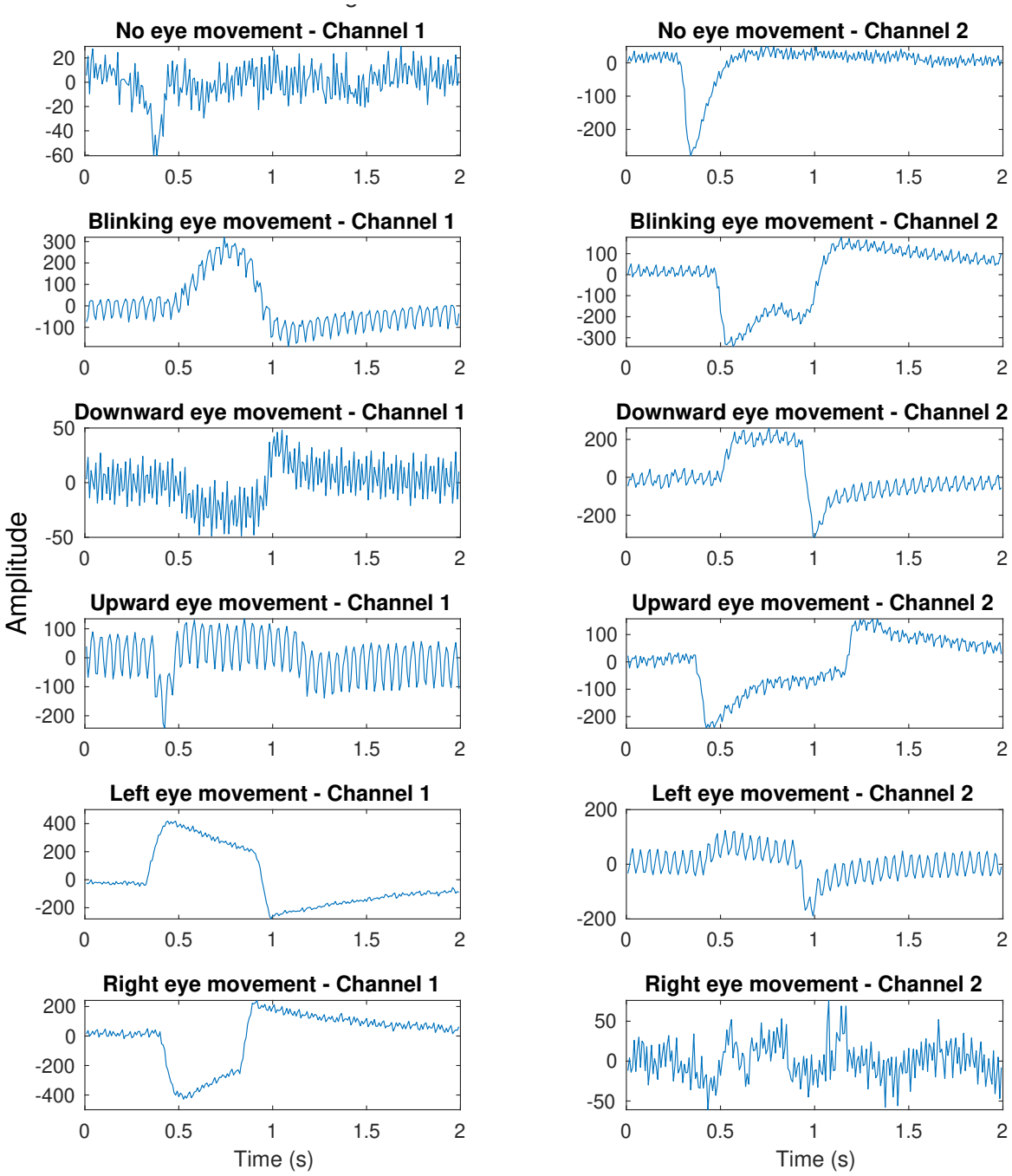

Figure 3.3: Plots of all the different eye movements.

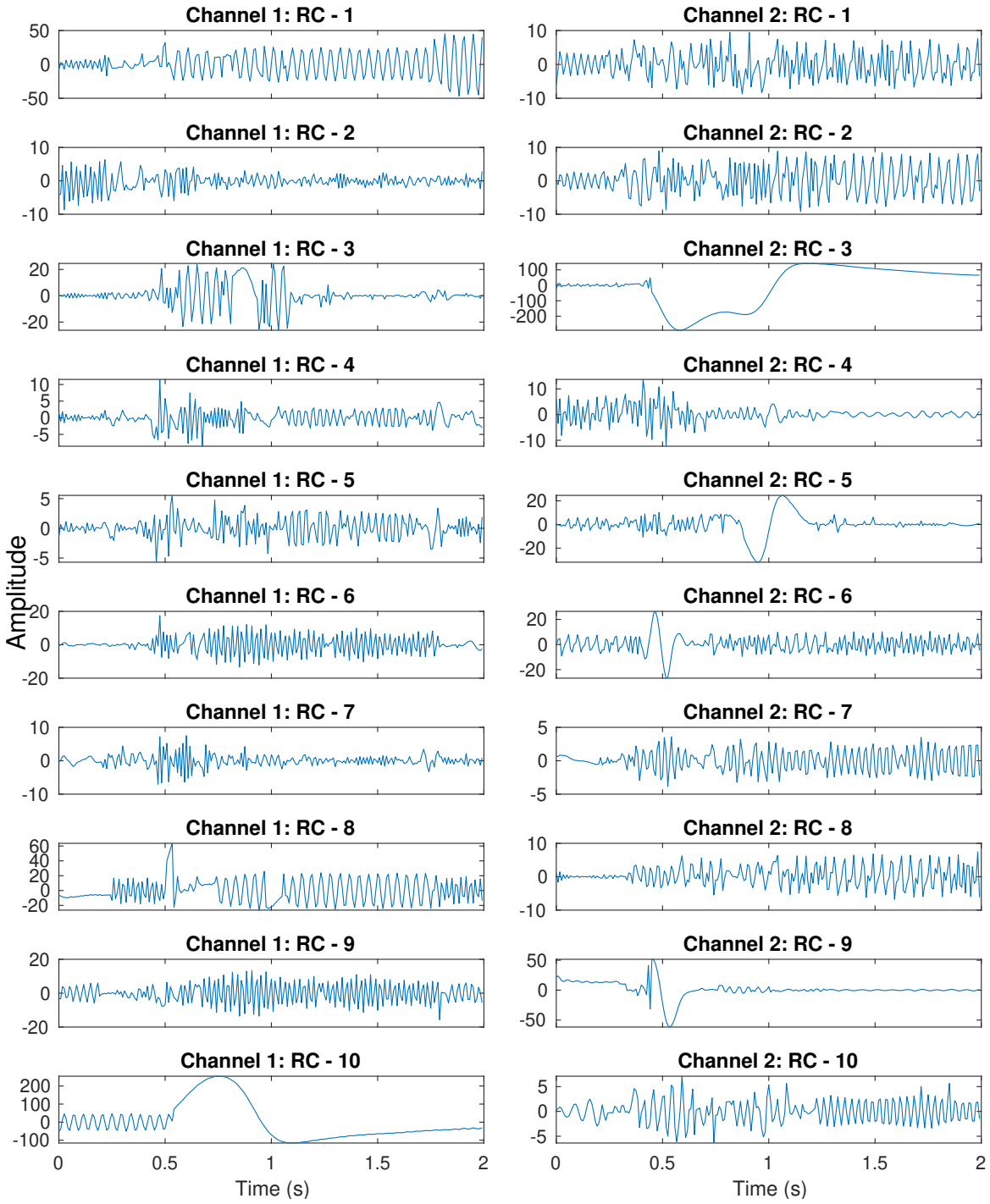

Figure 3.4: SMSSA decomposition of EMG signal for blinking movement (shown in Fig. 3)

sampled at 120 Hz.

The dataset, available on IEEE Dataport [167], includes recordings from 10 subjects performing six distinct eye movement tasks—up (MU), down (MD), left (ML),

right (MR), blink (MP), and no movement (CN)—each repeated 10 times. Each recording consists of 25,000 samples captured over 2.083 seconds. For analysis, each signal is divided into 100 segments of 250 samples each.

3.3.2 Proposed framework for eye movement detection

For accurate eye movement detection, the EOG signal is decomposed into a set of reconstruction components using SMSSA technique, the features are extracted from the obtained RCs and significant features are selected using NCA, then these features are used for eye-movement detection using QCNN. The desciption of each of the steps is presented as follows:-

3.3.2.1 Sliding mode singular spectrum analysis

Signal $x[n]$ for $n = 1, 2, \ldots, N$ is decomposed using SMSSA as follows:

Step 1: The signal $x[n]$ is divided into frames of length W samples and step size Δ samples.

Step 2: Each frame is divided into R RCs using automated SSA.

Step 3: If the current frame number is 1, $\hat{x}_r[n] = \hat{a}_r[n]$ for $n = 1, 2, 3, \ldots, a$ and $r = 1, 2, 3, \ldots, R$ where $a = \frac{W-1}{2}$.

Otherwise, if the current frame number is less than $N - W + 1$, the decomposed components of the current frame are matched with the decomposed components of the previous frame by minimizing the distance between them. If it is not the last frame, $\hat{x}_r[n] = \hat{a}_r[n]$ for $n = a - \Delta + 1, a - \Delta, \ldots, a$ and $r = 1, 2, 3, \ldots, R$ else, $\hat{x}_r[n] = \hat{a}_r[n]$ for $n = a - \Delta + 1, a - \Delta, \ldots, W$ and $r = 1, 2, 3, \ldots, R$.

Steps for framewise automated SSA decomposition is as under:

Step 1: Embedding: Consider a signal $x[n]$ for $n = 1, 2, 3, \ldots, N$. The Hankel matrix

of $x[n]$ is obtained as [23, 143],

$$\mathbf{X} = \begin{bmatrix} x[1] & x[2] & \dots & x[K] \\ x[2] & x[3] & \dots & x[K+1] \\ \vdots & \vdots & \ddots & \vdots \\ x[L] & x[L+1] & \dots & x[N] \end{bmatrix} \tag{3.1}$$

where L is the embedding dimension and $K = N - L + 1$.

Step 2: Singular value decomposition: The SVD of the Hankel matrix X is expressed as [23],

$$X = U\Sigma V^T = \sum_{k=1}^{R} X_k = \sum_{k=1}^{R} \sigma_k u_k v_k^T \tag{3.2}$$

where $U = (u_1, u_2, \dots, u_L)$, $\Sigma = \text{diag}(\sigma_1, \sigma_2, \dots, \sigma_L)$, $V = (v_1, v_2, \dots, v_K)$, and T is the transpose operator.

Step 3: Diagonal averaging: Diagonal averaging of the k^{th} trajectory X_k yields the k^{th} reconstructed component $x_k[n]$ of signal [23].

Step 4: Grouping: The hierarchical clustering is performed on $\{x_1[n], x_2[n], \dots, x_R[n]\}$, grouping the components into C clusters. The components of each cluster are added together to obtain the reconstructed components $x_{\text{RC},k}[n]$ for $k = 1, 2, \dots, C$ [23, 143].

In this study, $L = 10$ and $N = 40$ were chosen, greatly improving classification. Fig. 3.4 shows the 10 extracted left and right EOM signals, revealing crucial multi-resolution information.

3.3.2.2 Feature extraction

In this work, features were extracted for each component from the signals, i.e., renyi entropy, activity, mobility, complexity, spectral entropy, and normalized spectral entropy, etc for creating a feature vector consisting of 100 features per channel and 200 features per signal sample.

In our work, we have employed the NCA algorithm [146] to select the most significant features from the obtained RCs. In our simulations, NCA with a parametric

configuration (population size = 20, iteration = 10, $L = 40$ and $K = 10$) was selected empirically to achieve the best-optimized features. At each iteration, the NCA algorithm evaluates each particle's feature subset using a fitness function (mean of input data) and generates the global best subsets. The best subset (gbest) is identified as the optimal feature set for machine learning, enhancing model performance. In our study, all 10 RCs from both channels were used as input to NCA, extracting the top 64 features.

These selected features are used as inputs for the QML algorithm, specifically QCNN (Fig. 4.1), in the proposed model to decode the type of eye movement from the most significant features in the decomposed signals. In Fig. 4.1, U3 is a single-qubit gate that applies an arbitrary rotation defined by three angles. IsingXX, IsingYY, and IsingZZ are gates that create entanglement between qubits by applying a rotation around the XX, YY, and ZZ axis for a pair of qubits respectively. Further, Fig. 3.2, depicts the overall prediction method for preprocessing and classification using the QML algorithm.

In this study, parameters from entropy, complexity, and frequency domain are computed from the decomposed signal and used as inputs to NCA to extract 64 significant features:

Entropy: Various entropy measures, including Rényi entropy (H_α), spectral entropy (H_s), and normalized spectral entropy (H_{ns}), are computed from the decomposed signal components to quantify the information content [169, 170]. The mathematical formulations are as follows:

- ***Rényi entropy:*** It is defined as

$$H_\alpha = \frac{1}{1-\alpha} \log \left(\sum_{i=1}^{n} p_i^\alpha \right),$$

  where α is the order of the entropy, p_i is the probability of the i-th event, and n is the total number of events [169, 170].

- ***Shannon entropy:*** When $\alpha \to 1$, Rényi entropy simplifies to Shannon entropy

(or spectral entropy), which is given by

$$H_s = -\sum_{i=1}^{n} p_i \log(p_i),$$

where p_i represents the spectral component probability [169, 170].

- ***Normalized spectral entropy:*** The normalized spectral entropy is computed as

$$H_{ns} = \frac{H_s}{\log(n)},$$

where n is the number of events [169, 170].

Complexity: Various complexity measures, including activity (A), mobility (M), and complexity index (C), are computed from the decomposed signal components to evaluate the dynamical characteristics relevant to the study [171]. The mathematical formulations for these measures are derived as follows:

- ***Activity***: Activity is computed as

$$A = \sum_{i=1}^{N} x_i^2,$$

where x_i is the signal value at the i-th time step, and N is the total number of time steps.

- ***Mobility***: It is defined as

$$M = \frac{\sqrt{\sum_{i=2}^{N}(x_i - x_{i-1})^2}}{A},$$

where A is the previously defined activity. This reflects the signal's rate of change normalized by its activity.

- ***Complexity index***: It is calculated as

$$C = \frac{M}{A},$$

which characterizes the signal's structural variation.

Frequency-domain: Various frequency-domain parameters, including peak frequency (f_{peak}), spectral centroid (f_c), spectral bandwidth (BW), and spectral flatness (SF), are computed from the decomposed signal components to analyze the frequency characteristics relevant to the study [171]. The mathematical formulations for these parameters are derived as follows:

- ***Peak Frequency***: The peak frequency is defined as

$$f_{\text{peak}} = \arg\max_X |X(f)|$$

where $X(f)$ is the frequency spectrum, and f_{peak} is the frequency where $|X(f)|$ is maximum.

- ***Spectral centroid***:The spectral centroid is calculated using

$$f_c = \frac{\sum_{k=1}^{N} k|X(k)|}{\sum_{k=1}^{N} |X(k)|}$$

where k is the index of frequency bins, and $X(k)$ is the magnitude of the frequency component at the k-th bin.

- ***Spectral bandwidth***: The spectral bandwidth is obtained as

$$BW = \frac{\sum_{k=1}^{N} (f_k - f_c)^2 |X(k)|}{\sum_{k=1}^{N} |X(k)|}$$

where f_k is the frequency at the k-th bin, and f_c is the spectral centroid.

- ***Spectral flatness***: The spectral flatness is calculated as

$$SF = \frac{\exp\left(\frac{1}{N}\sum_{k=1}^{N} \log(X(k))\right)}{\frac{1}{N}\sum_{k=1}^{N} X(k)}$$

where $X(k)$ is the magnitude of the frequency component at the k-th bin.

3.3.2.3 NCA

NCA was employed to optimize feature selection from a diverse range of physiological signals [172, 146]. By leveraging NCA's ability to enhance classification accuracy through learned feature relevance, the top 64 features were identified based on their discriminative power, enhancing the interpretability and efficiency of signal analysis. This approach ensures robust feature selection in complex datasets, thereby improving the efficacy of classification models in biomedical applications.

The resulting optimized feature subset significantly contributes to the improved performance of the proposed QCNN framework, as shown in Table 3.1 and illustrated in Figure 3.2. These optimized features were used as inputs to the Quantum Convolutional Neural Network (QCNN) classifier.

3.3.2.4 QCNN Classification

QCNNs, introduced by Cong et al. [147], are inspired by classical CNNs and prioritize generalization in machine learning. Generalization ensures optimized model performance across the data distribution despite limited training data, encapsulating the model's ability to predict unseen instances.

In this study, a QCNN model is employed for classifying features obtained from NCA to detect eye movement. Here, features (x) undergo encoding into quantum states ($\rho(x)$) through a mapping ($x \mapsto \rho(x)$) and are processed via learnable quantum channels ($\mathcal{E}\alpha(\rho(x))$). The QCNN operates on a subsystem of the state $\rho(x)$, producing an output state $(\mathcal{E}\alpha \otimes \mathrm{id})(\rho(x))$, where $\alpha = (\theta, k)$. Here, θ represents continuous parameters within gates, and k denotes discrete gate structures optimized during training [59].

The block diagram of a 6-qubit QCNN classifier is shown in Fig.3.1(a). The internal structure of the U3 Layer is illustrated in Fig.3.1(b), which depicts two single-qubit gates applying arbitrary rotations. The measurement layer is presented in Fig.3.1(c), showing the measurement operation on two qubits. Finally, Fig.3.1(d) illustrates the entanglement layer, which details the circuit structure for two qubits using IsingXX,

IsingYY, and IsingZZ gates to create entanglement through rotations around the XX, YY, and ZZ axes, respectively.

The layered structure of the QCNN—comprising encoding, entanglement, variational rotation, and measurement—enables it to efficiently extract and classify subtle patterns embedded within high-dimensional biomedical signals. Its performance, in comparison to classical classifiers, is quantitatively demonstrated in Table 3.1, validating the superiority of the proposed framework for eye movement detection from extraocular EMG signals.

3.3.2.5 Classical Classifiers

In this study for better comparison of existing algorithms all classical algorithms were compared and studied for classification of the dataset. The performance of the top ten classical algorithms is given in Table 3.1. The table shows that QCNN achieves the highest accuracy of 98.70%, with a corresponding loss of 0.2465, thus outperforming the existing classical algorithms.

Table 3.1: Comparison of classifier performance

Classifier	**Accuracy (%)**		**Loss**	
	Train	**Test**	**Train**	**Test**
Discriminant				
Linear	86.5	83.3	0.135	0.167
Ensemble subspace	85.2	80.0	0.148	0.200
SVM				
Linear	81.7	80.0	0.183	0.200
Quadratic	83.9	81.7	0.161	0.183
Cubic	83.1	83.3	0.169	0.167
Medium gaussian	82.0	80.0	0.180	0.200
Coarse gaussian	81.5	76.6	0.185	0.233
Kernel	79.4	81.7	0.206	0.183
NN				
Medium NN	82.8	66.7	0.172	0.333
Wide NN	83.1	80.0	0.169	0.200
QCNN	**98.99**	**98.70**	**0.2439**	**0.2465**

Note: ***SVM*** *= support vector machine,* ***NN*** *= neural network*

Table 3.2: NCA Feature Selection Results

Training Size	Loss		Accuracy	
	Training	Testing	Training	Testing
8	0.2037	0.2951	0.9588	0.8558
16	0.2262	0.2703	0.9744	0.9365
32	0.2353	0.2559	0.9803	0.9655
64	0.2371	0.2457	0.9880	0.9828
128	0.2434	0.2484	0.9891	0.9857
256	0.2439	0.2465	0.9899	0.9870

3.4 Results and discussion

To assess the effectiveness of the proposed SMSSA and QCNN-based classification framework, we employed a publicly available dataset from IEEE Dataport [167]. The extraocular muscle (EOM) dataset contains electromyographic (EMG) signals recorded at a sampling frequency of 120 Hz over a period of 2.083 seconds from 10 subjects. Each subject performed 10 pseudo-random repetitions of six distinct eye movement tasks: upward (MU), downward (MD), rightward (MR), leftward (ML), blinking (MP), and no movement (CN). Each individual recording comprises 25,000 samples [167]. For processing and analysis, these signals were divided into 100 equal-length segments, each containing 250 samples.

The recordings were collected using a five-surface electrode configuration as outlined by López et al. [67]. Specifically, an electrode (D) was placed on the forehead as a reference, two electrodes (A and B) were positioned vertically above and below the eyes to capture vertical ocular activity, and two additional electrodes (C and E) were placed laterally to detect horizontal gaze shifts. The signals from these electrodes were amplified using an AD620 instrumentation amplifier, which helped capture positive and negative potential changes based on eye movement direction [167].

Following segmentation, the signals were decomposed using SMSSA with a tolerance threshold of $\epsilon = 10^{-4}$ and an embedding dimension of 40. Each segmented sample was transformed into a 250×10 matrix representing ten reconstructed components. Figure 3.4 presents the SMSSA-based decomposition results of EOM signals obtained from both vertical and horizontal channels.

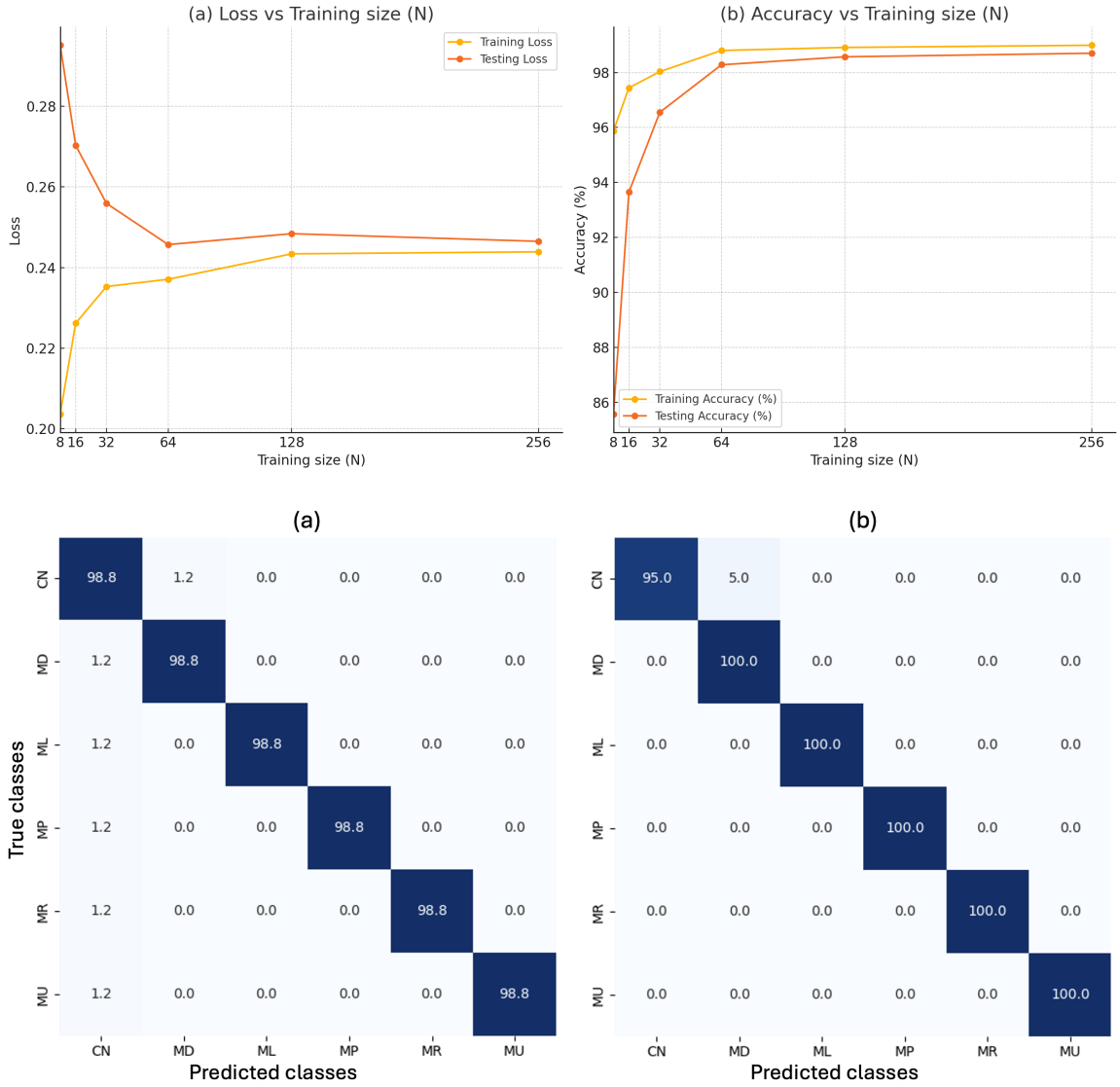

Figure 3.6: Confusion matrix (a) Training (b) Testing

From these reconstructed components, a comprehensive set of features was extracted. These included Renyi entropy, activity, mobility, complexity, spectral entropy, and normalized spectral entropy, resulting in a 120-dimensional feature vector per signal segment. The Neighborhood Component Analysis (NCA) algorithm was then applied to select the 64 most discriminative features for classification purposes.

Although Singh et al. [152] used the same two-channel dataset, their framework is based on multichannel eigenvalue decomposition of Hankel matrices (MCh-EVDHM), which jointly decomposes both channels while preserving cross-channel structural alignment, i.e., a multivariate analysis. In contrast, the proposed method applies SM-SSA separately to each channel as a single-channel decomposition approach. Because

Table 3.3: Efficiency of existing algorithms and proposed work

Reference	**Algorithm**	**Accuracy (%)**
Asanza et al. [132]	Fine KNN	92.0%
	Kernel naive bayes	92.3%
	Medium gaussian SVM	93.0%
	Quadratic SVM	93.3%
	Quadratic discriminant	93.3%
	SVM cubic	93.5%
Proposed framework	**SMSSA, NCA, QCNN**	**98.70%**

the nature, dimensionality, and channel dependence of the decomposed components differ fundamentally between the two frameworks, a direct numerical comparison was not included in Table 3.3 to avoid methodological inconsistency.

These selected features were evaluated using several classical classifiers. Table 3.1 presents the classification accuracies and loss values for the top ten models, including linear discriminant analysis and cubic SVM, both of which achieved a maximum accuracy of 83.3%. Despite these results, quantum models demonstrated significant performance gains. When the same features were used to train a Quantum Convolutional Neural Network (QCNN), the model achieved a testing accuracy of 98.70%.

The classifier's performance over varying training set sizes is detailed in Table 3.2, revealing consistent improvements in both training and testing accuracy, along with reduced loss. Figure 3.5 visually illustrates these trends. Notably, the highest performance was achieved at a training size of 256, validating the QCNN's ability to generalize well even in relatively low-data regimes.

Furthermore, Table 3.3 provides a comparative analysis of our proposed method with existing techniques as referenced in [132]. Our framework, integrating SMSSA, NCA, and QCNN, achieved an accuracy of 98.70% with precision: 0.9405, recall: 0.9875, F1-score: 0.9634, and specificity: 0.9875, outperforming traditional approaches such as cubic SVM, which reached only 93.5% . The confusion matrix is shown in Figure 3.6. This significant improvement highlights the superior efficacy of quantum machine learning in biomedical signal classification, especially for non-stationary, noisy EMG signals.

The combination of a high testing accuracy of 98.70% and the ability to operate on a relatively modest sample size illustrates the practical viability of the proposed approach. This success, combined with emerging advancements in quantum computing technologies—including thermal stability [161] and miniaturization [162]—underscores the future potential of deploying quantum intelligent sensors. Such innovations may revolutionize medical diagnostics, enabling precise real-time eye movement detection for applications ranging from assistive human-computer interaction systems to advanced clinical diagnostics and eye-controlled targeting systems.

3.5 Summary

This chapter presented a novel framework for the classification of electromyographic (EMG) signals acquired from extraocular muscles (EOM), leveraging a combination of advanced signal decomposition and quantum machine learning techniques. The methodology incorporated Sliding Mode Singular Spectrum Analysis (SMSSA) to extract meaningful reconstructed components from non-stationary and noisy EMG signals. Neighborhood Component Analysis (NCA) was subsequently used to identify the most significant features from the decomposed signal set, thereby optimizing the input space for classification.

The selected features were then classified using a Quantum Convolutional Neural Network (QCNN), a quantum-enhanced learning architecture inspired by classical CNNs. The proposed QCNN-based model achieved a testing accuracy of 98.70%, significantly outperforming traditional classifiers such as Support Vector Machines and Neural Networks. This result not only underscores the robustness of the QCNN framework but also illustrates the synergistic value of combining quantum computation with domain-specific feature extraction in biomedical applications.

The findings from this study demonstrate the feasibility and effectiveness of quantum machine learning models in interpreting biomedical signals with high precision. Beyond academic merit, the proposed approach offers practical implications for future assistive technologies. Specifically, the framework shows potential for integration into

next-generation prosthetics and exoskeletons, enabling more accurate control through bioelectrical signals. Additionally, its relevance extends to the design of eye-controlled targeting systems in autonomous tools, such as those used in robotic surgery or remote operations in hazardous environments.

The demonstrated success of the QCNN model, alongside the growing advancements in quantum computing—particularly in areas of room-temperature operation [161] and device miniaturization [162]—highlights a promising pathway toward the development of quantum intelligent sensors. Such sensors could provide real-time, high-resolution diagnostics and control capabilities, potentially transforming the landscape of medical diagnostics, human-computer interaction, and precision bioengineering.

Chapter 4

HAR from multi-channel sEMG using MSSA and optimized QCNN

In Chapters 2 and 3, we explored non-adaptive signal decomposition techniques such as Auto-SSA and SMSSA, integrated with QCNNs, to detect neuromuscular conditions like ALS and decode eye movement tasks using EMG signals. These frameworks demonstrated the effectiveness of combining structured signal decomposition with quantum machine learning for biomedical signal classification, particularly in single-channel or dual-channel EMG configurations.

Building on these foundations, this chapter extends the scope to multi-channel surface electromyogram (sEMG)-based HAR, a more complex and practical application in the domain of wearable systems and HCI. Here, we introduce an adaptive, multi-dimensional decomposition technique—MSSA —which is capable of extracting channel-aligned components from sEMG recordings distributed across multiple body locations. This enhances robustness against noise and channel misalignment, both of which are common in real-world HAR settings.

The proposed HAR framework integrates MSSA for signal preprocessing, multi-domain feature extraction, and the minimum redundancy maximum relevance (MRMR) algorithm for optimal feature selection. These features are then classified using a custom-designed QCNN architecture. By incorporating quantum learning principles into a multi-channel setup, this work not only addresses the inherent non-stationarity and noise in sEMG signals but also leverages quantum computational

advantages to improve classification efficiency and accuracy.

With a classification accuracy of 98.81% across twenty activity classes, this framework demonstrates significant improvements in precision and robustness for HAR applications. It serves as a natural progression from earlier chapters—shifting from disease detection and ocular motor control to a comprehensive human activity recognition system—thereby advancing the use of quantum machine learning in biomedical signal analysis and wearable HCI technologies.

4.1 Introduction

HAR plays a critical role in HMI technologies, enabled by advancements in compact sensors like surface EMG (sEMG), accelerometers, and gyroscopes [173]. Among these, sEMG-based HAR (HAR-sEMG) supports diverse applications, including health monitoring, prosthetic control, and rehabilitation systems, positioning it as a cornerstone of modern assistive technologies [174]. EMG sensors capture electrical signals from muscle contractions, offering precise insights into physical activities [175, 176]. Unlike other wearable sensors, sEMG non-invasively records muscle activity and identifies activity patterns with higher accuracy. These sensors are particularly effective for multi-class HAR in prosthetic control because they provide accurate gait analysis and have low computation times.

However, analyzing sEMG signals remains challenging due to their nonstationary nature and additive artifacts, which impact the reliability and accuracy of signal measurement and processing. Existing single-channel sEMG analysis faces inherent limitations, including reduced inter-channel information and decreased classification performance when handling a large number of HAR-sEMG classes. These challenges highlight the critical need for innovative methodologies to improve sEMG signal decomposition, feature extraction, and classification for enhanced measurement accuracy.

HAR-sEMG-based approaches have proven valuable in clinical rehabilitation, such as exoskeletons for mobility-impaired patients [177], and have broader applications in domains such as prosthetic control and human-computer interaction [178, 179, 180,

181]. To address these challenges, this study introduces a novel framework that leverages multivariate singular spectrum analysis (MSSA) for signal decomposition and noise reduction, advancing the accuracy and reliability of HAR-sEMG signal measurement. Additionally, the proposed integration of quantum machine learning (QML) optimizes feature detection, enabling precise classification of multi-class human activity tasks. These advancements contribute directly to the field of sensor measurement by introducing innovative methodologies for processing multi-channel sEMG signals."

Advancements in quantum computing, particularly in temperature optimization [161] and miniaturization [162], highlight the potential for developing quantum intelligent sensors. These sensors promise transformative capabilities for real-time pathological diagnostics and precise control in applications such as exoskeletons and advanced HCI systems, further extending the functionality and scope of modern measurement technologies.

Unlike previous approaches that rely on univariate sEMG signal decomposition, this work integrates MSSA for enhanced multi-channel feature extraction and a quantum CNN for robust classification, achieving state-of-the-art accuracy in HAR.

4.2 Related work

In the past decade, researchers have extensively explored multi-channel sEMG signals to effectively recognize muscle activity for various HAR-based applications. Nurhanim et al. [182] used random forest, a machine learning classifier, to classify data from sEMG wireless sensors for six different activities, achieving 82.08% accuracy. Vamsi et al. employed a CNN-LSTM framework for complex HAR systems using sEMG, achieving an accuracy of 87.18% [183]. Ju et al. [184] achieved 96.7% accuracy in HAR task classification from multi-channel EMG signals using fuzzy Gaussian mixture models (FGMMs) with recurrence plots (RP). Silva et al. [185] employed support vector machines (SVM) and recurrence quantification analysis (RQA) to achieve 98.28% accuracy in multi-class HAR classification from multi-channel EMG signals. Similarly, Sukumar et al. [186] obtained 98.17% accuracy using variational mode de-

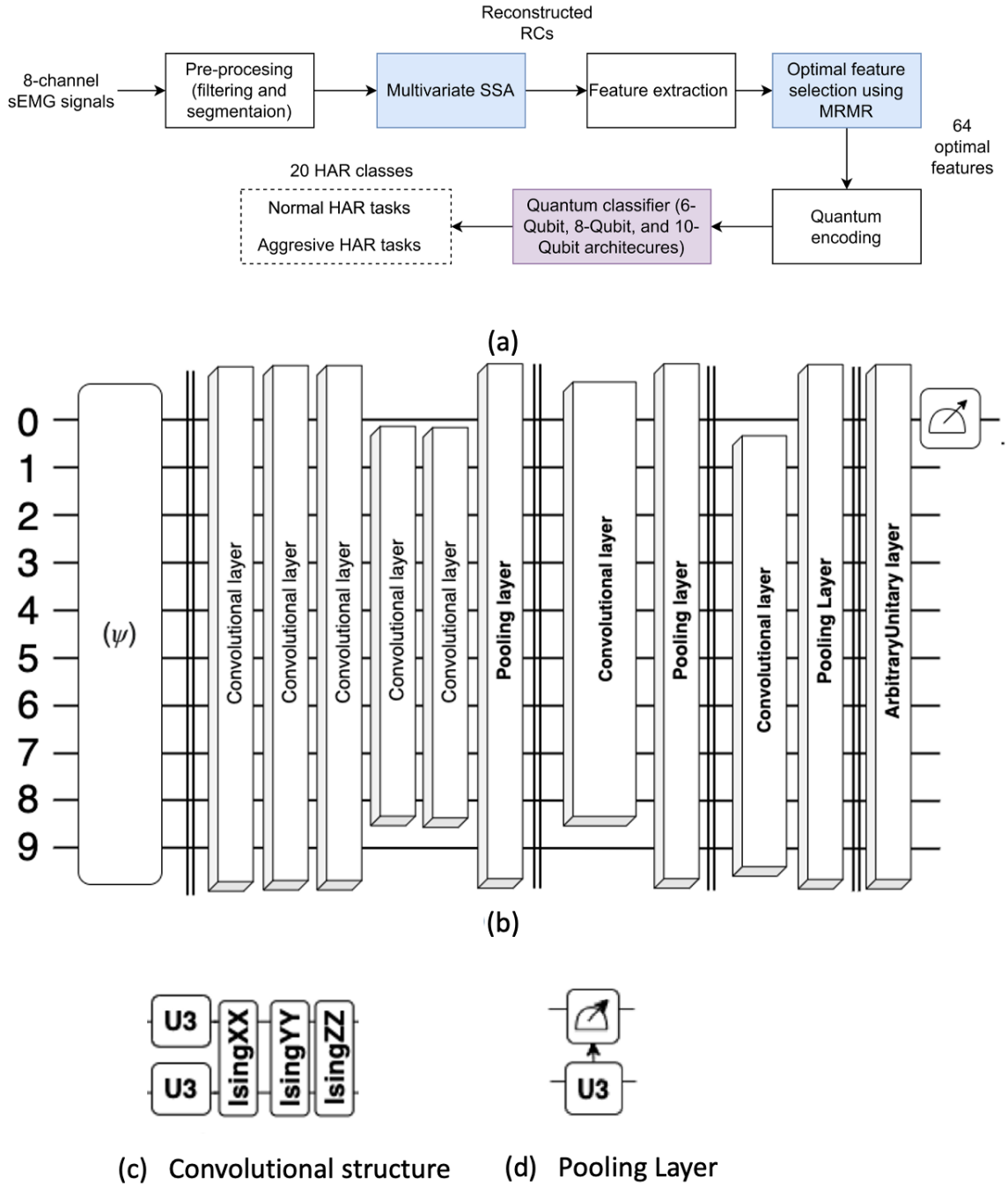

Figure 4.1: (a) Proposed MSSA-QCNN framework and (b) designed architecture of 10-Qubit QCNN classifier with internal structure as in (c)-(d).

composition (VMD) on EMG data for the classification of multiple physical gesture patterns. Chada et al. [187] proposed a framework for gesture pattern classification and achieved 97.74% accuracy using tunable-Q wavelet transform (TQWT). Ajayan et al. [188] employed the Inception-ResNet-v2 model with RP analysis for HAR task recognition, achieving 98.41%. Similarly, Choudhury et al. [189] used CNN-LSTM models to achieve 98% accuracy for EMG-based HAR task classification. While these works demonstrate progress in HAR-sEMG systems, they primarily focus on univariate sEMG analysis, limiting their ability to extract mutual patterns across multiple channels and achieve consistent performance for complex HAR tasks.

Recent advancements in quantum machine learning (QML) frameworks have demonstrated their transformative potential in sensors and instrumentation for EMG-based applications, achieving high accuracy in tasks such as amyotrophic lateral sclerosis classification and showing promise for HAR systems [190]. In extension of the development of sensor measurement systems, Yang et al. proposed a C3-QCNN framework for signal modulation classification, achieving 91% accuracy in 2022 [191], while Yijie Zhu et al. employed a multigate QCNN in 2024, achieving 96% accuracy [192]. However, existing works [184, 185, 186, 188, 190, 193, 194, 195, 196] rely heavily on single-channel sEMG analysis, which limits their classification performance and robustness for a large-scale multi-class HAR task-based measurement system.

To address these limitations, this study proposes the multivariate singular spectrum analysis-QCNN (MSSA-QCNN) framework, which leverages multivariate signal decomposition techniques to extract channel-aligned reconstructed components (RCs) and mutual spectral characteristics across multiple channels. By integrating MSSA and QCNN, the framework achieves a superior accuracy of 98.8% across all HAR-sEMG task categories, significantly advancing the measurement precision and robustness in HAR systems.

The novelty of the proposed MSSA-QCNN framework is rooted in its customized QCNN architecture, which is engineered to efficiently recognize HAR tasks using sEMG signals, even with minimal input data and reduced memory requirements. This advancement builds upon established signal decomposition methodologies—such as

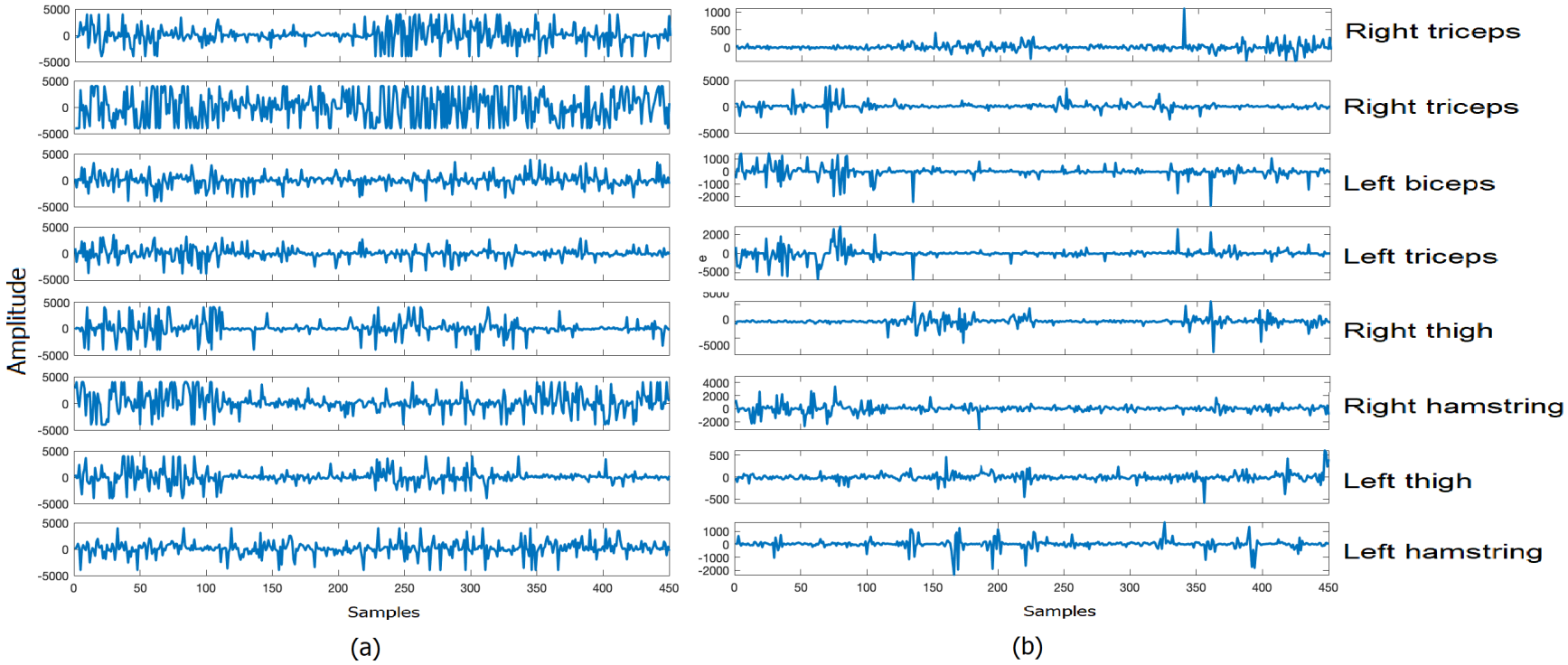

Figure 4.2: The 8-channel sEMG signals: (**a**) aggressive HAR task and (**b**) normal HAR task.

MSSA, EMD, and synchrosqueezing—by optimizing component reconstruction quality and feature extraction processes specifically for EMG signal analysis. The framework significantly contributes to the precision instrumentation required for prosthetic and exoskeleton applications, offering robust solutions for real-time, wearable, and embedded systems.

This study pioneers the application of the MSSA-QCNN framework to HAR-sEMG datasets, marking a significant step forward in the field of neuromuscular signal processing for activity recognition. By leveraging the multivariate capabilities of MSSA, the proposed approach demonstrates improved mutual information and channel alignment when compared to traditional univariate SSA methods, thereby enhancing the fidelity and reliability of signal measurements. This is particularly valuable in scenarios where accurate component separation and feature extraction are critical for downstream classification tasks.

A series of Qubit MSSA-QCNN architectures were systematically designed and rigorously tested using cross-subject validation protocols, ensuring adaptability and generalizability across diverse measurement scenarios and user populations. The flexibility inherent in these architectures allows the framework to accommodate varying signal complexities and noise profiles commonly encountered in real-world EMG data.

Furthermore, the study presents a detailed analysis of HAR-sEMG classification performance, underpinned by MRMR-based fusion feature selection. This approach not only improves classification accuracy but also provides a principled method for identifying the most informative features from multichannel EMG signals, thereby reducing computational overhead and enhancing interpretability.

Experimentally, the MSSA-QCNN framework has demonstrated high efficacy for HAR-sEMG recognition, particularly in the context of prosthetic exoskeleton devices. The framework's ability to process and classify sEMG signals with high precision makes it well-suited for integration into wearable device technologies and real-time measurement systems. These results highlight the transformative potential of the proposed approach for advancing the state-of-the-art in prosthetics, exoskeleton devices, assistive robotics, clinical diagnostics, and intelligent sensor systems etc.

4.3 Methodology

The proposed MSSA-QCNN framework integrates a multivariate extension of singular spectrum analysis (MSSA) and QCNN for HAR-sEMG task classification. The complete MSSA-QCNN framework for HAR-sEMG detection is depicted in Figure 4.1a, which includes pre-processing, extraction of RCs using MSSA across channels, feature extraction, feature ranking, and classification stages utilizing the QCNN algorithm. This integration demonstrates advancements in signal processing, decomposition, and analysis techniques, contributing significantly to modern measurement technologies. The designed architecture of the QCNN structure is shown in Figure 4.1b.

4.3.1 Dataset

In this work, we have used the physical action dataset [1], which comprises EMG recordings of 10 normal and 10 aggressive HAR activities collected from four healthy individuals (ages 25–30) using a wireless Delsys EMG device. Data from three males and one female were recorded across 20 trials, with approximately 10,000 samples per signal at a 1 kHz sampling rate. The device recorded 8-channel EMG signals from electrodes on participants' upper arms and legs, generating eight-channel time series of approximately 9,000 samples each.

This dataset provides an ideal foundation for testing advanced measurement and processing methods, aligning with the objectives of precision signal analysis and processing. The recorded raw 8-channel sEMG signals corresponding to the normal and aggressive HAR activities are shown in Figure 2. In our study, these samples were segmented into 450-sample clips, producing 20 segments per HAR activity per subject for further analysis. This resulted in 80 data segments per activity across all participants, facilitating training and testing for HAR-sEMG task classification. The detailed information on the used EMG physical activity dataset is presented in Table 4.1.

This study employs an **ethically approved** sEMG dataset recorded from four healthy individuals (3 males, 1 female, aged 25–30) using a **standardized** protocol

with a Delsys wireless system. Sensors were strategically placed on the upper arms and legs to ensure **consistent and reproducible measurements**. All participants provided written informed consent.

Table 4.1: The detailed description of EMG physical activity dataset [1]

HAR task	**Number of subjects**	**Sample length**	**Number of clips**
Aggressive activity: Elbowing, pushing, pulling, slapping, kneeing, hammering, headering, punching, sidekicking, frontkicking	4 (3 males and 1 female)	10 seconds	80
Normal activity: Walking, waving, standing, seating, running, jumping, hugging, bowing, handshaking, clapping	4 (3 males and 1 female)	10 seconds	80

4.3.2 Multivariate sliding mode singular spectrum analysis (MSSA)

MSSA is an advanced multivariate signal decomposition technique designed to process multi-channel data and extract mutual information across channels. It extends univariate SSA to effectively capture both stationary and oscillatory components in multivariate time series, contributing to the advancement of signal measurement and processing techniques [197]. MSSA is particularly advantageous where traditional multivariate SSA struggles to reconstruct mutual information among all channel data [13].

To address the limitations of static windowing in traditional multivariate SSA, MSSA employs a dynamic sliding window approach to decompose nonstationary components across signals. For each sliding window, the components are aligned and reconstructed by minimizing the Euclidean distance between the current components and their prior estimates. MSSA has demonstrated improved reconstruction quality factor (QRF) [198], making it highly effective in analyzing complex datasets such as biomedical signals and environmental monitoring. The MSSA technique comprises the following five steps:

4.3.2.1 Trajectory matrix construction

For a multichannel signal $Z = \{z_i(t) : i = 1, \ldots, I; t = 1, \ldots, T\}$ with I channels and T samples, the trajectory matrix H_j is constructed for each channel with an embedding dimension M.

$$H_j = \begin{bmatrix} z_j(1) & z_j(2) & \cdots & z_j(T-M+1) \\ z_j(2) & z_j(3) & \cdots & z_j(T-M+2) \\ \vdots & \vdots & \ddots & \vdots \\ z_j(M) & z_j(M+1) & \cdots & z_j(T) \end{bmatrix} \tag{4.1}$$

where $L = T - M + 1$.

4.3.2.2 Grand trajectory matrix

A grand trejectory matrix is H of size H is $M \times IL$ is computed using a concatenated trajectory matrix of different channels, which is expressed as follows:

$$H = [H_1, H_2, \ldots, H_I] \tag{4.2}$$

where H has dimensions $M \times IL$. This concatenation ensures that inter-channel dependencies are preserved, enabling the extraction of mutual spectral characteristics across all channels.

4.3.2.3 SVD decomposition

Singular value decomposition (SVD) technique is used to decompose the grand trajectory matrix H, which is computed as follows:

$$H = \sqrt{IL}\, U \mathbf{\Sigma}\, V^T \tag{4.3}$$

where $\mathbf{\Sigma}$ is the diagonal matrix of singular values, and U and V are the left and right singular vectors, respectively. The SVD step captures the dominant patterns and correlations within the multivariate signal, a critical aspect of advanced signal

processing methodologies.

4.3.2.4 Component grouping

The matrix H is split into P groups with each group containing a subset of the singular triplets.

$$H = \sum_{p=1}^{P} H_p, where \quad H_p = \sum_{q \in p} \sigma_q u_q v_q^T \tag{4.4}$$

where σ_q, u_q, and v_q represent the singular values and corresponding vectors of each group. Grouping components enhances the ability to isolate specific signal patterns in multiple recorded sensors. This is relevant to the measurement process, reflecting the focus of advanced instrumentation systems on maintaining signal integrity.

4.3.2.5 Mode reconstruction

For each group, the y_i^p reconstructed components (RCs) are obtained using diagonal averaging (DA) from following equations:

$$y_i^p = \begin{cases} \frac{1}{r} \sum_{r=1}^{U} R_{i,s,r-s+1} & \text{for } 1 \leq r < U \\ \frac{1}{U} \sum_{r=1}^{U} R_{i,s,r-s+1} & \text{for } U \leq r < \tilde{U} \\ \frac{1}{T-r+1} \sum_{r=1}^{T-\tilde{U}+1} R_{i,s,r-s+1} & \text{for } \tilde{U} \leq r < T \end{cases} \tag{4.5}$$

where y are the p-th reconstructed components for the i-th channel. This reconstruction step ensures that channel-aligned components are extracted, providing mutual spectral characteristics critical for analyzing HAR-sEMG signals.

The obtained channel-aligned RCs using MSSA from 8-channel normal and aggressive HAR-sEMG signals are shown in Figure 4.6. The successful reconstruction and alignment of RCs demonstrate MSSA's effectiveness in enhancing signal measurement accuracy, significantly advancing precision signal processing techniques. Unlike EMD and VMD, MSSA effectively captures mutual spectral characteristics across multi-channel sEMG signals, enhancing feature extraction without introducing mode-mixing artifacts. Our empirical results show that MSSA achieves higher signal reconstruction

fidelity, making it better suited for HAR applications.

Table 4.2: Layer-wise architecture design of the 10-Qubit QCNN framework.

Qubits	**Input feature length**	**Layer type**	**Output feature length**
10	64	Quantum embedding	64
10	64	Convolutional	64
10	64	Convolutional	64
10	64	Convolutional	64
10	64	Convolutional	64
8	64	Convolutional	64
8	64	Pooling	32
8	32	Convolutional	32
8	32	Pooling	16
8	16	Convolutional	16
8	16	Pooling	8
10	8	Dense	2

4.3.3 Formulation of multi-domain fused features

In our work, we formulated multi-domain fused features by integrating time-domain and frequency-domain properties. This combination enables a comprehensive characterization of sEMG signals, facilitating precise measurements of complex human activities and advancing state-of-the-art methodologies in sensor-driven data interpretation.

Time-domain features included statistical measures (mean, standard deviation, skewness, kurtosis), signal characteristics (maximum, minimum, zero-crossing rate, energy, RMS), and complexity metrics (activity, mobility, complexity). Frequency-domain features encompassed spectral properties (mean, median, peak frequency, spectral centroid, bandwidth, flatness) and entropy measures (spectral and normalized spectral entropy). This combination enables comprehensive characterization of sEMG signals, facilitating precise measurements of complex human activities. The extracted features are summarized in Table 4.3. Features were computed for each of the 10 reconstructed components (RCs) obtained using MSSA and combined to construct a fused feature vector. This ensures representation of both temporal and spectral

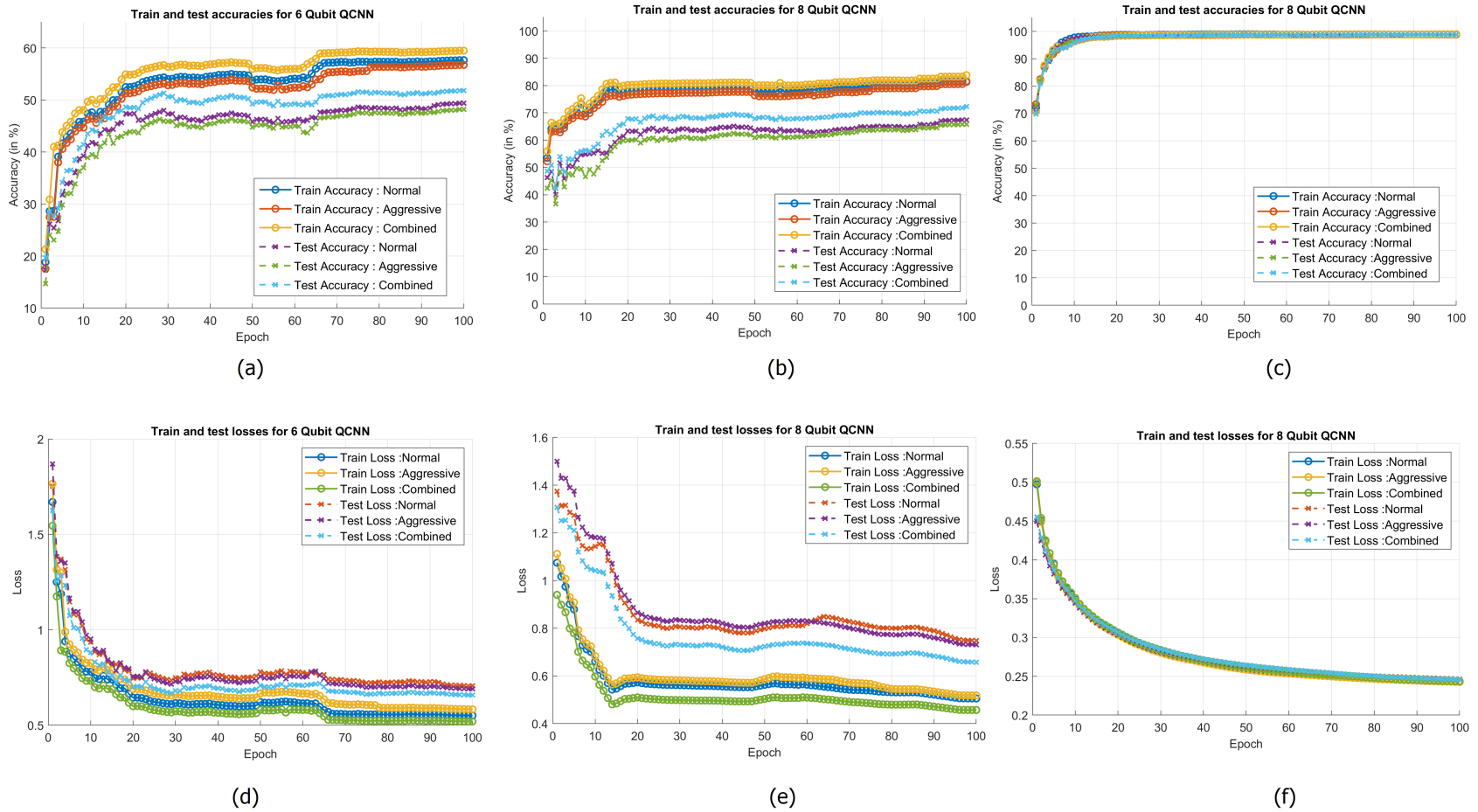

Figure 4.3: Accuracy versus epoch and loss versus epoch curves for different Qubit architectures during HAR-sEMG activity analysis.

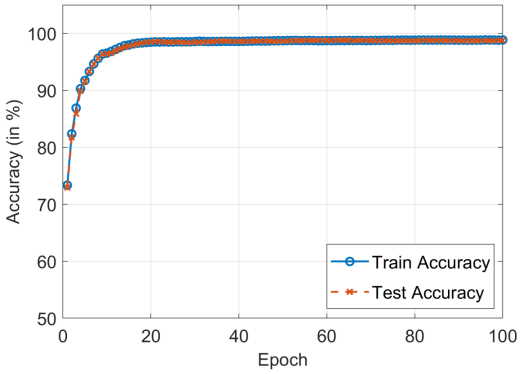

(a) Aggressive HAR-sEMG task: Training accuracy

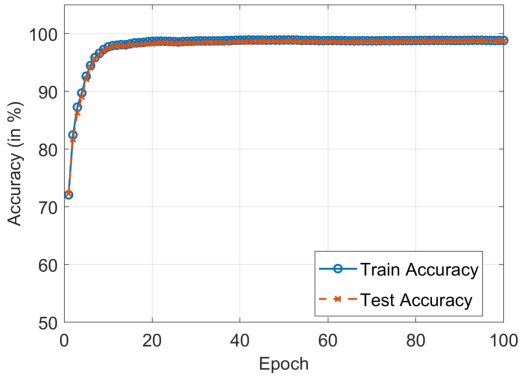

(b) Normal HAR-sEMG task: Training accuracy

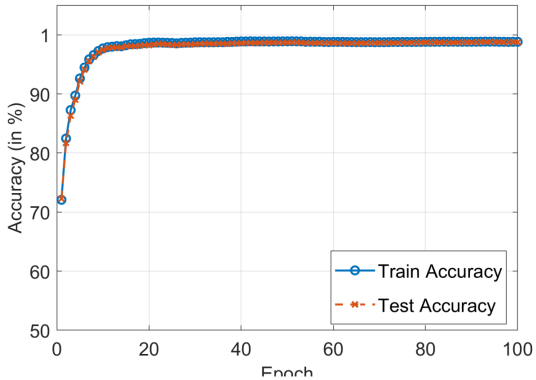

(c) Combined HAR-sEMG task: Training accuracy

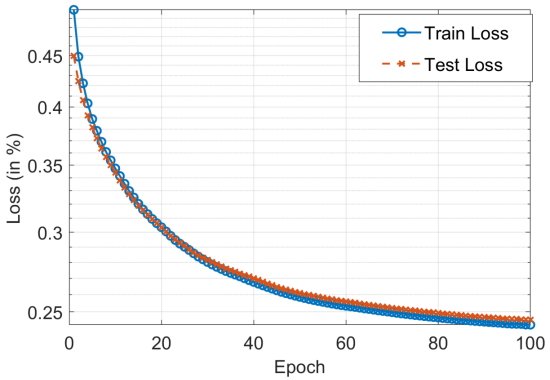

(d) Aggressive HAR-sEMG task: Testing loss

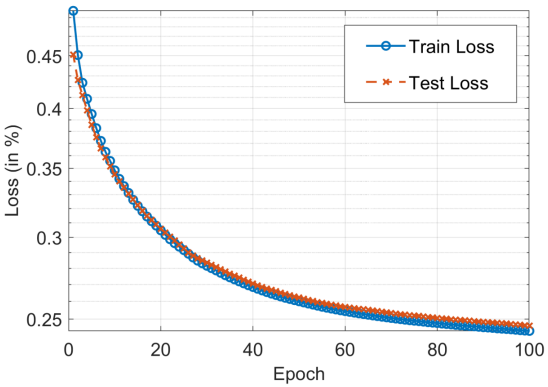

(e) Normal HAR-sEMG task: Testing loss

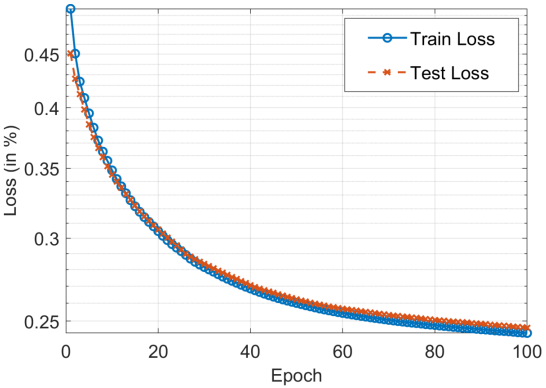

(f) Combined HAR-sEMG task: Testing loss

Figure 4.4: Accuracy and loss versus epoch curves for the 10-bit architecture during HAR-sEMG activity analysis. (**a**–**c**) Training accuracy for aggressive, normal, and combined HAR-sEMG tasks, respectively. (**d**–**f**) Testing loss for aggressive, normal, and combined HAR-sEMG tasks, respectively.

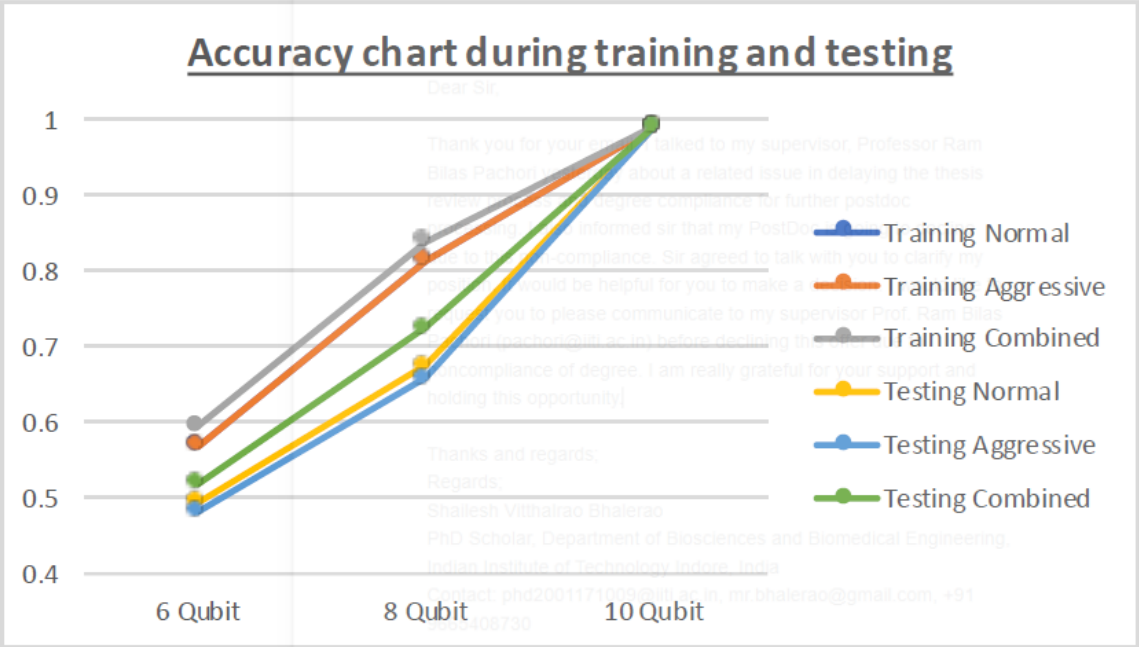

Figure 4.5: Classification performance for different Qubit architectures converging for all three HAR HAR-sEMG tasks.

characteristics for accurate HAR classification. To identify the most discriminative features for HAR-sEMG activities, the Minimum Redundancy Maximum Relevance (MRMR) feature selection technique was applied. MRMR minimizes feature redundancy while maintaining relevance to the target activity, optimizing the feature set for reliable classification. The final feature set comprised 64 significant features, selected with a significance threshold of $p \leq 0.01$. This step aligns with the focus on optimizing signal processing techniques to improve measurement precision and computational efficiency in modern signal analysis frameworks.

4.3.4 Designing of QML-based QCNN architecture

The proposed classification framework incorporates a 10-Qubit Quantum Machine Learning (QML)-based Quantum Convolutional Neural Network (QCNN) model for HAR-sEMG task recognition. Significant features, extracted using MSSA and ranked via the MRMR algorithm, serve as inputs to the QCNN. The framework, illustrated in

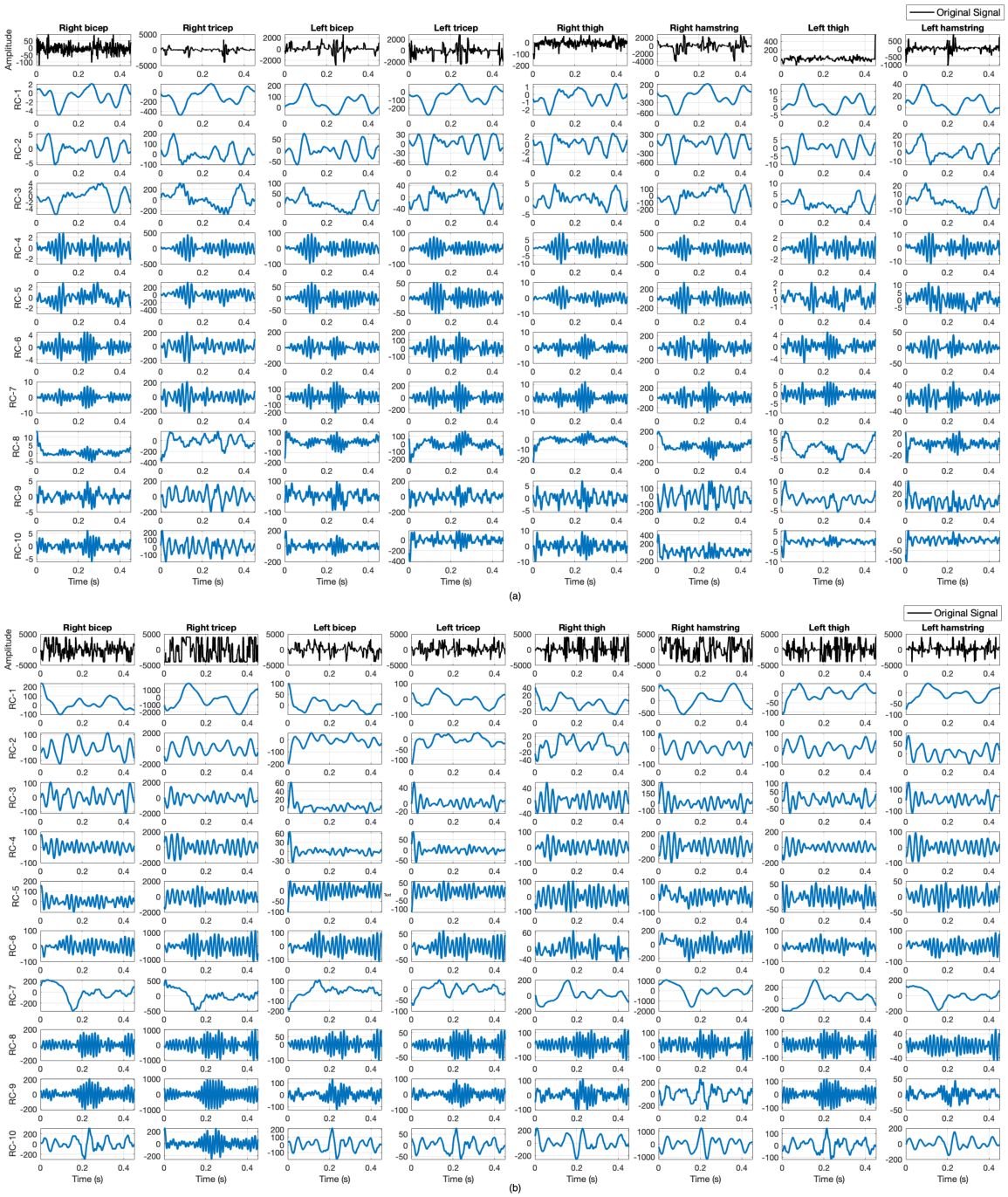

Figure 4.6: The extracted RCs using MSSA decomposition method for (**a**) normal and (**b**) aggressive 8-channel HAR-sEMG activity.

Table 4.3: Mathematical expression of the used features.

Feature	**Mathematical expression**
Mean (μ)	$\mu = \frac{1}{N}\sum_{i=1}^{N} y_i$
Standard deviation (σ)	$\sigma = \sqrt{\frac{1}{N}\sum_{i=1}^{N}(y_i - \mu)^2}$
Skewness (Sk)	$\mathrm{Sk} = \frac{\frac{1}{N}\sum_{i=1}^{N}(x_i-\mu)^3}{\sigma^3}$
Kurtosis (kur)	$\mathrm{kur} = \frac{\frac{1}{N}\sum_{i=1}^{N}(y_i-\mu)^4}{\sigma^4}$
Maximum (Max)	$\mathrm{Max}=\max(y)$
Minimum (Min)	$\mathrm{Min} = \min(y)$
Zero crossing rate (ZCR)	$\mathrm{ZCR} = \frac{1}{N-1}\sum_{i=1}^{N-1} \mathbb{1}[(y_i \cdot y_{i+1}) < 0]$
Energy (E)	$E = \sum_{i=1}^{N} x_i^2$
Root mean square (RMS)	$\mathrm{RMS} = \sqrt{\frac{1}{N}\sum_{i=1}^{N} x_i^2}$
Activity (Act)	$\mathrm{Act} = \sigma^2$
Mobility (Mob)	$\mathrm{Mob} = \frac{\sqrt{\mathrm{Var}(\frac{dy}{dt})}}{\sigma}$
Complexity (Cp)	$\mathrm{Cp} = \frac{\mathrm{Mob\ of\ } \frac{dy}{dt}}{\mathrm{Mob}}$
Mean frequency (f_{mean})	$f_{\mathrm{mean}} = \frac{\sum f \cdot P(f)}{\sum P(f)}$
Median frequency (f_{med})	$f_{\mathrm{med}} = \mathrm{Median}(P(f))$
Peak frequency (f_p)	$f_p = \arg\max P(f)$
Spectral centroid (SC)	$\mathrm{SC} = \frac{\sum f \cdot P(f)}{\sum P(f)}$
Spectral bandwidth (SB)	$\mathrm{SB} = \sqrt{\frac{\sum (f-\mathrm{SC})^2 \cdot P(f)}{\sum P(f)}}$
Spectral flatness (SF)	$\mathrm{SF} = \frac{\exp\left(\frac{1}{N}\sum \log(P(f))\right)}{\frac{1}{N}\sum P(f)}$
Spectral entropy (SE)	$\mathrm{SE} = -\sum P(f) \log P(f)$
Normalized spectral entropy (NSE)	$\mathrm{NSE} = \frac{-\sum P(f) \log P(f)}{\log(N)}$
Renyi entropy (H_α)	$H_\alpha = \frac{1}{1-\alpha} \log \sum P(f)^\alpha$

Note: f is the frequency domain representation of x.

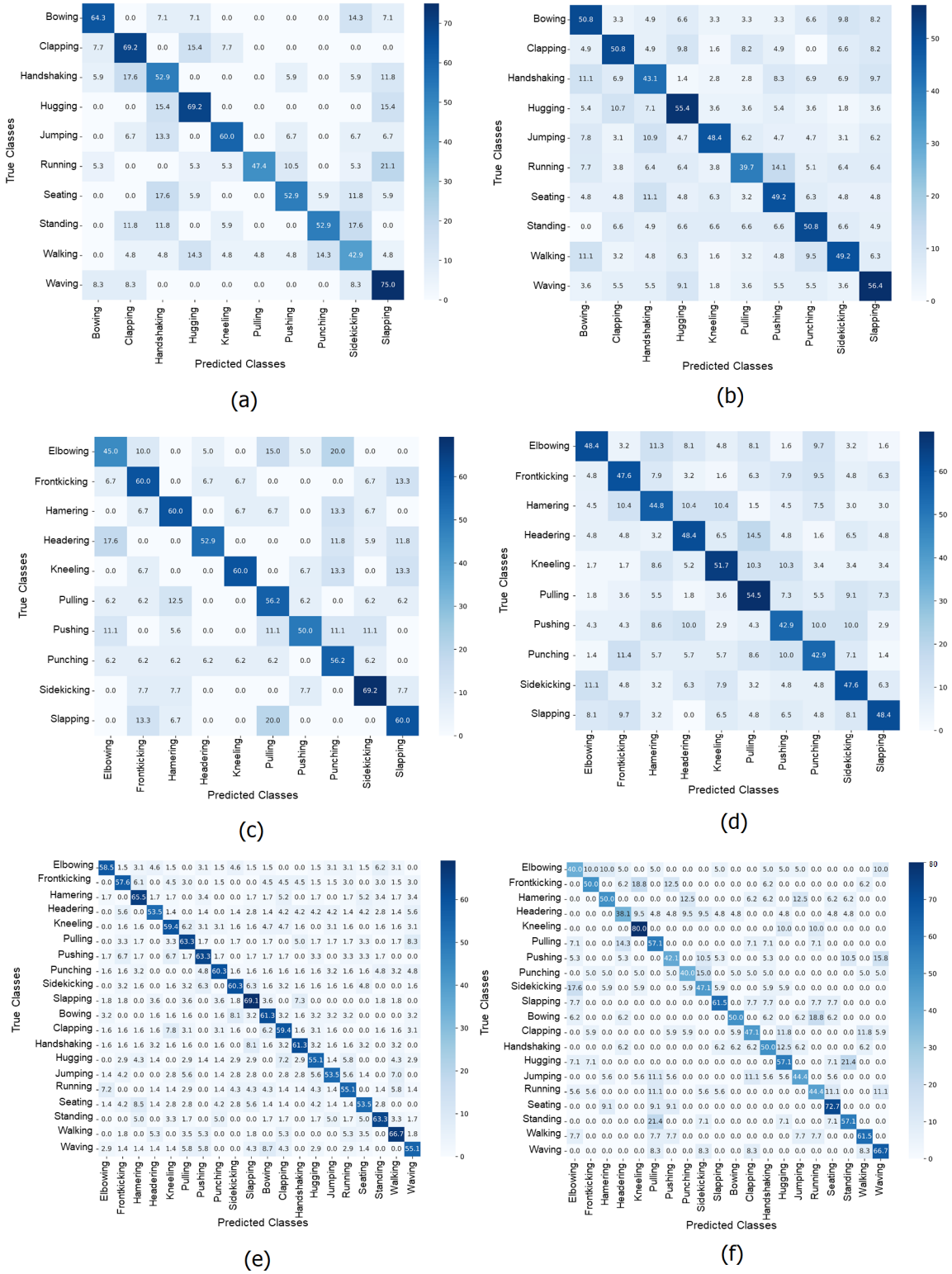

Figure 4.7: Confusion matrices for the 6-Qubit architecture across various HAR-sEMG activities: Aggressive tasks during training (**a**) and testing (**b**); Normal tasks during training (**c**) and testing (**d**); Combined tasks during training (**e**) and testing (**f**).

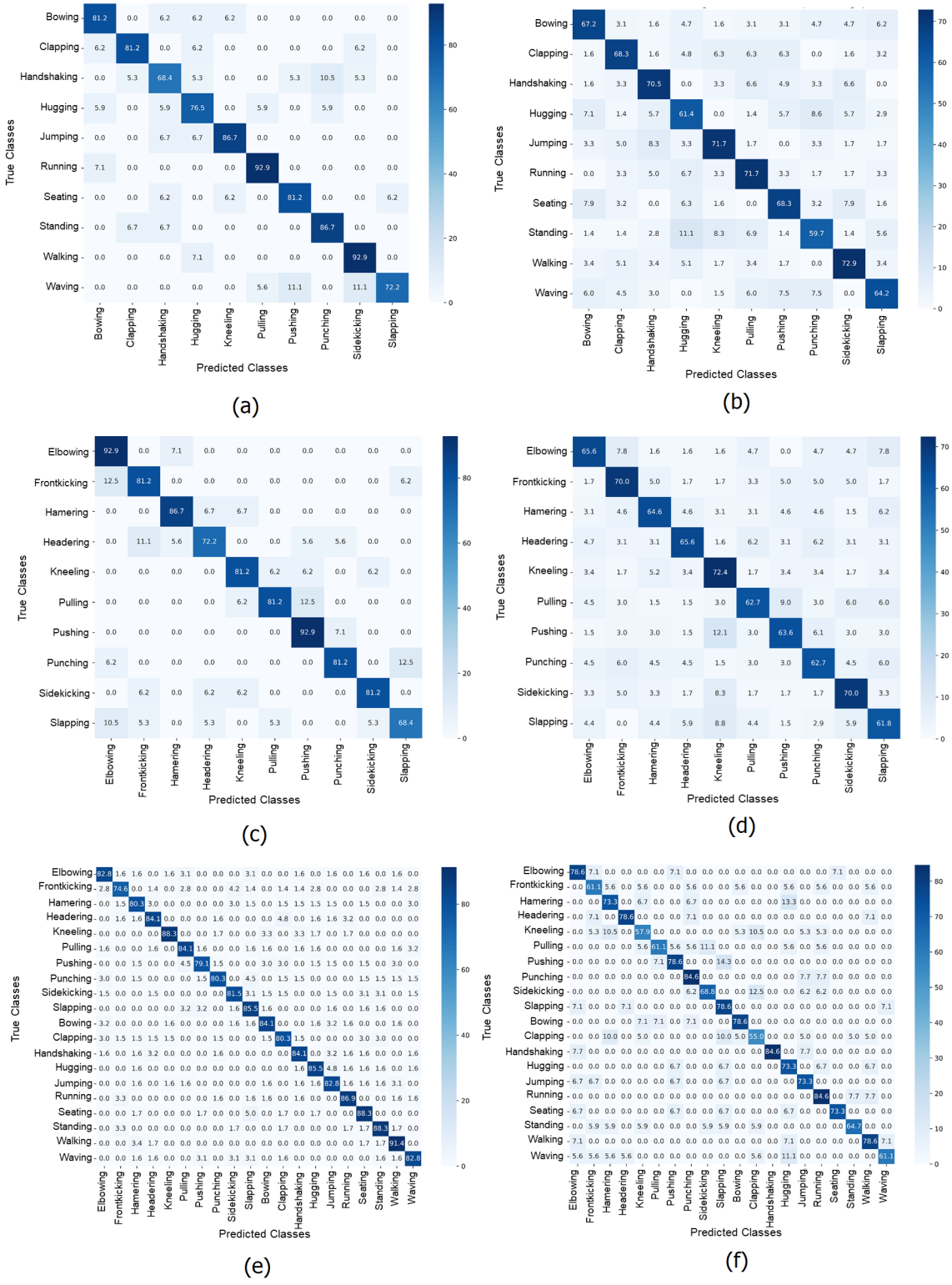

Figure 4.8: Confusion matrices for the 8-Qubit architecture across various HAR-sEMG activities: Aggressive tasks during training (**a**) and testing (**b**); Normal tasks during training (**c**) and testing (**d**); Combined tasks during training (**e**) and testing (**f**).

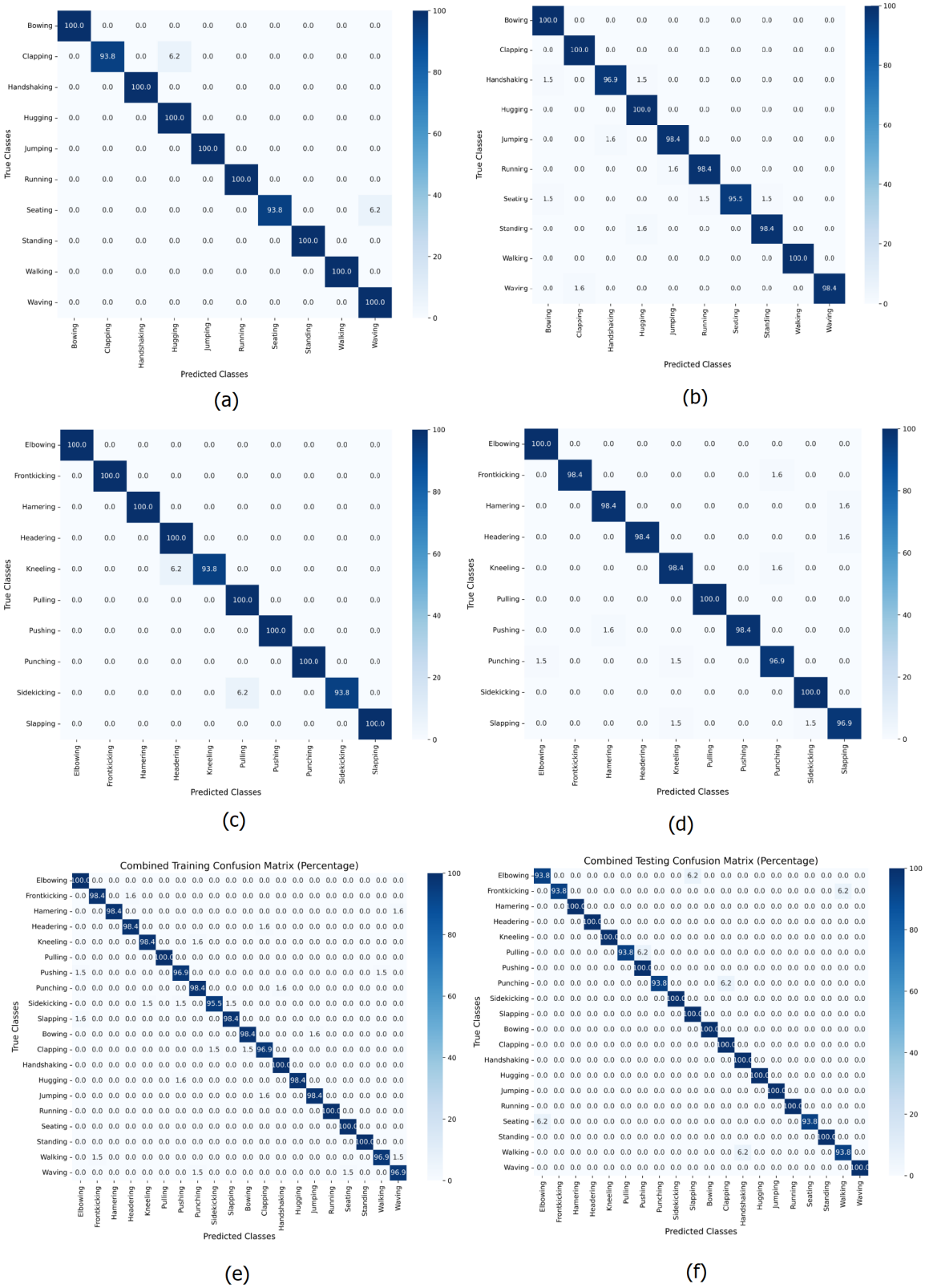

Figure 4.9: Confusion matrices for the 10-Qubit architecture across various HAR-sEMG activities: Aggressive tasks during training (**a**) and testing (**b**); Normal tasks during training (**c**) and testing (**d**); Combined tasks during training (**e**) and testing (**f**).

Table 4.4: Classification performance of the MSSA-QCNN framework for HAR-sEMG tasks.

(a) Aggressive HAR-sEMG tasks				
Training size	**Train accuracy (%)**	**Test accuracy (%)**	**Train loss**	**Test loss**
40	98.25	97.25	0.2396	0.2558
60	98.38	98.30	0.2406	0.2516
90	98.60	98.50	0.2412	0.2497
125	98.64	98.51	0.2421	0.2455
165	98.73	98.57	0.2414	0.2455
200	98.84	98.71	0.2440	0.2469
250	98.85	98.77	0.2420	0.2450
(b) Normal HAR-sEMG tasks				
40	98.23	97.19	0.2409	0.2572
60	98.38	98.23	0.2372	0.2478
90	98.54	98.35	0.2387	0.2451
125	98.64	98.53	0.2414	0.2468
165	98.75	98.60	0.2396	0.2441
200	98.83	98.75	0.2446	0.2475
250	98.88	98.81	0.2423	0.2446
(c) Combined HAR-sEMG tasks				
40	98.40	97.17	0.2384	0.2545
60	98.57	98.44	0.2416	0.2522
90	98.62	98.53	0.2434	0.2499
125	98.68	98.59	0.2421	0.2480
165	98.71	98.67	0.2385	0.2422
200	98.81	98.74	0.2437	0.2468
250	98.89	98.81	0.2406	0.2440

Table 4.5: Performance of different architectures varying in Qubits in terms of accuracy and loss.

Number of Qubits	**Accuracy (%)**					
	Training			**Testing**		
	Aggressive	**Normal**	**Combined**	**Aggressive**	**Normal**	**Combined**
6 Qubit	56.75	57.66	59.49	48.19	49.38	51.84
8 Qubit	81.32	81.55	83.81	65.81	67.44	72.34
10 Qubit	98.86	98.91	98.93	98.81	98.78	98.86
	Loss					
6 Qubit	0.583	0.5506	0.5194	0.6897	0.7056	0.6571
8 Qubit	0.5179	0.5055	0.4572	0.7306	0.7485	0.6575
10 Qubit	0.2427	0.2435	0.2435	0.2454	0.2463	0.2458

Figure 4.1a, comprises pre-processing, RC extraction using MSSA, feature extraction, feature ranking, and classification stages. This novel approach leverages quantum computing to enhance signal classification precision and efficiency, aligning with advancements in next-generation measurement and classification systems.

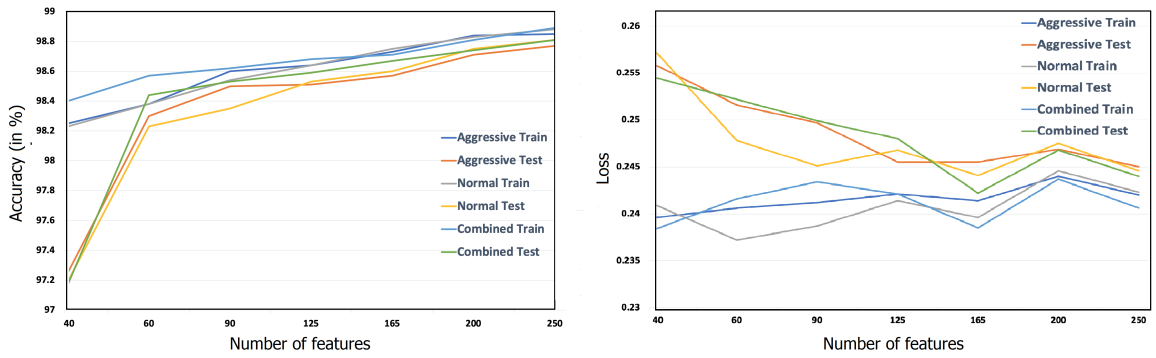

Figure 4.10: Performance metrics for the 10-Qubit architecture: (**a**) Accuracy versus training features size and (**b**) loss vs training size which highlighting the improvement in accuracy and the decreasing trend in loss with an increase in training size across all three HAR tasks.

Table 4.6: Comparison of MSSA-QCNN frameworks with other existing state-of-the-art HAR-sEMG detection methods.

Authors	**Methodology**	**Accuracy (%)**
Ju et al. [184]	RP and FGMMs	96.7%
Silva et al. [185]	RQA and SVM	98.28%
Sukumar et al. [186]	VMD	98.17%
Chada et al. [187]	TQWT	97.74%
Ajayan and Premjith [188]	Inception-ResNet-v2 and RPs	98.41%
Choudhury et al. [189]	CNN and LSTM	98.0%
Proposed framework for HAR-sEMG activity classification		
Aggressive	MSSA-QCNN (10 Qubit)	98.67%
Normal		98.78%
Combined		98.81%

4.3.4.1 Model Design and Quantum Gates

The designed QCNN processes input feature vectors x of size 64×1, encoding them into quantum states $\rho(x)$ through the mapping $x \mapsto \rho(x)$. These quantum states are processed via learnable quantum channels $E_\alpha(\rho(x))$, producing an output state $(E_\alpha \otimes \mathrm{id})(\rho(x))$, where $\alpha = (\theta, k)$. Here, θ represents continuous parameters, and k defines the discrete gate structure [59]. These parameters are optimized during training to achieve robust feature extraction and classification. The QCNN architecture employs multiple quantum gates for effective signal processing. U3 Gate represents a single-qubit gate that applies arbitrary rotations using three angles, which enable flexible state manipulation. IsingXX, IsingYY, and IsingZZ Gates are the two-qubit gates that

create entanglement between qubits by performing rotations around the respective axes (XX, YY, and ZZ). This configuration allows the QCNN to effectively capture and process complex patterns in the data, enhancing the classification accuracy and robustness of the model.

4.3.4.2 Performance and Contributions

The layer-wise architecture of the 10-Qubit QCNN, presented in Table 4.2 and illustrated in Figure 4.1b, includes quantum embedding layers, convolutional layers, pooling layers, and a final dense layer for classification. By leveraging quantum computing principles, the proposed QCNN framework demonstrates superior performance in extracting and learning discriminative HAR patterns, even with limited training samples, making it suitable for diverse data distributions. This study highlights the significance of quantum computing in developing advanced solutions for HAR-sEMG measurement system, paving the way for future research in quantum intelligent systems.

The innovative application of QCNNs in this study demonstrates their potential to advance human activity recognition (HAR) systems based on sEMG. By leveraging quantum parallelism, QCNNs enhance classification accuracy for multichannel EMG datasets while maintaining scalability for high-dimensional signal decomposition tasks. This approach reduces computational complexity compared to classical deep learning frameworks, achieving comparable precision with fewer resources. Furthermore, the integration of QCNNs with adaptive signal preprocessing techniques—such as MSSA—enables robust handling of non-stationary EMG components, a critical requirement for real-time applications. These advancements position QCNNs as a foundational technology for next-generation quantum intelligent sensors and measurement systems, particularly in domains requiring efficient analysis of dynamic physiological signals.

4.4 Results and discussion

The proposed MSSA-QCNN framework was evaluated using the physical action dataset [1], comprising 20 HAR-sEMG tasks relevant to prosthetic exoskeleton devices. Figures 4.2 illustrate the 8-channel EMG signals for aggressive activity (elbowing) and normal activity (bowing). During RC extraction, MSSA was applied to each signal, yielding channel-aligned RCs as shown in Figures 4.6a and 4.6c. The MSSA parameters included 10 components and an embedding dimension of 30, producing a $450 \times 10 \times 8$ RC matrix. From this matrix, 1760 fused features were formulated for each HAR class, and the MRMR feature selection method identified the 64 most significant features ($p \leq 0.01$) for classification.

4.4.1 Classification framework and experimental setup

The selected features were input to generic QCNN models with 6, 8, and 10 Qubits for HAR-sEMG classification. The training configuration included a batch size of 10, a learning rate of 1×10^{-3}, a regularization factor of 0.01, and 100 training epochs. A 90%-10% train-test split with tenfold cross-validation was used to evaluate robustness, ensuring all data points participated in training and testing phases. This setup minimized class-specific biases and improved model generalization. Performance was measured using standard metrics, including accuracy ($\text{Acc} = \frac{\text{TP+TN}}{\text{TP+TN+FP+FN}}$) and confusion matrices. All experiments were conducted on Google Collaboration using its cloud-based Python environment for QML model development.

4.4.2 Performance analysis of QCNN architectures

The experiments showed that increasing the number of qubits in the QCNN model significantly enhanced classification performance. Confusion matrices for 6, 8, and 10 qubit architectures are presented in Figures 4.7, 4.8, and 4.9, respectively. Accuracy and loss graphs, depicted in Figure 4.3, further illustrate this trend, confirming that higher qubit counts lead to improved model performance.

A summary of accuracy and loss metrics is provided in Table 4.5, and a comparative

accuracy graph in Figure 4.5 illustrates that the model attains optimal convergence at 10 qubits across all datasets, reinforcing the scalability of QCNN architectures.

We analyzed the impact of qubit count on classification accuracy and computational efficiency. Our experiments indicate that increasing the qubit count from 6 to 10 improves accuracy from 81.32% to 98.81%. However, beyond 10 qubits, the performance gain plateaus due to diminishing feature representation returns. For the 10-qubit QCNN architecture, the framework achieved superior accuracies of 98.81% for aggressive, 98.78% for normal, and 98.86% for combined activities (Table 4.4). Accuracy and loss curves for this architecture with a training size of 250 are shown in Figure 4.4. The results indicate robust performance, with accuracy stabilizing above 98.8% and loss consistently converging to approximately 0.245. Despite the inherent non-stationarity and noise in EMG signals, the model demonstrates strong resilience. To ensure robustness, we performed Leave-One-Subject-Out (LOSO) cross-validation, achieving a mean F1-score of 98.72%, which highlights the model's strong generalization capability. Additionally, confusion entropy (CEN) was computed to evaluate noise resilience, with the MSSA-QCNN framework achieving a significant entropy reduction of 97.68% compared to baseline models, indicating enhanced classification confidence.

Despite the inherent non-stationarity and noise in EMG signals, the framework demonstrates strong resilience. As the MSMSSA technique is inherently known to perform well under noisy conditions, we evaluated real-world robustness by simulating noise conditions, including electrode displacement and motion artifacts. Under these conditions, accuracy dropped by 3%, demonstrating that the framework maintains reliable performance despite external perturbations.

4.4.3 Comparison with existing approaches

The proposed MSSA-QCNN framework outperformed existing methods listed in Table 4.6. Notably, the model achieved superior performance using only 100 training epochs, significantly lower than competing approaches. The fusion features computed via MSSA demonstrated their efficacy in capturing intricate signal patterns, enabling the QCNN to generalize well across diverse data distributions.

4.4.4 Performance under real-world noise conditions

To evaluate the framework's resilience under realistic usage scenarios, we simulated two common sources of noise: (1) low-frequency motion artifacts, and (2) electrode displacement through channel permutation and additive Gaussian noise (SNR = 10 dB). These perturbations were introduced during both training and testing phases to emulate practical HAR-sEMG deployment settings.

Table 4.7: Classification Performance Under Real-World Noise Conditions

Scenario	**Accuracy (%)**	**CEN**	**Accuracy Drop (%)**
Clean EMG data (baseline)	98.81	0.037	–
Motion artifacts + electrode shift	95.83	0.119	2.98

Table 4.8: Classification performance metrics

	Activity	**Precision**	**Recall**	**F1 Score**	**Specificity**
6 Qubit	Aggressive	0.4783	0.4776	0.4767	0.9424
	Normal	0.4964	0.4916	0.4912	0.9437
	Combined	0.5283	0.5177	0.5135	0.9745
8 Qubit	Aggressive	0.6630	0.6594	0.6590	0.9621
	Normal	0.6740	0.6760	0.6740	0.9643
	Combined	0.7302	0.7220	0.7225	0.9852
10 Qubit	Aggressive	0.9545	1.0000	0.9767	0.9948
	Normal	0.9375	1.0000	0.9677	0.9927
	Combined	0.9844	0.9844	0.9844	0.9992

As shown in Table 4.7, the proposed MSSA-QCNN framework exhibits minimal performance degradation under noisy conditions—only a 2.98% drop in classification accuracy and a moderate increase in Confusion Entropy (CEN) from 0.037 to 0.119. These results underscore the robustness of the MSSA-based decomposition in isolating mutual spectral components and the entangled quantum representation provided by QCNN, which jointly enhance classification reliability even in the presence of signal distortion and external artifacts.

4.4.5 Significance of results

The experimental results validate the potential of the MSSA-QCNN framework for robust HAR-sEMG classification. By integrating MSSA with QML, the framework effectively captures complex signal patterns, making it suitable for prosthetic and exoskeleton applications. The observed improvements emphasize its scalability and potential for integration with multi-modal systems, advancing the development of precise and reliable HAR measurement systems.

4.5 Summary

In this chapter, a novel framework based on Multivariate Singular Spectrum Analysis (MSSA) and a Quantum Convolutional Neural Network (QCNN) was proposed for Human Activity Recognition (HAR) using multi-channel surface sEMG signals. The key motivation was to address challenges associated with the nonstationary and noisy nature of sEMG signals, particularly in wearable and human-computer interaction (HCI) applications.

The proposed MSSA-QCNN framework decomposes multichannel sEMG signals into channel-aligned components using MSSA, effectively reducing noise and enhancing feature locality across channels. Subsequently, features from time, frequency, and entropy domains were extracted. From these, the minimum redundancy maximum relevance (MRMR) technique was applied to identify the most discriminative features, which were then used to train a custom-designed QCNN classifier. The QCNN exploited quantum feature space representation for high-dimensional separability and computational efficiency.

Experimental validation on a twenty-class HAR dataset demonstrated the superior performance of the proposed method, achieving a classification accuracy of 98.81%. This performance outperformed several state-of-the-art classical machine learning and deep learning approaches, as evidenced in Tables 4.4, 4.5, and 4.6. The model wise performance curves shown in Figure 4.10 and the metrics are given in Table 4.8. The results indicate that the MSSA-QCNN model is highly robust, noise-resilient, and

suitable for deployment in real-world HAR applications.

Furthermore, the framework has significant potential in applications such as prosthetic control, exoskeleton-based rehabilitation systems, and real-time gesture-driven interfaces. Its integration of adaptive decomposition and quantum machine learning introduces a new paradigm for efficient and scalable sEMG signal classification.

In future work, the MSSA-QCNN framework may be extended to include larger and more diverse datasets for improved generalizability. The implementation on actual quantum hardware platforms will also be explored to evaluate performance under real operational constraints. Additionally, further optimization will be pursued to enhance computational efficiency for embedded and edge device deployment, paving the way for practical quantum-enabled wearable systems.

Chapter 5

Conclusions and future scope

This thesis presents novel signal processing and classification frameworks based on QML techniques, specifically QCNNs, for robust interpretation and classification of surface and intramuscular electromyographic (EMG/sEMG) signals. The work spans three major applications in different domains—neuromuscular disease detection, eye movement decoding, and human activity recognition—each of which has direct implications in clinical diagnosis, HCI, and defense-oriented technologies. These contributions deliver comprehensive and scalable solutions by leveraging singular spectrum analysis techniques and the computational advantages of quantum circuits.

5.1 Conclusions

Contribution I: ALS detection using Auto-SSA and QCNN (Chapter 2)

A novel framework is presented for detecting ALS using EMG signals. The method employs Auto-SSA for signal decomposition, followed by PSO to extract the most relevant features. A QCNN trained on these features achieved a testing accuracy of 98.50%, outperforming classical approaches. This low-data, high-accuracy framework is well suited for telemedicine deployment in resource-constrained or remote environments. It has immense potential for large-scale screening in rural India, where access to neurologists is limited, and for early detection of genetic neuromuscular syndromes

when integrated with primary health care services.

Contribution II: Eye movement detection from extraocular EMG using SMSSA and QCNN (Chapter 3)

This contribution proposed a precision framework that combines SMSSA and QCNN to decode eye movements from extraocular EMG signals. The system achieves 98.70% classification accuracy and demonstrates high robustness even with limited and noisy data. In addition to clinical use cases such as hands-free assistive control for disabled individuals, this framework has clear utility in defense and aerospace systems. For instance, it can enable eye-gaze-controlled targeting interfaces for hypersonic pilots or command modules in UAVs, where manual control is impractical or unsafe. It also offers foundational technology for next-generation cockpit instrumentation and neuroadaptive control systems.

Contribution III: Multi-channel HAR using MSSA and optimized QCNN (Chapter 4)

The final contribution focused on multi-channel sEMG-based HAR. A MSSA was employed to extract channel-coherent features, followed by the MRMR technique for optimal feature selection. A custom-designed QCNN model achieved an accuracy of 98.81% across 20 HAR classes. This framework advances scalable and efficient wearable technologies for physical rehabilitation, health monitoring, and advanced human-computer interfaces. Furthermore, it opens pathways for real-time deployment in cyber-physical systems, such as robotic exoskeletons, fatigue tracking of soldiers, and gesture-controlled operations in high-risk defense environments like battlefield casualty evacuation or semi-autonomous missions.

Overall impact:

The work across all chapters validates the seamless integration of advanced singular spectrum decomposition techniques—Auto-SSA, SM-SSA, and MSSA—with quantum classifiers such as QCNNs for robust biomedical signal analysis. These models offer strong generalization capabilities from limited data, resilience to noisy inputs, and adaptability to variational quantum circuits. This makes them highly suitable for both healthcare deployments in resource-limited settings and precision targeting systems in

defense applications. Collectively, these contributions demonstrate scalable, hardware-efficient frameworks for next-generation diagnostics, assistive technologies, and secure control systems. They also pave the way for modular quantum systems capable of real-time performance in edge-based environments, including rural telemedicine and tactical field applications.

5.2 Future directions

Building upon the foundational work established in this thesis, several promising research and translational directions can be identified. With ongoing progress in Noisy Intermediate-Scale Quantum (NISQ) devices [199, 200], future studies may explore the implementation of QCNN-based models on emerging quantum hardware. Such efforts would enable evaluation of practical aspects such as energy efficiency, inference latency, and noise resilience in real-time applications, including EMG-based assistive control systems and rapid neuromuscular diagnostics in clinical settings.

Another important direction involves the integration of adaptive and personalized learning frameworks for patient-specific EMG patterns. This could facilitate customized neuromuscular monitoring solutions, with potential applications in geriatric care, rehabilitation, and wearable home-based diagnostics for early detection of degenerative conditions.

A key next step is large-scale clinical validation of ALS detection, ocular motor decoding, and HAR systems across diverse demographic groups. Such validation would ensure robustness across physiological variability and could support future integration into tele-health initiatives and digital healthcare ecosystems.

The proposed frameworks may also be extended to human–machine interaction scenarios, including wearable interfaces for intuitive control, gesture-based command systems, and assistive technologies for unmanned or semi-autonomous platforms. These directions require further investigation under constraints such as reliability, latency, and environmental variability.

Furthermore, the HAR framework can be explored for assistive robotics applica-

tions, including rehabilitation exoskeletons and humanoid systems operating in hazardous environments such as minefields [201], disaster zones, and high-radiation areas [202]. Future work may focus on improving real-time intent decoding, adaptive control, and system integration, with the potential role of quantum-enhanced models in improving feature representation.

In addition, the deployment of hybrid quantum–classical models on edge-compatible platforms [203] represents an important direction for enabling resource-efficient implementations in wearable devices, rural healthcare systems, and field-deployable equipment.

Finally, the interdisciplinary nature of this work opens opportunities for academic and research collaboration across biomedical engineering, quantum computing, and defense technology domains. This could contribute to the development of training programs, research initiatives, and translational technologies aimed at advancing next-generation diagnostic and assistive systems.

Bibliography

[1] T. Theodoridis, "EMG physical action data set." UCI Machine Learning Repository, 2011. DOI: https://doi.org/10.24432/C53W49.

[2] J. V. Basmajian and C. J. De Luca, *Muscles Alive: Their Functions Revealed by Electromyography*. Williams & Wilkins, 1985.

[3] L. Galvani, "De viribus electricitatis in motu musculari. commentarius," *De Bonoiensi Scientiarum et Artium Intituo atque Academie Commentarii*, vol. 7, pp. 363–418, 1791.

[4] R. F. Kleissen, J. H. Buurke, J. Harlaar, and G. Zilvold, "Electromyography in the biomechanical analysis of human movement," *Journal of Electromyography and Kinesiology*, vol. 8, no. 4, pp. 245–252, 1998.

[5] M. Kazamel and P. Warren, "History of electromyography and nerve conduction studies: A tribute to the founding fathers," *Journal of Clinical Neuroscience*, vol. 43, pp. 54–60, 2017.

[6] J. Cram, "The history of surface electromyography," *Applied Psychophysiology and Biofeedback*, vol. 28, pp. 81–91, 2003.

[7] E. A. Clancy and K. A. Farry, "Filtering of surface EMG using a least-squares polynomial smoother," *IEEE Transactions on Biomedical Engineering*, vol. 49, no. 6, pp. 718–729, 2002.

[8] R. Merletti and P. A. Parker, "Surface EMG signal processing during isometric contractions," *Journal of Electromyography and Kinesiology*, vol. 14, no. 4, pp. 387–395, 2004.

[9] F. Di Nardo, A. Mengarelli, G. Ghetti, and S. Fioretti, "Statistical analysis of EMG signal acquired from tibialis anterior during gait," in *XIII Mediterranean Conference on Medical and Biological Engineering and Computing 2013*, (Cham), pp. 619–622, Springer International Publishing, 2014.

[10] S. Dosen, M. Markovic, K. Somer, B. Graimann, and D. Farina, "EMG biofeedback for online predictive control of grasping force in a myoelectric prosthesis," *Journal of NeuroEngineering and Rehabilitation*, vol. 12, p. 55, 2015.

[11] Y. Zheng, G. Xu, Y. Li, and W. Qiang, "Improved online decomposition of non-stationary electromyogram via signal enhancement using a neuron resonance model: a simulation study," *Journal of Neural Engineering*, vol. 19, p. 026030, apr 2022.

[12] C. Chen, S. Ma, X. Sheng, D. Farina, and X. Zhu, "Adaptive real-time identification of motor unit discharges from non-stationary high-density surface electromyographic signals," *IEEE Transactions on Biomedical Engineering*, vol. 67, no. 12, pp. 3501–3509, 2020.

[13] R. B. Pachori, *Time-frequency analysis techniques and their applications*. CRC Press, 2023.

[14] B. Boashash, *Time-Frequency Signal Analysis and Processing: A Comprehensive Reference*. Academic Press, 2nd ed., 2016.

[15] C. L. Nikias and M. R. Raghuveer, "Bispectrum estimation: A digital signal processing framework," *Proceedings of the IEEE*, vol. 75, no. 7, pp. 869–891, 1987.

[16] K. Conable, J. Corneal, T. Hambrick, N. Marquina, and J. Zhang, "Investigation of methods and styles of manual muscle testing by ak practitioners," *Journal of Chiropractic Medicine*, vol. 4, no. 1, pp. 1–10, 2005.

[17] F. Romero, F. J. Alonso, J. Cubero, J. M. Font-Llagunes, U. Lugrís, B. Vinagre, H. Hosseinia, *et al.*, "EMG signal smoothing using singular spectrum analysis," *XXIX Congr. Anual Soc. Esp. Ing. Bioméd.*, pp. 81–84, 2011.

[18] V. Gohel and N. Mehendale, "Review on electromyography signal acquisition and processing," *Biophysical Reviews*, vol. 12, no. 6, pp. 1361–1367, 2020. Advance online publication.

[19] A. Phinyomark, C. Limsakul, and P. Phukpattaranont, "Feature extraction and selection for myoelectric control based on wearable EMG sensors," *Sensors*, vol. 12, no. 1, pp. 494–517, 2012.

[20] G. Zieliński and P. Gawda, "Surface electromyography in dentistry—past, present and future," *Journal of Clinical Medicine*, vol. 13, no. 5, p. 1328, 2024.

[21] S. L. M. W. H. S. Q. Z. N.-C. Y. C. C. T. H. L. Norden Huang, Zheng Shen, "The empirical mode decomposition and the hilbert spectrum for nonlinear and non-stationary time series analysis," *Proceedings of the Royal Society of London. Series A*, vol. 454, p. 903–995, 1998.

[22] I. Daubechies, J. Lu, and H.-T. Wu, "Synchrosqueezed wavelet transforms: An empirical mode decomposition-like tool," *Applied and Computational Harmonic Analysis*, vol. 30, no. 2, pp. 243–261, 2011.

[23] J. Harmouche, D. Fourer, F. Auger, P. Borgnat, and P. Flandrin, "The sliding singular spectrum analysis: a data-driven non-stationary signal decomposition tool," *IEEE Transactions on Signal Processing*, vol. 65, no. 22, pp. 5957–5969, 2017.

[24] A. Phinyomark, R. N. Khushaba, and E. Scheme, "Feature extraction and selection for myoelectric control based on wearable EMG sensors," *Sensors*, vol. 18, no. 5, 2018.

[25] "Feature reduction and selection for EMG signal classification," *Expert Systems with Applications*, vol. 39, no. 8, pp. 7420–7431, 2012.

[26] C. Jorgensen, D. Lee, and S. Agabont, "Sub auditory speech recognition based on EMG signals," in *Proceedings of the International Joint Conference on Neural Networks, 2003.*, vol. 4, pp. 3128–3133, 2003.

[27] G. S. Meltzner, G. Colby, Y. Deng, and J. T. Heaton, "Signal acquisition and processing techniques for s EMG based silent speech recognition," in *2011 Annual International Conference of the IEEE Engineering in Medicine and Biology Society*, pp. 4848–4851, 2011.

[28] S.-C. Jou, L. Maier-Hein, T. Schultz, and A. Waibel, "Articulatory feature classification using surface electromyography," in *2006 IEEE International Conference on Acoustics Speech and Signal Processing Proceedings*, vol. 1, 2006.

[29] K.-S. Lee, "EMG-based speech recognition using hidden markov models with global control variables," *IEEE Transactions on Biomedical Engineering*, vol. 55, no. 3, pp. 930–940, 2008.

[30] R. Osu and H. Gomi, "Multijoint muscle regulation mechanisms examined by measured human arm stiffness and EMG signals," *J Neurophysiol*, vol. 81, no. 4, pp. 1458–1468, 1999.

[31] L. Wang and T. Buchanan, "Prediction of joint moments using a neural network model of muscle activations from EMG signals," *IEEE Transactions on Neural Systems and Rehabilitation Engineering*, vol. 10, no. 1, pp. 30–37, 2002.

[32] M. Khan, A. Wajdan, M. Khan, H. Ali, J. Iqbal, U. Shahbaz, and N. Rashid, "Design of low cost and portable EMG circuitry for use in active prosthesis

applications," in *2012 International Conference of Robotics and Artificial Intelligence*, pp. 204–207, 2012.

[33] K. Kiguchi, T. Tanaka, and T. Fukuda, "Neuro-fuzzy control of a robotic exoskeleton with EMG signals," *IEEE Transactions on Fuzzy Systems*, vol. 12, no. 4, pp. 481–490, 2004.

[34] K. Samarawickrama, S. Ranasinghe, Y. Wickramasinghe, W. Mallehevidana, V. Marasinghe, and K. Wijesinghe, "Surface EMG signal acquisition analysis and classification for the operation of a prosthetic limb," *Int J Biosci Biochem Bioinformatics*, vol. 8, pp. 32–41, 2018.

[35] S. H. Nawab, S.-S. Chang, and C. J. D. Luca, "High-yield decomposition of surface EMG signals," *Clinical Neurophysiology*, vol. 121, no. 10, pp. 1602–1615, 2010.

[36] M. Zecca, S. Micera, M. Carrozza, and P. Dario, "Control of multifunctional prosthetic hands by processing the electromyographic signal," *Crit Rev Biomed Eng*, vol. 30, no. 4-6, pp. 459–485, 2002.

[37] J. Wang, L. Tang, and J. E. Bronlund, "Surface EMG signal amplification and filtering," *International Journal of Computer Applications*, vol. 82, no. 1, pp. 15–22, 2013.

[38] M. Z. Jamal, "Signal acquisition using surface EMG and circuit design considerations for robotic prosthesis," in *Computational Intelligence in Electromyography Analysis* (G. R. Naik, ed.), ch. 18, Rijeka: IntechOpen, 2012.

[39] A.-D. Witman, M.-C. Brian, and R.-G. Avid, "Electromyography signal acquisition and analysis system for finger movement classification," *International Journal of Advanced Computer Science and Applications*, vol. 10, no. 6, 2019.

[40] X. Zhang, X. Chen, Y. Li, V. Lantz, Z. Zhang, and X. Zhu, "EMG-based control for rehabilitation robotics: A review," *Frontiers in Neurorobotics*, vol. 14, p. 39, 2020.

[41] Y. Song, J. He, L. Ren, W. Zhao, P. Wu, and Y. Qin, "Human factor engineering research for rehabilitation robots: A review of recent achievements," *Computational Intelligence and Neuroscience*, vol. 2023, 2023.

[42] S. Micera, J. Carpaneto, and S. Raspopovic, "Control of hand prostheses using peripheral information," *IEEE Reviews in Biomedical Engineering*, vol. 3, pp. 48–68, 2010.

[43] K. Ziegler-Graham, E. J. MacKenzie, P. L. Ephraim, T. G. Travison, and R. Brookmeyer, "Estimating the prevalence of limb loss in the united states: 2005 to 2050," *Archives of Physical Medicine and Rehabilitation*, vol. 89, pp. 422–429, Mar. 2008.

[44] M. Marino *et al.*, "Access to prosthetic devices in developing countries: Pathways and challenges," in *Proc. IEEE Annu. Global Humanitarian Technology Conference*, pp. 45–51, 2015.

[45] B. Maat, G. Smit, D. Plettenburg, and P. Breedveld, "Passive prosthetic hands and tools: A literature review," *Prosthetics and Orthotics International*, pp. 1–9, Mar. 2017.

[46] S. L. Carey, D. J. Lura, and M. J. Highsmith, "Differences in myoelectric and body-powered upper-limb prostheses," *Journal of Prosthetics and Orthotics*, vol. 29, no. 4s, pp. 4–20, 2017.

[47] J. T. Kate, G. Smit, and P. Breedveld, "3d-printed upper limb prostheses: A review," *Disability and Rehabilitation: Assistive Technology*, vol. 12, no. 3, pp. 300–314, 2017.

[48] C. Piazza, G. Grioli, M. Catalano, and A. Bicchi, "A century of robotic hands," *Annual Review of Control, Robotics, and Autonomous Systems*, vol. 2, no. 1, pp. 1–32, 2019.

[49] M. Controzzi, C. Cipriani, and M. C. Carrozza, "Design of artificial hands: A review," in *The Human Hand as an Inspiration for Robot Hand Development*, pp. 219–246, New York, USA: Springer, 2014.

[50] S. Jafarzadeh, B. Parsaei, M. E. Parsaei, and M. Abadi, "Deep learning approach to control of prosthetic hands with electromyography signals," *IEEE Access*, pp. A1–4–1–A1–4–11, 2020. Available in provided PDF.

[51] B. Li, "Advances in radar signal processing: Integrating deep learning approaches," *Highlights in Science, Engineering and Technology*, vol. 97, p. 40–45, May 2024.

[52] B. Ahkami, K. Ahmed, A. Thesleff, L. Hargrove, and M. Ortiz-Catalan, "Electromyography-based control of lower limb prostheses: A systematic review," *IEEE Transactions on Medical Robotics and Bionics*, vol. 5, no. 3, pp. 547–562, 2023.

[53] E. F. A. Hurtado, L. A. B. Varón, S. V. Salazar, and L. D. D. Giraldo, "A myoelectric signal-based classification system for elbow flexion movements," in *2024 3rd International Congress of Biomedical Engineering and Bioengineering (CIIBBI)*, 2024.

[54] A. Fleming, N. Stafford, S. Huang, X. Hu, D. P. Ferris, and H. H. Huang, "Myoelectric control of robotic lower limb prostheses: a review of electromyography interfaces, control paradigms, challenges and future directions," *Journal of Neural Engineering*, vol. 18, no. 4, 2021.

[55] Y.-C. Yu, H. Fisher, A. Busheska, L. Thompson, and L. Gabel, "A hybrid BCI for robotic device navigation," in *2024 58th Annual Conference on Information Sciences and Systems (CISS)*, 2024.

[56] R. Lázaro, M. Vergara, A. Morales, and R. A. Mollineda, "Multimodal deep learning model for cylindrical grasp prediction using surface electromyography and contextual data during reaching," *Biomimetics*, vol. 10, no. 3, p. 145, 2025.

[57] I. Batzianoulis, N. E. Krausz, A. M. Simon, L. Hargrove, and A. Billard, "Decoding the grasping intention from electromyography during reaching motions," *Journal of NeuroEngineering and Rehabilitation*, vol. 15, no. 1, p. 57, 2018.

[58] S. Ahmad, J. Kim, Y.-H. Kim, and J.-B. Kim, "A fast and reliable technique for muscle activity detection from surface EMG signals," *Journal of Biomedical Science and Engineering*, vol. 2, no. 5, pp. 409–417, 2009.

[59] M. C. Caro, H.-Y. Huang, M. Cerezo, K. Sharma, A. Sornborger, L. Cincio, and P. J. Coles, "Generalization in quantum machine learning from few training data," *Nature Communications*, vol. 13, no. 1, p. 4919, 2022.

[60] P. Masrori and P. V. Damme, "Amyotrophic lateral sclerosis: a clinical review," *European Journal of Neurology*, vol. 27, no. 10, pp. 1918–1929, 2020.

[61] R. Dubbioso, M. Spisto, L. Verde, *et al.*, "Voice signals database of als patients with different dysarthria severity and healthy controls," *Scientific Data*, vol. 11, p. 800, 2024.

[62] P. M. Andersen, "The genetics of amyotrophic lateral sclerosis (als)," *Supplements to Clinical Neurophysiology*, vol. 57, pp. 211–227, 2003.

[63] M. B. Raez, M. S. Hussain, and F. Mohd-Yasin, "Techniques of EMG signal analysis: detection, processing, classification and applications," *Biological Procedures Online*, vol. 8, pp. 11–35, 2006.

[64] R. Merletti and P. J. Parker, *Electromyography: physiology, engineering, and non-invasive applications*. John Wiley & Sons, 2004.

[65] D. Stashuk, "EMG signal decomposition: how can it be accomplished and used?," *Journal of Electromyography and Kinesiology*, vol. 11, no. 3, pp. 151–173, 2001.

[66] M. B. I. Reaz, M. S. Hussain, and F. Mohd-Yasin, "Techniques of EMG signal analysis: detection, processing, classification and applications," *Biological procedures online*, vol. 8, pp. 11–35, 2006.

[67] A. López, F. Ferrero, M. Valledor, J. Campo, and O. Postolache, "A study on electrode placement in EOG systems for medical applications," in *2016 IEEE International Symposium on Medical Measurements and Applications (MeMeA)*, 2016.

[68] Y.-C. Yu, H. Fisher, A. Busheska, L. Thompson, and L. Gabel, "A hybrid BCI for robotic device navigation," in *2024 58th Annual Conference on Information Sciences and Systems (CISS)*, 2024.

[69] M. D. Olmo and R. Domingo, "EMG characterization and processing in production engineering," *Materials (Basel)*, vol. 13, no. 24, p. 5815, 2020.

[70] L. Myers, M. Lowery, M. O'Malley, C. Vaughan, C. Heneghan, A. S. C. Gibson, Y. Harley, and R. Sreenivasan, "Rectification and non-linear pre-processing of EMG signals for cortico-muscular analysis," *Journal of Neuroscience Methods*, vol. 124, no. 2, pp. 157–165, 2003.

[71] P. Flandrin, *Explorations in Time-Frequency Analysis*. Cambridge University Press, 2018.

[72] B. M. K. Y. D. I. Wu HT, Hseu SS, "Evaluating physiological dynamics via synchrosqueezing: prediction of ventilator weaning," *IEEE Transactions on Biomedical Engineering*, vol. 61, p. 736–744, 2014.

[73] K. Dragomiretskiy and D. Zosso, "Variational mode decomposition," *IEEE Transactions on Signal Processing*, vol. 62, no. 3, pp. 531–544, 2014.

[74] S. Wadekar, A. Mahalkari, A. Ali, and A. Gupta, "A review on singular spectrum analysis," in *2022 IEEE International Conference on Current Development in Engineering and Technology (CCET)*, pp. 1–6, 2022.

[75] N. Golyandina, A. Zhigljavsky, N. Golyandina, and A. Zhigljavsky, "Basic ssa," *Singular Spectrum Analysis for time series*, pp. 21–90, 2020.

[76] R. Rekapalli and R. Tiwari, "A short note on the application of singular spectrum analysis for geophysical data processing," *J. Ind. Geophys. Union*, vol. 19, pp. 77–85, 2015.

[77] Y. Peng, X. Chen, X. Jiang, *et al.*, "Auto-identification of dominant modal parameters from multi-batch signals based on weighted SSA to suppress milling vibration," *The International Journal of Advanced Manufacturing Technology*, vol. 128, pp. 4077–4090, 2023.

[78] A. Phinyomark, F. Quaine, S. Charbonnier, C. Serviere, F. TarpinBernard, and Y. Laurillau, "EMG feature evaluation for improving myoelectric pattern recognition robustness," *Expert Systems with Applications*, vol. 40, no. 12, pp. 4832–4840, 2013.

[79] C. J. D. Luca, R. Jung, and Z. G. K. Z. Nawab, "Techniques of emg signal analysis: detection, processing, classification and applications," *Biological Procedures Online*, vol. 8, pp. 11–35, 2006.

[80] R. Panda, S. Jain, R. K. Tripathy, R. R. Sharma, and R. B. Pachori, "Sliding mode singular spectrum analysis for the elimination of cross-terms in wigner–ville distribution," *Springer Science+Business Media, LLC, part of Springer Nature*, p. 1207–1232, 2020.

[81] H. Hassani, "Singular spectrum analysis: Methodology and comparison," *Journal of Data Science*, vol. 5, no. 2, pp. 239–257, 2022.

[82] S. Jain, R. Panda, and R. Tripathy, "Multivariate sliding-mode singular spectrum analysis for the decomposition of multisensor time series," *IEEE Sensors Letters*, 2020.

[83] J. Manit and P. Youngkong, "Neighborhood components analysis in s EMG signal dimensionality reduction for gait phase pattern recognition," in *7th International Conference on Broadband Communications and Biomedical Applications*, pp. 86–90, 2011.

[84] J. Kennedy and R. Eberhart, "Particle swarm optimization," in *Proceedings of IEEE International Conference on Neural Networks*, vol. IV, pp. 1942–1948, 1995.

[85] M. R. Bonyadi and Z. Michalewicz, "Particle swarm optimization for single objective continuous space problems: A review," *Evolutionary Computation*, vol. 25, no. 1, pp. 1–54, 2017.

[86] A. Esmin, R. Coelho, and S. Matwin, "A review on particle swarm optimization algorithm and its variants to clustering high-dimensional data," *Artificial Intelligence Review*, vol. 44, pp. 23–45, June 2015.

[87] D. Bratton and J. Kennedy, "Defining a standard for particle swarm optimization," in *2007 IEEE Swarm Intelligence Symposium*, pp. 120–127, 2007.

[88] X. Cui, J. M. Beaver, J. St. Charles, and T. E. Potok, "Dimensionality reduction particle swarm algorithm for high dimensional clustering," in *2008 IEEE Swarm Intelligence Symposium*, pp. 1–6, 2008.

[89] Y. Zhang, S. Wang, and G. Ji, "A comprehensive survey on Particle Swarm Optimization Algorithm and Its Applications," *Mathematical Problems in Engineering*, vol. 2015, no. 1, 2015.

[90] W. Yang, K. Wang, and W. Zuo, "Neighborhood component feature selection for high-dimensional data," *Journal of Computers*, vol. 7, no. 1, pp. 161–168, 2012.

[91] S. Ramírez-Gallego, I. Lastra, D. Martínez-Rego, V. Bolón-Canedo, J. M. Benítez, F. Herrera, and A. Alonso-Betanzos, "Fast-MRMR: Fast minimum redundancy maximum relevance algorithm for high-dimensional big data," *International Journal of Intelligent Systems*, vol. 32, no. 2, pp. 134–152, 2017.

[92] H. Peng, F. Long, and C. Ding, "Feature selection based on mutual information: criteria of max-dependency, max-relevance, and min-redundancy," *IEEE Trans-*

actions on Pattern Analysis and Machine Intelligence, no. 8, pp. 1226–1238, 2005.

[93] P. A. Estévez, M. Tesmer, C. A. Perez, and J. M. Zurada, "Normalized mutual information feature selection," *IEEE Transactions on Neural Networks*, vol. 20, no. 2, pp. 189–201, 2009.

[94] N. D. Thang and Y.-K. Lee, "An improved maximum relevance and minimum redundancy feature selection algorithm based on normalized mutual information," in *2010 10th IEEE/IPSJ International Symposium on Applications and the Internet*, pp. 395–398, IEEE, 2010.

[95] A. Senawi, H.-L. Wei, and S. A. Billings, "A new maximum relevance-minimum multicollinearity (mrmmc) method for feature selection and ranking," *Pattern Recognition*, vol. 67, pp. 47–61, 2017.

[96] C. Ding and H. Peng, "Minimum redundancy feature selection from microarray gene expression data," *Journal of Bioinformatics and Computational Biology*, vol. 3, no. 2, pp. 185–205, 2005.

[97] D. Lopez-Paz, P. Hennig, and B. Schölkopf, "The randomized dependence coefficient," in *Advances in Neural Information Processing Systems*, pp. 1–9, 2013.

[98] S. P. Jordan, "Quantum algorithm zoo." `https://quantumalgorithmzoo.org`.

[99] A. M. Childs and W. Van Dam, "Quantum algorithms for algebraic problems," *Reviews of Modern Physics*, vol. 82, no. 1, pp. 1–52, 2010.

[100] M. Santha, "Quantum walk based search algorithms," in *International Conference on Theory and Applications of Models of Computation*, pp. 31–46, Springer, 2008.

[101] D. Bacon and W. van Dam, "Recent progress in quantum algorithms," *Commun. ACM*, vol. 53, p. 84–93, Feb. 2010.

[102] A. Jadhav, A. Rasool, and M. Gyanchandani, "Quantum machine learning: Scope for real-world problems," *Procedia Computer Science*, vol. 218, pp. 2612–2625, 2023. International Conference on Machine Learning and Data Engineering.

[103] M. Schulda, I. Sinayskiy, and F. Petruccione, "An introduction to quantum machine learning," *Quantum Research Group, School of Chemistry and Physics, University of KwaZulu-Natal*, September 11 2014. National Institute for Theoretical Physics (NITheP), KwaZulu-Natal, 4001, South Africa.

[104] M. A. Nielsen and I. L. Chuang, *Quantum Computation and Quantum Information*. Cambridge University Press, 10th anniversary ed., 2010.

[105] S. Oh, J. Choi, and J. Kim, "A tutorial on quantum convolutional neural networks QCNN," in *2020 International Conference on Information and Communication Technology Convergence (ICTC)*, (Jeju, Korea (South)), pp. 236–239, 2020.

[106] J. Korvenaho, "Spoken command recognition with quantum convolutional neural networks." `https://erepo.uef.fi/items/4359c4f4-4f06-4487-9f4f-153cd314bee1`, 2022. University of Eastern Finland.

[107] I. Cong, S. Choi, and M. D. Lukin, "Quantum convolutional neural networks," *Nature Physics*, vol. 15, no. 12, pp. 1273–1278, 2019.

[108] W. Li, P.-C. Chu, G.-Z. Liu, Y.-B. Tian, T.-H. Qiu, and S.-M. Wang, "An image classification algorithm based on hybrid quantum classical convolutional neural network," *Quantum Engineering*, p. 5701479, 2022.

[109] F. Fan, Y. Shi, T. Guggemos, and X. X. Zhu, "Hybrid quantum-classical convolutional neural network model for image classification," *IEEE Transactions on Neural Networks and Learning Systems*, 2023.

[110] Y. Li, R.-G. Zhou, R. Xu, J. Luo, and W. Hu, "A quantum deep convolutional neural network for image recognition," *Quantum Science and Technology*, vol. 5, 2020.

[111] A. Sebastianelli, D. A. Zaidenberg, D. Spiller, B. L. Saux, and S. L. Ullo, "On circuit-based hybrid quantum neural networks for remote sensing imagery classification," *IEEE Journal of Selected Topics in Applied Earth Observations and Remote Sensing*, vol. 15, p. 565, 2021.

[112] A. Chalumuri, R. Kune, S. Kannan, and B. Manoj, "Quantum–classical image processing for scene classification," *IEEE Sensors Letters*, vol. 6, no. 1, 2022.

[113] X. Zhang, J. Xia, X. Tan, X. Zhou, and T. Wang, "Polsar image classification via learned superpixels and QCNN integrating color features," *Remote Sensing*, vol. 11, p. 1831, 2019.

[114] S. Y. Chang, B. L. Saux, S. Vallecorsa, and M. Grossi, "Quantum convolutional circuits for earth observation image classification," in *IGARSS 2022-2022 IEEE International Geoscience and Remote Sensing Symposium*, pp. 4907–4910, 2022.

[115] Z. N. Aldoski and C. Koren, "Impact of traffic sign diversity on autonomous vehicles: a literature review," *Periodica Polytechnica Transportation Engineering*, vol. 51, p. 338, 2023.

[116] M. A. Khan, H. Park, and J. Chae, "A lightweight convolutional neural network (cnn) architecture for traffic sign recognition in urban road networks," *Electronics*, vol. 12, p. 1802, 2023.

[117] S. Y.-C. Chen, T.-C. Wei, C. Zhang, H. Yu, and S. Yoo, "Quantum convolutional neural networks for high energy physics data analysis," *Physical Review Research*, vol. 4, Mar 2022.

[118] S. Monaco, O. Kiss, A. Mandarino, S. Vallecorsa, and M. Grossi, "Quantum phase detection generalization from marginal quantum neural network models," *Physical Review B*, vol. 107, p. L081105, 2023.

[119] A. J. Ferreira-Martins, L. Silva, A. Palhares, R. Pereira, D. O. Soares-Pinto, R. Chaves, and A. Canabarro, "Detecting quantum phase transitions in a frustrated spin chain via transfer learning of a quantum classifier algorithm," *Physical Review A*, vol. 109, p. 052623, 2024.

[120] I. MacCormack, C. Delaney, A. Galda, N. Aggarwal, and P. Narang, "Branching quantum convolutional neural networks," *Physical Review Research*, vol. 4, p. 013117, 2022.

[121] J. Herrmann, S. M. Llima, A. Remm, P. Zapletal, N. A. McMahon, C. Scarato, F. Swiadek, C. K. Andersen, C. Hellings, S. Krinner, *et al.*, "Realizing quantum convolutional neural networks on a superconducting quantum processor to recognize quantum phases," *Nature Communications*, vol. 13, p. 1, 2022.

[122] N. Wrobel, A. Baul, K.-M. Tam, and J. Moreno, "Detecting quantum critical points of correlated systems by quantum convolutional neural network using data from variational quantum eigensolver," *Quantum Reports*, vol. 4, p. 574, 2022.

[123] Y.-J. Liu, A. Smith, M. Knap, and F. Pollmann, "Modelindependent learning of quantum phases of matter with quantum convolutional neural networks," *Physical Review Letters*, vol. 130, p. 220603, 2023.

[124] L.-H. Gong, J.-J. Pei, T.-F. Zhang, and N.-R. Zhou, "Quantum convolutional neural network based on variational quantum circuits," *Optics Communications*, vol. 550, p. 129993, 2024.

[125] D. Bokhan, A. S. Mastiukova, A. S. Boev, D. N. Trubnikov, and A. K. Fedorov, "Multiclass classification using quantum convolutional neural networks with hybrid quantum-classical learning," *Frontiers in Physics*, vol. 10, p. 1069985, 2022.

[126] E. Gil-Fuster, J. Eisert, and C. Bravo-Prieto, "Understanding quantum machine learning also requires rethinking generalization," *Nature Communications*, vol. 15, p. 2277, 2024.

[127] M. Henderson, S. Shakya, S. Pradhan, and T. Cook, "Quanvolutional neural networks: powering image recognition with quantum circuits," *Quantum Machine Intelligence*, vol. 2, no. 1, p. 2, 2020.

[128] A. Montanaro, "Quantum algorithms: an overview," *npj Quantum Information*, vol. 2, p. 15023, 2016.

[129] A. Şengür, Ü. Budak, and Y. Akbulut, "Classification of amyotrophic lateral sclerosis and healthy electromyography signals based on transfer learning," *European Journal of Technique (EJT)*, vol. 8, no. 2, pp. 179–185, 2018.

[130] K. N. Hassan, M. S. A. Hridoy, N. Tasnim, A. F. Chowdhury, T. A. Roni, S. Tabrez, A. Subhana, and C. Shahnaz, "ALSNet: A dilated 1-D CNN for identifying ALS from raw EMG signal," in *ICASSP 2022-2022 IEEE International Conference on Acoustics, Speech and Signal Processing (ICASSP)*, pp. 1181–1185, IEEE, 2022.

[131] M. Nikolic and J. A. Sørensen, *Detailed Analysis of Clinical Electromyography Signals: EMG Decomposition, Findings and Firing Pattern Analysis in Controls and Patients with Myopathy and Amyotrophic Lateral Sclerosis*. PhD thesis, Faculty of Health Science, IT University of Copenhagen, 2001.

[132] V. Asanza, J. Miranda, J. Miranda, L. Rivas, D. H. Peluffo-Ordóñez, E. Pelaez, F. Loayza, and O. Alejandro, "Electrooculography signals classification for FPGA-based human-computer interaction," in *2022 IEEE ANDESCON*, pp. 1–7, 2022.

[133] S. Zarei, K. Carr, L. Reiley, K. Diaz, O. Guerra, P. F. Altamirano, W. Pagani, D. Lodin, G. Orozco, and A. Chinea, "A comprehensive review of amyotrophic lateral sclerosis," *Surgical Neurology International*, vol. 6, 2015.

[134] S. Carrera-Juliá, M. L. Moreno, C. Barrios, J. E. de la Rubia Ortí, and E. Drehmer, "Antioxidant alternatives in the treatment of amyotrophic lateral sclerosis: a comprehensive review," *Frontiers in Physiology*, vol. 11, p. 63, 2020.

[135] S. Dukic, R. McMackin, E. Costello, M. Metzger, T. Buxo, A. Fasano, R. Chipika, M. Pinto-Grau, C. Schuster, M. Hammond, *et al.*, "Resting-state EEG reveals four subphenotypes of amyotrophic lateral sclerosis," *Brain*, vol. 145, no. 2, pp. 621–631, 2022.

[136] A. Doulah and S. Fattah, "Neuromuscular disease classification based on mel frequency cepstrum of motor unit action potential," in *2014 International Conference on Electrical Engineering and Information & Communication Technology*, pp. 1–4, IEEE, 2014.

[137] A. Sengur, M. Gedikpinar, Y. Akbulut, E. Deniz, V. Bajaj, and Y. Guo, "Deep EMGnet: an application for efficient discrimination of ALS and normal EMG signals," in *Mechatronics 2017: Recent Technological and Scientific Advances*, pp. 619–625, Springer, 2018.

[138] A. Mokdad, S. M. E. A. Debbal, and F. Meziani, "Diagnosis of amyotrophic lateral sclerosis (ALS) disorders based on electromyogram (EMG) signal analysis and feature selection," *Polish Journal of Medical Physics and Engineering*, vol. 26, no. 3, pp. 155–160, 2020.

[139] S. Chatterjee, K. Samanta, N. R. Choudhury, and R. Bose, "Detection of myopathy and ALS electromyograms employing modified window Stockwell transform," *IEEE Sensors Letters*, vol. 3, no. 7, p. 7001204, 2019.

[140] V. K. Mishra, V. Bajaj, A. Kumar, and G. K. Singh, "Analysis of ALS and normal EMG signals based on empirical mode decomposition," *IET Science, Measurement & Technology*, vol. 10, no. 8, pp. 963–971, 2016.

[141] C. Hou, F. Cai, F. Liu, S. Cheng, and H. Wang, "A method for removing ECG interference from lumbar EMG based on signal segmentation and SSA," *IEEE Sensors Journal*, vol. 22, no. 13, pp. 13309–13317, 2022.

[142] S. De and A. K. Gupta, "A quantum machine learning framework for driver drowsiness detection using biopotential signals and head movement analysis,"

in *2024 IEEE International Conference for Women in Innovation, Technology and Entrepreneurship (ICWITE)*, pp. 461–466, 2024.

[143] R. Panda, S. Jain, R. Tripathy, R. R. Sharma, and R. B. Pachori, "Sliding mode singular spectrum analysis for the elimination of cross-terms in Wigner–Ville distribution," *Circuits, Systems, and Signal Processing*, vol. 40, no. 3, pp. 1207–1232, 2021.

[144] R. Eberhart and X. Hu, "Human tremor analysis using particle swarm optimization," in *Proceedings of the 1999 Congress on Evolutionary Computation-CEC99 (Cat. No. 99TH8406)*, vol. 3, pp. 1927–1930 Vol. 3, 1999.

[145] R. Hassan, B. Cohanim, and O. de Weck, "A comparison of particle swarm optimization and the genetic algorithm," vol. 2, 04 2005.

[146] S. Ahmed, M. Frikha, T. D. H. Hussein, and J. Rahebi, "Optimum feature selection with particle swarm optimization to face recognition system using Gabor wavelet transform and deep learning," *BioMed Research International*, vol. 2021, no. 1, p. 6621540, 2021.

[147] I. Cong, S. Choi, and M. D. Lukin, "Quantum convolutional neural networks," *Nature Physics*, vol. 15, no. 12, pp. 1273–1278, 2019.

[148] R. Liguori, A. Fuglsang-Frederiksen, W. Nix, P. Fawcett, and K. Andersen, "Electromyography in myopathy," *Neurophysiologie Clinique/Clinical Neurophysiology*, vol. 27, no. 3, pp. 200–203, 1997.

[149] K. J. Felice, "Differential diagnosis of distal myopathies," *Practical Neurology*, vol. 18, pp. 82–91, July 2019.

[150] S. Sriram, K. Rajagopal, O. Krejcar, and H. Namazi, "Decoding of the extraocular muscles activations by complexity-based analysis of electromyogram (EMG) signals," *Fractals*, vol. 32, no. 03, p. 2450067, 2024.

[151] M. R. Ahsan, M. I. Ibrahimy, and O. O. Khalifa, "EMG signal classification for human computer interaction: a review," vol. 33, pp. 480–501, 2009.

[152] V. K. Singh and R. B. Pachori, "Multichannel eigenvalue decomposition of Hankel matrix based classification of eye movements from electrooculogram," *IEEE Sensors Letters*, vol. 8, pp. 1–4, 2024.

[153] J. J. A. M. Junior, C. E. Pontim, T. S. Dias, and D. P. Campos, "How do s EMG segmentation parameters influence the pattern recognition process? an approach based on a wearable s EMG sensor," *Biomedical Signal Processing and Control*, vol. 81, p. 104546, 2023.

[154] M. Soundirarajan, M. H. Babini, S. Sim, V. Nathan, A. Subasi, and H. Namazi, "Analysis of brain-facial muscle connection in the static fractal visual stimulation," *International Journal of Imaging Systems and Technology*, vol. 31, no. 2, pp. 548–554, 2021.

[155] M. Soundirarajan, E. Aghasian, O. Krejcar, and H. Namazi, "Complexity-based analysis of the coupling between facial muscle and brain activities," *Biomedical Signal Processing and Control*, vol. 67, p. 102511, 2021.

[156] J. Ramadoss, K. Rajagopal, N. M. Dawi, H. Namazi, and N. Pakniyat, "Decoding the correlation among leg muscle and brain activations in different body movements," *Fractals*, vol. 30, no. 04, p. 2250120, 2022.

[157] H.-S. Choi, "Electromyogram (EMG) signal classification based on light-weight neural network with FPGAs for wearable application," *Electronics*, vol. 12, no. 6, p. 1398, 2023.

[158] M. Barfi, H. Karami, F. Faridi, Z. Sohrabi, and M. Hosseini, "Improving robotic hand control via adaptive fuzzy-pi controller using classification of EMG signals," *Heliyon*, vol. 8, no. 12, 2022.

[159] F. Pérez-Reynoso, N. Farrera-Vazquez, C. Capetillo, N. Méndez-Lozano, C. González-Gutiérrez, and E. López-Neri, "Pattern recognition of EMG signals

by machine learning for the control of a manipulator robot," *Sensors*, vol. 22, no. 9, 2022.

[160] N. Nazmi, M. A. Abdul Rahman, S.-i. Yamamoto, S. A. Ahmad, M. Malarvili, S. A. Mazlan, and H. Zamzuri, "Assessment on stationarity of EMG signals with different windows size during isotonic contractions," *Applied Sciences*, vol. 7, no. 10, p. 1050, 2017.

[161] A. Yamauchi, K. Tanaka, M. Fuki, S. Fujiwara, N. Kimizuka, T. Ryu, M. Saigo, K. Onda, R. Kusumoto, N. Ueno, *et al.*, "Room-temperature quantum coherence of entangled multiexcitons in a metal-organic framework," *Science Advances*, vol. 10, no. 1, p. eadi3147, 2024.

[162] E. Mykkänen, J. S. Lehtinen, L. Grönberg, A. Shchepetov, A. V. Timofeev, D. Gunnarsson, A. Kemppinen, A. J. Manninen, and M. Prunnila, "Thermionic junction devices utilizing phonon blocking," *Science Advances*, vol. 6, no. 15, p. eaax9191, 2020.

[163] L. Gila, A. Villanueva, and R. Cabeza, "Fisiopatología y técnicas de registro de los movimientos oculares," in *Anales del sistema sanitario de Navarra*, vol. 32, pp. 9–26, SciELO Espana, 2009.

[164] R. Wu, J. Xiao, and F. Zhao, "Design and implementation of pulse diagnosis instrument based on wavelet transform," in *Journal of Physics: Conference Series*, vol. 2396, p. 012007, IOP Publishing, 2022.

[165] J. P. Vásconez, L. I. Barona López, Á. L. Valdivieso Caraguay, and M. E. Benalcázar, "Hand gesture recognition using EMG-IMU signals and deep q-networks," *Sensors*, vol. 22, no. 24, p. 9613, 2022.

[166] H. R. Namazi, "Fractal based analysis of movement behavior in animal foraging," *ARC Journal of Neuroscience*, vol. 2, no. 3, pp. 1–3, 2017.

[167] V. Asanza, J. Miranda, N. Sánchez, E. Peláez, F. Loayza, and D. H. Peluffo-Ordóñez, "Electromyography (EMG) of the extraocular muscles (EOM)," 2021.

[168] M. Kalantari and H. Hassani, "Automatic grouping in singular spectrum analysis," *Forecasting*, vol. 1, no. 1, pp. 189–204, 2019.

[169] A. Rényi, "On measures of entropy and information," in *Proceedings of the Fourth Berkeley Symposium on Mathematical Statistics and Probability, Volume 1: Contributions to the Theory of Statistics*, pp. 547–561, University of California Press, 1961.

[170] N. Singh and B. Lall, "Spectral entropy features based analysis of impulse noise sources for plc systems," in *2018 IEEE Global Communications Conference (GLOBECOM)*, pp. 1–6, 2018.

[171] G. Sharma, K. Umapathy, and S. Krishnan, "Trends in audio signal feature extraction methods," *Applied Acoustics*, vol. 158, p. 107020, 2020.

[172] W. Yang, K. Wang, and W. Zuo, "Neighborhood component feature selection for high-dimensional data.," *J. Comput.*, vol. 7, no. 1, pp. 161–168, 2012.

[173] S. Mekruksavanich, P. Jantawong, N. Hnoohom, and A. Jitpattanakul, "Deep learning models for daily living activity recognition based on wearable inertial sensors," in *2022 19th International Joint Conference on Computer Science and Software Engineering (JCSSE)*, pp. 1–5, 2022.

[174] N. Hnoohom, A. Jitpattanakul, and S. Mekruksavanich, "Real-life human activity recognition with tri-axial accelerometer data from smartphone using hybrid long short-term memory networks," in *2020 15th International Joint Symposium on Artificial Intelligence and Natural Language Processing (iSAI-NLP)*, pp. 1–6, 2020.

[175] S. Mekruksavanich and A. Jitpattanakul, "A deep learning network with aggregation residual transformation for human activity recognition using inertial and stretch sensors," *Computers*, vol. 12, no. 7, 2023.

[176] C. Zhu and W. Sheng, "Realtime recognition of complex human daily activities using human motion and location data," *IEEE Transactions on Biomedical Engineering*, vol. 59, no. 9, pp. 2422–2430, 2012.

[177] M. S. AL-Quraishi, I. Elamvazuthi, S. A. Daud, S. Parasuraman, and A. Borboni, "EEG-based control for upper and lower limb exoskeletons and prostheses: A systematic review," *Sensors*, vol. 18, no. 10, 2018.

[178] K. Kiguchi and Y. Hayashi, "An EMG-based control for an upper-limb power-assist exoskeleton robot," *IEEE Transactions on Systems, Man, and Cybernetics, Part B (Cybernetics)*, vol. 42, no. 4, pp. 1064–1071, 2012.

[179] P. W. Kong, A. H. Koh, M. Y. M. Ho, M. N. S. Iskandar, and C. X. E. Lim, "Effectiveness of a passive military exoskeleton in off-loading weight during static and dynamic load carriage: A randomised cross-over study," *Applied Ergonomics*, vol. 119, p. 104293, 2024.

[180] M. Scattolini, A. Tigrini, F. Verdini, G. Iadarola, S. Spinsante, S. Fioretti, L. Burattini, and A. Mengarelli, "Leveraging inertial information from a single IMU for human daily activity recognition," in *2024 IEEE International Symposium on Medical Measurements and Applications (MeMeA)*, pp. 1–6, 2024.

[181] A. Vijayvargiya, B. Dhanka, V. Gupta, and R. Kumar, "Implementation of machine learning algorithms for automated human gait activity recognition using s EMG signals," *International Journal of Biomedical Engineering and Technology*, vol. 42, no. 2, pp. 150–166, 2023.

[182] K. Nurhanim, I. Elamvazuthi, L. Izhar, G. Capi, and S. Su, "EMG signals classification on human activity recognition using machine learning algorithm," in *2021 8th NAFOSTED Conference on Information and Computer Science (NICS)*, pp. 369–373, 2021.

[183] R. M. Vamsi, N. Adapa, D. Yelamanchili, N. A. Choudhury, and B. Soni, "An efficient and optimized CNN-LSTM framework for complex human activity recog-

nition system using surface EMG physiological sensors and feature engineering," in *2024 IEEE Students Conference on Engineering and Systems (SCES)*, pp. 1–6, 2024.

[184] Z. Ju, G. Ouyang, M. Wilamowska-Korsak, and H. Liu, "Surface EMG based hand manipulation identification via nonlinear feature extraction and classification," *IEEE Sensors Journal*, vol. 13, no. 9, pp. 3302–3311, 2013.

[185] L. Silva, J. Vaz, M. Castro, P. Serranho, J. Cabri, and P. Pezarat-Correia, "Recurrence quantification analysis and support vector machines for golf handicap and low back pain EMG classification," *Journal of Electromyography and Kinesiology*, vol. 25, no. 4, pp. 637–647, 2015.

[186] N. Sukumar, S. Taran, and V. Bajaj, "Physical actions classification of surface EMG signals using VMD," in *2018 International Conference on Communication and Signal Processing (ICCSP)*, pp. 0705–0709, IEEE, 2018.

[187] S. Chada, S. Taran, and V. Bajaj, "An efficient approach for physical actions classification using surface EMG signals," *Health Information Science and Systems*, vol. 8, no. 1, p. 3, 2019.

[188] A. K. Ajayan and P. B., "EMG physical action detection using recurrence plot approach," *Procedia Computer Science*, vol. 235, pp. 1539–1547, 2024. International Conference on Machine Learning and Data Engineering (ICMLDE 2023).

[189] N. A. Choudhury and B. Soni, "An efficient and lightweight deep learning model for human activity recognition on raw sensor data in uncontrolled environment," *IEEE Sensors Journal*, vol. 23, no. 20, pp. 25579–25586, 2023.

[190] K. K. Makam, V. K. Singh, and R. B. Pachori, "ALS detection framework based on automatic singular spectrum analysis and quantum convolutional neural network from EMG signals," *IEEE Sensors Letters*, vol. 8, no. 9, pp. 1–4, 2024.

[191] C. Yang, S. Yang, Z. Feng, and M. Wang, "Quadruplet convolution neural network with c3 loss (c3-qcnn) for signal classification," *IEEE Transactions on Instrumentation and Measurement*, vol. 71, pp. 1–8, 2022.

[192] Y. Zhu, A. Bouridane, M. E. Celebi, D. Konar, P. Angelov, Q. Ni, and R. Jiang, "Quantum face recognition with multigate quantum convolutional neural network," *IEEE Transactions on Artificial Intelligence*, vol. 5, no. 12, pp. 6330–6341, 2024.

[193] A. Vijayvargiya, R. Kumar, and P. Sharma, "PC-GNN: Pearson correlation-based graph neural network for recognition of human lower limb activity using s EMG signal," *IEEE Transactions on Human-Machine Systems*, vol. 53, no. 6, pp. 945–954, 2023.

[194] H. Liu and Z. Liu, "A multimodal dynamic hand gesture recognition based on radar–vision fusion," *IEEE Transactions on Instrumentation and Measurement*, vol. 72, pp. 1–15, 2023.

[195] H. Zhang and L. Xu, "Multi-STMT: Multi-level network for human activity recognition based on wearable sensors," *IEEE Transactions on Instrumentation and Measurement*, vol. 73, pp. 1–12, 2024.

[196] S. Ullah and D.-H. Kim, "Multi-accent EMG-to-speech optimized transduction with PerFL and MAML adaptations," *IEEE Transactions on Instrumentation and Measurement*, vol. 73, p. 2528317, 2024.

[197] P. C. Rodrigues and R. Mahmoudvand, "The benefits of multivariate singular spectrum analysis over the univariate version," *Journal of the Franklin Institute*, vol. 355, no. 1, pp. 544–564, 2018.

[198] S. Jain, R. Panda, and R. K. Tripathy, "Multivariate sliding-mode singular spectrum analysis for the decomposition of multisensor time series," *IEEE Sensors Letters*, vol. 4, no. 6, pp. 1–4, 2020.

[199] D. Vashaee and J. Abouie, "Microwave-induced cooling in double quantum dots: Achieving millikelvin temperatures to reduce thermal noise around spin qubits," *Phys. Rev. B*, vol. 111, p. 014305, Jan 2025.

[200] N. Delfosse and E. Tham, "Low-cost noise reduction for clifford circuits," *Phys. Rev. Lett.*, vol. 134, p. 090603, Mar 2025.

[201] D. Chappell, B. Mulvey, S. Perera, F. Bello, P. Kormushev, and N. Rojas, "Beyond humanoid prosthetic hands: Modular terminal devices that improve user performance," *IEEE Transactions on Neural Systems and Rehabilitation Engineering*, vol. 33, pp. 466–475, 2025.

[202] M. Karimi and M. Ahmadi, "iLeAD: An EMG-based adaptive shared control framework for exoskeleton assistance via deep reinforcement learning," *IEEE Transactions on Artificial Intelligence*, pp. 1–13, 2025.

[203] S. G. Thomas and P. K. Myakala, "Beyond the cloud: Federated learning and edge AI for the next decade," *Journal of Computer and Communications*, vol. 13, no. 2, pp. 37–50, 2025.

List of Publications

A. Published

A1. In Refereed Journals

1. K. K. Makam, V. K. Singh and R. B. Pachori, "ALS detection framework based on automatic singular spectrum analysis and quantum convolutional neural network from EMG signals," *IEEE Sensors Letters*, vol. 8, no. 9, pp. 1-4, Sept. 2024.

2. K. K. Makam, V. K. Singh and R. B. Pachori, "Eye movement detection based on SM-SSA and quantum CNN from EMG of EOM signals," *IEEE Sensors Letters*, vol. 9, no. 5, pp. 1-4, May 2025.

B. Communicated

In Refereed Journals

1. K. K. Makam, S. V. Bhalerao and R. B. Pachori, "Enhanced human activity recognition using multivariate singular spectrum analysis with optimized quantum CNN model," *IEEE Transactions on Human-Machine Systems.*

C. Other publications

C1. In Refereed Journals

1. A. Shirumalla, M. Bajpai and K.K. Makam, "YOLO Models for Security and Surveillance Applications," *International Journal for Research in Applied Science and Engineering Technology (ISRAJET)*, vol. 12, no. VI, pp. 2513-2518, Jun. 2024.

C2. In Refereed Conferences

1. K.K. Makam and N.B. Agarwal, "Hybrid quantum-based machine learning algorithm for ALS detection using EMG signals," in *Innovations in Electrical and Electronics Engineering. ICEEE 2024, Lecture Notes in Electrical Engineering, Springer.*

2. P.K. Srimal and K.K. Makam, "Decoding human languages: A transfer learning approach for language translation for low resource languages – Nepali, Urdu, Pashto, and Punjabi," in *Proceedings of the 2024 International Conference on Computer, Electronics, Electrical Engineering & their Applications (IC2E3), Srinagar Garhwal, Uttarakhand, India*, 2024, pp. 1–6. (Awarded Best Paper)